Synthesis and Properties of Cationic Nitrogen-Doped Carbon Materials via Solution Plasma

Sangwoo CHAE

Synthesis and Properties of Cationic Nitrogen-Doped Carbon Materials via Solution Plasma

A Doctoral Dissertation by

Sangwoo CHAE

2019

Graduate School of Engineering,

Department of Material Science and Engineering,

Nagoya University

Table of contents

Abstract

The discovery of new form of low-dimension carbon materials (graphene, carbon nanotube) with exceptional electrical properties, such as high conductivity and high charge mobility, has revolutionized the electronics industry by dramatically expanding the potential applications of these types of materials. Graphene and carbon nanotube (CNT) have high electrical conductivity in the case of a single layer/wall. However, when they were used in material that has an applying physical force, the conductivity get drastically decreased. Although, the carbonaceous material still has low conductivity when compared to the other electrical conductors. Thus, the rational design and development of new form of carbon material with high performance are still challenging.

At the molecular scale, there is a possibly new form of nitrogen in carbon framework, the cationic nitrogen (N^+), which is not much concentrated in the literature. The cationic nitrogen-doped carbon (CN–C) can maintain planarity and crystalline is manifested. The carbon atom has 4 valence electrons which are generally arranged in a planar hexagonal structure with sp^2 hybridization. However, that sp^2 cannot maintain planarity when a heteroatom, such as nitrogen atom which has five valence electrons, was introduced to carbon plane. To avoid this, it requires a species with 4 valence electrons, for examples, cationic nitrogen (N^+) and anionic boron (B^-), doped to carbon plane to maintain planarity with good crystallinity.

Solution plasma (SP) is an experimental tool successfully developed by our group. SP is a cold plasma in a gas at atmospheric pressure, outcoming from the liquid that surrounds the discharge. SP process provides a synthesis of nanocarbon and hetero-nanocarbon materials via the CH activation. For example, the nitrogen-doped carbon can be easily obtained by the SP produced in nitrogen-containing organic solvent. However, the synthesis of CN–C has not been

reported. In this context, we investigated methods to synthesize CN–C without thermal treatment in order to develop high-performance carbon with high electrical properties using SP.

Chapter 2, cationic nitrogen-containing functional groups functionalized few-layer graphene sheets (f-FLG) were synthesized through a new method called SP in an ionic liquid, from graphite at ambient temperature and atmospheric pressure. Graphene sheets synthesis is now challenging in material science field which trendy need a new, fast and simple way. In this paper we are presenting an alternative method with those challenges by using graphite submerges in an ionic liquid then discharging with a bi-polar pulse. CN-functionalized graphene sheets were then obtained. With this method, the graphite was peeled into graphene sheets simultaneously cooperated with CN-functionalization. The nitrogen content was found to be 7.7 at%. The structural properties and nitrogen content of synthesized sample was then confirmed by characterizations of X-ray diffraction (XRD), Raman spectroscopy, Transmission Electron Microscopy (TEM), Field emission scanning electron microscopy (FE-SEM), Fourier transform infrared spectroscopy (FTIR) and X-ray photoelectron spectroscopy (XPS).

Chapter 3, reveals that cationic nitrogen-doped graphene (CN–G) was successfully synthesized at the high-repetition frequency with mixture of ionic liquid (IL) / organic solution (OS) as precursor for carbon and nitrogen source. Furthermore, the few-layer structure was confirmed by the 2D band in the Raman spectrum, as well as the morphological images from TEM. XPS analysis confirmed that the synthesized few-layer graphene including 13.4 at% nitrogen where the nitrogen atoms were introduced at the edge or defect site of graphene sheet at the same time that graphene sheets were synthesized by SP. Electrical measurements indicated that CN–G exhibits p-type semiconducting behavior, indicating that the alternative doping can effectively control the electrical properties of graphene. Our discovery will provide

a new experimental example of CN–G and promote research and application of CN–G.

Chapter 4, CN–C and CN–C wrapping single-wall carbon nanotubes (CN–C@SWCNT) were synthesized using SP which was done at ambient temperature and atmospheric pressure, in the gas resulted from the surrounding liquid. Reactive species produced from SP results in the formation of cationic-doped nitrogen entirely wrapping over SWCNT. The evidence of cationic nitrogen was confirmed by Raman spectroscopy, electron diffraction (ED), and XPS. Characterization of CN–C@SWCNT shows a high electric conductivity and uniform wrapping of CN–C on SWCNT. CN–C@SWCNT synthesized by SP has high electrical conductivity of 120 S cm^{-1}, which is exhibits p-type semiconducting behavior with high carrier concentration of 4.6×10^{20} cm^{-3}. The high electrical conductivity is due to nitrogen cationic from CN–C material wrapping the surface of SWCNT and SWCNT acting as conductive bridges among CN–C domains.

In this study, SP successfully synthesized a new carbonaceous material with outstandingly high electrical properties. These high electrical properties were attributed by synergistic effect by maintaining planarity and crystallinity via doping cationic nitrogen on CN–C materials. The cationic nitrogen atom on basal plane contributed an increasing in electrical conductivity which is beneficial for electrochemical devices, such as capacitors, solar cells, lithium-based batteries and the next-generation batteries that needed to be placed on the electrode side with high electrical conductivity. To accomplish these tasks, we design a new carbon material containing cationic nitrogen via SP.

Chapter 1

General introduction

Chapter 1 – General introduction

1.1. Low-dimensional carbon materials

In 1985, Fullerene, a carbon in form of a soccer ball combined with 60 carbon atoms, was first discovered. Then the carbon nanotubes (CNTs) was produced by Professor Iijima of Japan in 1991, followed by researchers from the UK, Geim and Novoselov, who succeeded in obtaining graphene from graphite using scotch tape and won the Nobel Prize. In recent decades, many studies on carbon allotropes have been very active. The allotropic forms of carbon were shown in **Figure 1.1**. Graphene has been attracting much attention, and also carbon nanotubes, because of their excellent electrical, physical and thermal properties.[1,2]

Graphene was defined by the word "graphite" and the suffix "ene" which indicates the chemical bonding state of carbon atoms, and is named graphene.[3] In other words, graphene is a sheet of graphite in a pencil lead that was thinly peeled with a layer thickness of 0.2 nm. Graphene has very good electrical, mechanical, thermal and optical properties. It has a charge mobility up to 100 times greater than silicon and an allowable current density up to 100 times higher than copper. It also has the highest thermal conductivity among carbon materials.[4,5] In addition, chemical functionalization is possible, thus controlling the chemical properties can be done and can be applied to various materials. Moreover, it has greater transparency and flexibility than the conventional indium tin oxide (ITO), which is used as a transparent electrode material, and is attracting attention as a new material to change the paradigm of existing semiconductor and display information technology.[6,7]

There are many ways to make graphene with such excellent properties, but there are two major ways called Top-down method, for producing graphene from graphite, and bottom-up method for chemically synthesizing graphene from carbon source.

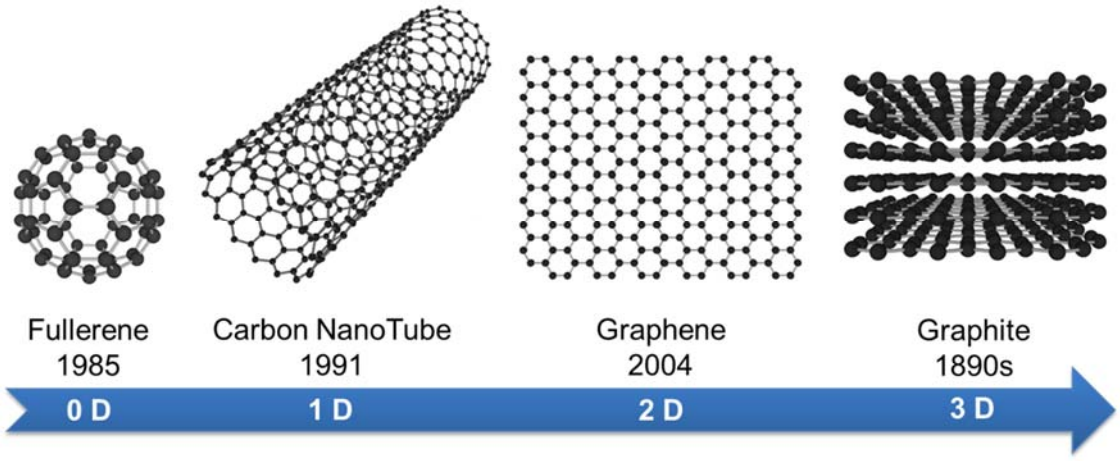

Figure 1.1. Allotropes of carbon; fullerene, carbon nanotubes graphene and graphite.

1.2 Graphene production method

There are two main methods of manufacturing graphene. The first is a top-down method for producing graphene from graphite, and the second is a bottom-up method for chemically synthesizing graphene from a carbon source (**Figure 1.2**).

1.2.1 *Top-down Methods*

The mechanical exfoliation is a method that mechanically separate graphene from graphite by using the adhesive force of scotch tape.[8,9] Graphite / Graphite intercalation compounds can be dispersed in solution through oxidation to graphite oxide. Then graphite oxide was exfoliated by ultrasonication to form graphene oxide (GO) and then was reduced to form reduced graphene oxide (rGO) which has lower electrical conductivity than graphite oxide.

Graphene, obtained by peeling of graphite, has an excellent crystallinity and also high conductivity, few defects and low production efficiency. This is not good enough in practical applications. Moreover, there is a possibility of contamination with organic impurities, and it is difficult to control the number of graphene layers. The GO and rGO are generally prepared by the Hummer's method, which oxidizes graphite to graphene. This method produces multi-layer graphene of several hundred nanometers to micrometers in size. Graphene flakes, which can

produce large quantities at low cost, can be applied to fillers, coatings, conductive inks and energy storage devices which is not necessary to be high purity. Thus, flake-type graphenes which have different sizes and contaminations are not suitable for applications in transparent flexible electrodes.

- Mechanical peeling from graphite -

The commonly known scotch tape peeling method was invented by Novoselov and Geim professor in 2004. It separates graphene from graphite stacks by using adhesive force of tape.[9] When you first remove the tape, the several layers of graphene sheet will come off. In order to obtain a few amounts of single-layered and double-layered graphene, it is necessary to repeat the operation of peeling off the tape. Then graphene is transferred to the desired target substrate and can be obtained by removing the adhesive component using a solvent such as acetone.

- Chemical exfoliation method -

The chemical exfoliation method is a separation of graphene layers by oxidizing graphite with strong acid.[10,11] The graphite oxide layers are dispersing in solution while the solvent is inserted between graphite layers making the gap between them far apart. Then GO reduced to rGO by reduction. This method can simply produce a lot of graphene for massive use applications. However, graphene obtained from this method has some defects and oxygen-containing functional groups which were left after reduction from oxidation of strong acids (eg, nitric acid (HNO_3), sulfuric acid (H_2SO_4)).

- Non-oxidative exfoliation -

A method designed to maintain the physical and electrical properties of graphene is to form graphene without defects and functional groups formed in the production of rGO through chemical exfoliation.[12,13] It is a method of inducing intercalation of graphite by using ionic

material and organic solvent, dispersing it, and separating single layer graphene by layer separation of dispersed solution by ultracentrifugation method. Although the above method is for forming high-quality graphene. However, it could get only a low yield of graphene which is the major drawback of this method. Thus, graphite peeling method is chosen to be a commercial method because of its massive producibility, and many researches are being focused on the mass production at present.

- Exfoliation of graphite in ionic liquid (IL) -

IL are presenting in a liquid state below 100 °C as the material, such as a salt consisting of ionic bond of cations and anions[14]. IL are called as green solvents and under consideration as an environmentally friendly solvent because they could exist as a stable liquid solution at high temperatures and their vapor pressure is almost close to zero. High dielectric constant of the IL are helping to block the stacking interaction that caused by Van der Waals interactions and effectively disperse the nanomaterials. With IL assistance, various methods have been employed, to successfully peel and disperse graphene sheet into the IL and IL mixtures, such as; mechanical, chemical, microwave, hydrothermal, electrochemical, and sonication techniques.[15]

IL has been known to be an intercalation material for the spaces between graphene sheets. Aida et al. were successful to fabricate the graphene sheets from graphite by using a heated IL.[16] Although microwave assisted method, which facilitated the intercalation and exfoliation of graphite oxide or expansion of graphite, have been reported.[17,18] We use the Ionic liquid that is mainly used for nitrogen-doped carbon synthesis, which is a process involving graphite peeling and nitrogen doping at the same time. The results showed that after microwave PF6-based IL, the graphite layers were peeling off and the peeling efficiency of graphene was decreased as the surface tension of IL shifted away from 40 mJ m^{-2}.[15]

1.2.2 *Bottom-up Methods*

Graphene can be formed by chemical vapor deposition (CVD) or epitaxial growth and grown from a carbon source. This method can control the number of layers and growth factors of graphene by using various kinds of substrates. In particular, the CVD synthesis method enables large-area, high-quality, and high-purity graphene production, which enables the mass production.

- Chemical vapor deposition (CVD) synthesis method -

In recent years, the CVD synthesis method is widely used to mass-produce high-quality graphene films. The CVD is a bottom-up method in which graphene directly grow on a substrate using a carbon source such as methane.[19-21] Large-area single-layer graphene grown on catalytic metal foils, primarily nickel or copper, can be transferred to the target substrate of interest. The synthesized graphene has higher crystallinity and electrical conductivity than general CVD graphene, but it has a problem that it is difficult to be commercially used due to the restriction of large-area synthesis and relatively expensive materials.

- Epitaxial growth method -

The epitaxial growth method is a production of graphene by heat-treating materials such as silicon carbide (SiC) containing carbon source at high temperature.[22,23] Graphene is formed as the carbon contained in the crystal grows along the grain surface at high temperature. The epitaxial growth method has a disadvantage that is relatively inferior in electrical characteristics to other synthetic methods and difficult to produce.

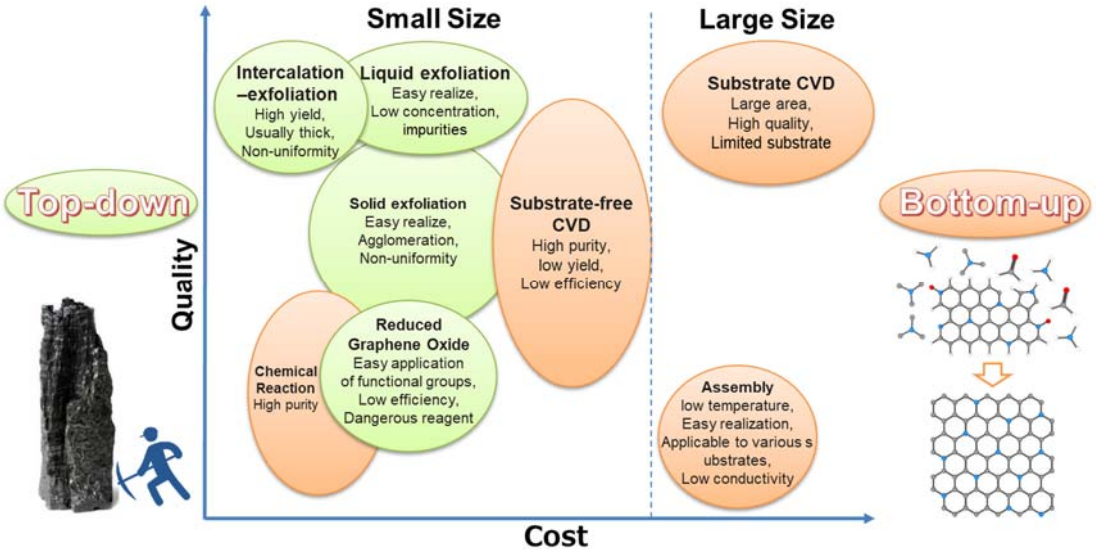

Figure 1.2. Quality versus cost for graphene synthesis techniques.

1.3 Doping Graphene

Graphene has a good electrical conductivity; however it has a unique energy band without bandgap, and research is being conducted to control electrical properties. In general, to use graphene as a semiconducting device, such as a transistor, it is necessary to open the bandgap or to improve the electrical characteristics by an appropriate method. Doping of heteroatom to material is known to be an effective way to modify the electrical properties of carbon materials.[24] There are two major types of doping which are p-type and n-type. The former, p-type, is a way to add an atom, which has lone pair electron that could be donated, to the carbon framework. This makes excessive electron in graphene layer which increases conductivity. Moreover, the Fermi level moves up and the work function decreases as well. The latter, n-type doping, is an atom provided a hole to the graphene layer. It increases conductivity and the Fermi level moves downwards resulting decrease in work function.[25] Amine-based materials are known to be effective dopants for N-doping graphene,[26-28] and NO_2[29] and tetrafluoro-tetracyanoquinodimethane (F4-TCNQ) are known to strongly p-dope graphene.[30] The graphene

whose electrical properties are changed by changing holes or number of electrons can be used as materials of various fields.

- Various nitrogen-bonding configurations in the graphene -

Ab-initio molecular orbital calculations confirmed the catalytic activity of the cationic nitrogen inside the basal plane of carbon layers, considering the Stone-Wales defect and curvature effect of the carbon sheet.[31] Density functional theory calculation demonstrated that among different nitrogen dopants of carbon as pyridinic, pyrrolic, and graphitic types, the last one creates the most active sites for electrocatalysis.[32]

The various types of nitrogen-bonding states observed in the carbon materials are shown in **Figure 1.3**. The most frequently noted types are pyridinic (N-6),[33,34] pyrrolic (N-5 (1))[35,36] and quaternary (N-Q (1))[37,38] nitrogen-bonding states. Others include amino (N-5 (2))[39,40] and pyridinic oxidized (N-X)[41,42] nitrogen-bonding states. The quaternary or graphitic (N-Q (1)) and cationic (N-Q (2))[43,44] nitrogen-bonding states are found in X-Q distinctions with similar XPS binding energies.

The graphitic nitrogen as dopant originates from the substitution of a tertiary carbon by a nitrogen atom, which becomes a cation changing the local charge density, and this cationic nitrogen plays an important role in the formation of the electron structure of sp^2-carbon (2D).[45] In addition, the graphitic nitrogen is also converted into stable quaternary nitrogen, but when the quaternary nitrogen is introduced, it cannot maintain the planarity. Therefore, planarity can be obtained by doping cationic nitrogen.[31]

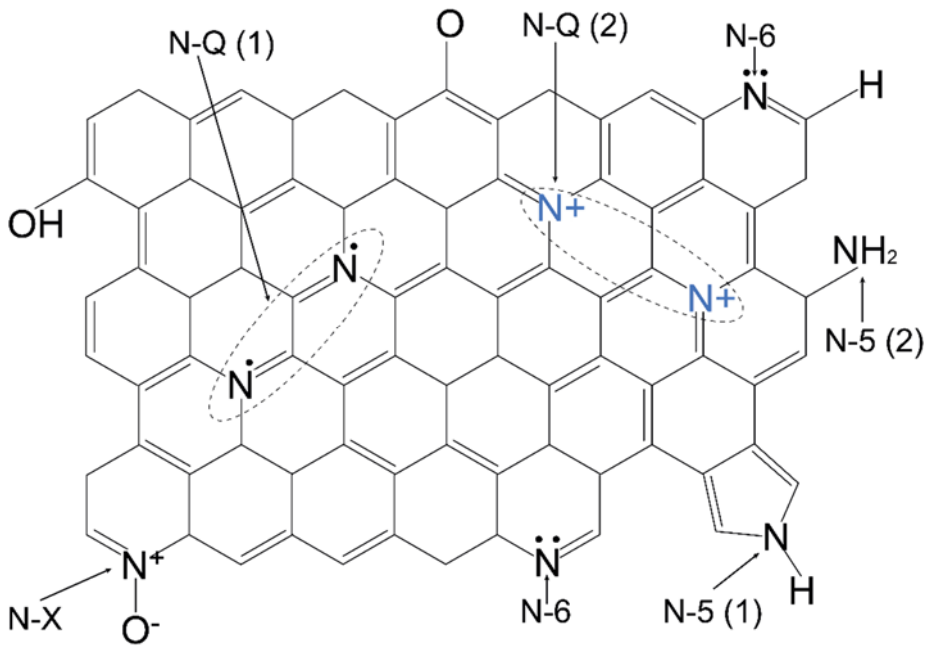

Figure 1.3. Various types of nitrogen-bonding configurations in the carbon structure

1.4. Graphene production via Solution plasma (SP)

There are some problems regarding the synthesis process of a significant amount of graphene. The peeling of HOPG by an adhesive tape and ball milling of graphite provide disordered stacks among layers although the number of layers was reduced.[46] The liquid–phase exfoliation of graphite in organic solvents with high surface tension, in IL, in ammonia, by using shear mixing and high-speed centrifugation, and the density differentiation in surfactants in various combinations with water are the most spread methods for a high-yield production of graphene sheets.[47-51] Unfortunately, these processes need multiple and more complex steps rather than graphene synthesis.

- *Top-down via SP*

We found a novel synthesis method for graphene sheets by erosion of graphite electrodes in SP.[52] SP is a non-equilibrium discharge at atmospheric pressure in the gas coming from the solution surrounding plasma. In the plasma field, high-energy electrons and activated species

such as H・, OH・, and carbon radicals depending on the solution used, can initiate and conduct plasma chemical reactions. The electron impact and especially ion collisions with the carbon electrodes produce erosion and generate graphene sheets. The chemical compounds from the liquid, transferred into the gas phase plasma, are dissociated by SP and form free radicals which are very active species. These activated or decomposed species can react with the electrons in the π-bond of graphite to form high molecular weight nanocarbon.[53]

- Bottom-up via SP

Recently, a SP for the synthesis of heteroatom-doped carbon has been reported. SP can produce hetero carbon with excellent electrical properties due to direct polymerization of liquid material and can design ideal high-performance carbon. In fact, it is possible to construct the heteroatom-doped carbon through a SP to synthesize carbon containing substantial heteroatoms, as mentioned above.

Plasma generation in a liquid medium containing carbon and a heteroatom precursor simultaneously induces dissociation and recombination with heteroatom insertion of the precursor. In other words, the molecule of precursor affects the formation of graphene through dissociation and recombination, and also during dissociates to form free radicals and bind electrons at the π-bond of the graphene. During this process, the dissociated nitrogen atoms interact and replace the carbon atoms of graphene sheet during growth and formation to form nitrogen doped graphene sheet. As a result, the heteroatom-doped graphene can be synthesized in one-step process. For example, the nitrogen-doped graphene sheets can be easily obtained by the SP produced in pyrrolidine, 2-pyrrolidone and N-methyl-2-pyrrolidone.[54,55]

1.5. Object and outline of the thesis

Essential factors of graphene manufacturing method evaluation; high content of nitrogen, selectivity towards few-layer graphene, structural integrity of graphene and processing time. So

far, there is no methods to satisfy all essential factors. The purpose of this study is to develop a high content nitrogen doped carbon material with simultaneously doping cationic nitrogen while satisfying all conditions at a high level.

Therefore, in this study, we investigated methods to improve the electrical properties without prior thermal treatment in order to produce cationic nitrogen doped high-performance carbon materials using SP. The work we have described is summarized in the **Figure 1.4**. We developed a new type of CN–C material using top-down and button-up methods using IL and SP. The study was carried out as follows.

In chapter 2, f-FLG sheets were synthesized through SP from graphite. The mechanism of FLG synthesis by the induced electron exchange in graphene flakes and the IL via SP were discussed.

In chapter 3, CN–G were successfully synthesized via SP in a mixture of ionic liquids (IL) / organic solution (OS) at room temperature. A detailed study on the change of properties of CN–G by cationic nitrogen was discussed.

In chapter 4, CN–C@SWCNT were synthesized via SP using an aniline aqueous solution with the SWCNT dispersion. A detailed study of the properties of CN–C and CN–C@SWCNT and the effects of cationic nitrogen was discussed.

Finally, chapter 5, it is a summary of all chapters.

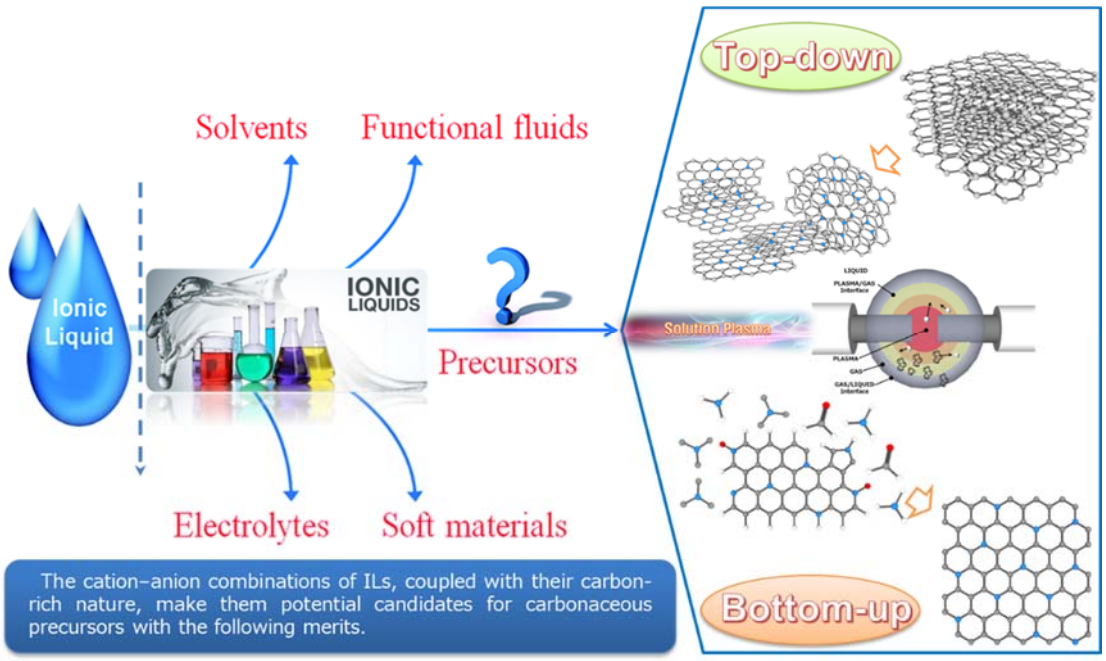

Figure 1.4. Ionic liquids (ILs) as novel precursors for carbon materials.

References

(1) K. S. Kim, Y. Zhao, H. Jang, S. Y. Lee, J. M. Kim, K. S. Kim, J.-H. Ahn, P. Kim, J.-Y. Choi and B. H. Hong, *Nature*, 2009, **457**, 706.

(2) L. L. Zhang and X. Zhao, *Chem. Soc. Rev.*, 2009, **38**, 2520-2531.

(3) H. P. Boehm, R. Setton and E. Stumpp, *Pure Appl. Chem.*, 1994, **66**, 1893-1901.

(4) X. Li, W. Cai, J. An, S. Kim, J. Nah, D. Yang, R. Piner, A. Velamakanni, I. Jung and E. Tutuc, *Science*, 2009, **324**, 1312-1314.

(5) C. Lee, X. Wei, J. W. Kysar and J. Hone, *Science*, 2008, **321**, 385-388.

(6) F. Schwierz, *Nat. Nanotechnol.*, 2010, **5**, 487.

(7) J.-H. Chen, C. Jang, S. Xiao, M. Ishigami and M. S. Fuhrer, *Nat. Nanotechnol.*, 2008, **3**, 206.

(8) Y. Zhang, J. P. Small, W. V. Pontius and P. Kim, *Appl. Phys. Lett.*, 2005, **86**, 073104.

(9) K. S. Novoselov, A. K. Geim, S. V. Morozov, D. Jiang, Y. Zhang, S. V. Dubonos, I. V. Grigorieva and A. A. Firsov, *Science*, 2004, **306**, 666-669.

(10) I. Jung, D. A. Dikin, R. D. Piner and R. S. Ruoff, *Nano Lett.*, 2008, **8**, 4283-4287.

(11) H. C. Schniepp, J.-L. Li, M. J. McAllister, H. Sai, M. Herrera-Alonso, D. H. Adamson, R. K. Prud'homme, R. Car, D. A. Saville and I. A. Aksay, *J. Phys. Chem. B*, 2006, **110**, 8535-8539.

(12) U. Khan, A. O'Neill, M. Lotya, S. De and J. N. Coleman, *Small*, 2010, **6**, 864-871.

(13) J. Lu, J.-x. Yang, J. Wang, A. Lim, S. Wang and K. P. Loh, *ACS Nano*, 2009, **3**, 2367-2375.

(14) M. J. Earle and K. R. Seddon, *Pure Appl. Chem.*, 2000, **72**, 1391-1398.

(15) S. Ravula, S. N. Baker, G. Kamath and G. A. Baker, *Nanoscale*, 2015, **7**, 4338-4353.

(16) M. Matsumoto, Y. Saito, C. Park, T. Fukushima and T. Aida, *Nat. Chem.*, 2015, **7**, 730-736.

(17) Y. Zhu, S. Murali, M. D. Stoller, A. Velamakanni, R. D. Piner and R. S. Ruoff, *Carbon*, 2010, **48**, 2118-2122.

(18) X. Liu, J. Liu, D. Zhan, J. Yan, J. Wang, D. Chao, L. Lai, M. Chen, J. Yin and Z. Shen, *RSC Adv.*, 2013, **3**, 11601-11606.

(19) X. Li, X. Wang, L. Zhang, S. Lee and H. Dai, *Science*, 2008, **319**, 1229-1232.

(20) A. Reina, X. Jia, J. Ho, D. Nezich, H. Son, V. Bulovic, M. S. Dresselhaus and J. J. N. l. Kong, 2008, **9**, 30-35.

(21) X. Li, C. W. Magnuson, A. Venugopal, R. M. Tromp, J. B. Hannon, E. M. Vogel, L. Colombo and R. S. Ruoff, *J. Am. Chem. Soc.*, 2011, **133**, 2816-2819.

(22) P. W. Sutter, J.-I. Flege and E. A. Sutter, *Nat. Mater.*, 2008, **7**, 406.

(23) C. Berger, Z. Song, X. Li, X. Wu, N. Brown, C. Naud, D. Mayou, T. Li, J. Hass and A. N. Marchenkov, *Science*, 2006, **312**, 1191-1196.

(24) C. Zhou, J. Kong, E. Yenilmez and H. Dai, *Science*, 2000, **290**, 1552-1555.

(25) A. Kasry, M. A. Kuroda, G. J. Martyna, G. S. Tulevski and A. A. Bol, *ACS Nano*, 2010, **4**, 3839-3844.

(26) D. Wei, Y. Liu, Y. Wang, H. Zhang, L. Huang and G. Yu, *Nano Lett.*, 2009, **9**, 1752-1758.

(27) D. Deng, X. Pan, L. Yu, Y. Cui, Y. Jiang, J. Qi, W.-X. Li, Q. Fu, X. Ma and Q. Xue, *Chem. Mater.*, 2011, **23**, 1188-1193.

(28) Y. Wang, Y. Shao, D. W. Matson, J. Li and Y. Lin, *ACS Nano*, 2010, **4**, 1790-1798.

(29) S. Zhou, D. Siegel, A. Fedorov and A. Lanzara, *Phys. Rev. Lett.*, 2008, **101**, 086402.

(30) W. Chen, S. Chen, D. C. Qi, X. Y. Gao and A. T. S. Wee, *J. Am. Chem. Soc.*, 2007, **129**, 10418-10422.

(31) G.-L. Chai, Z. Hou, D.-J. Shu, T. Ikeda and K. Terakura, *J. Am. Chem. Soc.*, 2014, **136**, 13629-13640.

(32) H. Kim, K. Lee, S. I. Woo and Y. Jung, *Phys. Chem. Chem. Phys.*, 2011, **13**, 17505-17510.

(33) B. Kumar, M. Asadi, D. Pisasale, S. Sinha-Ray, B. A. Rosen, R. Haasch, J. Abiade, A. L. Yarin and A. Salehi-Khojin, *Nat. Commun.*, 2013, **4**, 2819.

(34) J. Wu, S. Ma, J. Sun, J. I. Gold, C. Tiwary, B. Kim, L. Zhu, N. Chopra, I. N. Odeh and R. Vajtai, *Nat. Commun.*, 2016, **7**, 13869.

(35) J. Zhang, L. Qu, G. Shi, J. Liu, J. Chen and L. Dai, *Angew. Chem. Int. Ed.*, 2016, **55**, 2230-2234.

(36) N. Mahmood, C. Zhang, H. Yin and Y. Hou, *J. Mater. Chem. A*, 2014, **2**, 15-32.

(37) T. Kondo, S. Casolo, T. Suzuki, T. Shikano, M. Sakurai, Y. Harada, M. Saito, M. Oshima, M. I. Trioni and G. F. Tantardini, *Phys. Rev. B*, 2012, **86**, 035436.

(38) D. Zhou, Y. Cui, P.-W. Xiao, M.-Y. Jiang and B.-H. Han, *Nat. Commun.*, 2014, **5**, 4716.

(39) R. Arrigo, M. Hävecker, S. Wrabetz, R. Blume, M. Lerch, J. McGregor, E. P. Parrott, J. A. Zeitler, L. F. Gladden and A. Knop-Gericke, *J. Am. Chem. Soc.*, 2010, **132**, 9616-9630.

(40) R. Arrigo, M. Hävecker, R. Schlögl and D. S. Su, *Chem. Commun.*, 2008, **0**, 4891-4893.

(41) W. Ding, Z. Wei, S. Chen, X. Qi, T. Yang, J. Hu, D. Wang, L. J. Wan, S. F. Alvi and L. Li, *Angew. Chem.*, 2013, **125**, 11971-11975.

(42) X. Y. Chen, C. Chen, Z. J. Zhang, D. H. Xie, X. Deng and J. W. Liu, *J. Power Sources*, 2013, **230**, 50-58.

(43) B.-X. Zou, Y. Liang, X.-X. Liu, D. Diamond and K.-T. Lau, *J. Power Sources*, 2011, **196**, 4842-4848.

(44) E. Kang, K. Neoh and K. Tan, *Polym. J.*, 1989, **21**, 873.

(45) K. Xu, Y. Fu, Y. Zhou, F. Hennersdorf, P. Machata, I. Vincon, J. J. Weigand, A. A. Popov, R. Berger and X. Feng, *Angew. Chem. Int. Ed.*, 2017, **56**, 15876-15881.

(46) A. K. Geim and K. S. Novoselov, *Nat. Mater.*, 2007, **6**, 183-191.

(47) Y. Hernandez, V. Nicolosi, M. Lotya, F. M. Blighe, Z. Sun, S. De, I. McGovern, B. Holland, M. Byrne and Y. K. Gun'Ko, *Nat. Nanotechnol.*, 2008, **3**, 563-568.

(48) I. Janowska, K. Chizari, O. Ersen, S. Zafeiratos, D. Soubane, V. Da Costa, V. Speisser, C. Boeglin, M. Houllé and D. Bégin, *Nano Res.*, 2010, **3**, 126-137.

(49) K. R. Paton, E. Varrla, C. Backes, R. J. Smith, U. Khan, A. O'Neill, C. Boland, M. Lotya, O. M. Istrate and P. King, *Nat. Mater.*, 2014, **13**, 624-630.

(50) A. A. Green and M. C. Hersam, *Nano Lett.*, 2009, **9**, 4031-4036.

(51) M. Lotya, Y. Hernandez, P. J. King, R. J. Smith, V. Nicolosi, L. S. Karlsson, F. M. Blighe, S. De, Z. Wang and I. McGovern, *J. Am. Chem. Soc.*, 2009, **131**, 3611-3620.

(52) H. Lee, M. A. Bratescu, T. Ueno and N. Saito, *RSC Adv.*, 2014, **4**, 51758-51765.

(53) T. Morishita, T. Ueno, G. Panomsuwan, J. Hieda, A. Yoshida, M. A. Bratescu and N. Saito, *Sci. Rep.*, 2016, **6**, 36880.

(54) K. Hyun, T. Ueno, O. L. Li and N. Saito, *RSC Adv.*, 2016, **6**, 6990-6996.

(55) K. Hyun and N. Saito, *Sci. Rep.*, 2017, **7**, 3825.

Chapter 2

Synthesis of Few-Layer Graphene by Peeling Graphite Flakes via Electron Exchange in Solution Plasma

Chapter 2 - Synthesis of Few-Layer Graphene by Peeling Graphite Flakes via Electron Exchange in Solution Plasma

2.1. Introduction

Graphene is an attractive two-dimensional carbon material because of its excellent electrical, thermal, mechanical, and optical properties.[1] It has extensively been used in solar cells, energy storage assembly, fuel cells, capacitors, and electronic and sensing devices.[2-7] However, graphene in real systems does not retain the above-mentioned excellent properties because of the surrounding materials, such as the substrate or electrode.

Few-layer graphene is expected to be a more attractive material as the electrical conductivity of graphene is marginally retained in few-layer graphene, although the thermal conductivity drastically decreases. Thus, previous studies have indicated that the electronic band dispersion near the Fermi level in few-layer graphene does not strongly depend on the number of layers and stacking geometry.[8,9] On the other hand, the thermal conductivity of few-layer graphene decreases with the increase in the layer number of graphene, i.e., from two to four layers. Hence, few-layer graphene is expected to be used in ultrafast transistor electrodes and transparent electrodes with heat-shielding function.[10] For these, few-layer graphene has a potential of sensible material which outperforms graphene properties in the material system. Moreover, the functional groups in few-layer graphene provide additional possibilities to tune the properties[11] and improve the dispersion in solutions and the anti-oxidation characteristic.[12,13]

Several methods for fabricating graphene from graphite have been reported. To do this, the peeling force must be greater than the van der Waals attractive force between the layers. Thus, certain forms of energy, including heat, ultrasonication (US), torque in centrifugation, supply graphite in an organic solvent, a solution with ionic liquid (IL), or a surfactant.14 These

methods can be categorized into three strategies. The first strategy involves cleavage by a mechanically induced shear force. Graphene has frequently been peeled using an adhesive tape or ball milling by this method.[15,16] However, this approach is limited by low production throughput. The second strategy concerns in an increase of the steric hindrance via the introduction of oxidized functional groups such as hydroxyl groups into graphite using chemical, mechanochemical, and physical treatment.[17,18] However, a disordered structure is obtained because graphene bearing the oxidized functional groups must be reduced again using reducing agents. The third strategy involves chemical weakening of the van der Waals attraction force using a solution and a solute. This method means the chemical peeling of graphite in solutions with specific surface energy which is suitable to fabricate graphene.[19-21] Recent studies based on the third strategy have realized high-yield, high-purity graphene. However, this method is only appropriate for the fabrication of graphene, not few-layer graphene.

Solution plasma (SP) represents a non-equilibrium discharge in the gas originating from the solution surrounding plasma. The SP process using tungsten electrodes in an organic solution permits the fabrication of nanocarbon materials via CH activation.[22] During this procedure, the transfer of electrons between SP and the solution plays a key role in the synthesis of nanocarbon materials. Another SP process with carbon electrodes in an aqueous solution permits the easy fabrication of multilayer-stacked graphene and hetero-graphene via the exfoliation process of electrodes. The principal mechanism in this experiment was the collisions of the energetic ions produced in SP with the graphite electrodes. During the electrode exfoliation, the number of graphene layers was difficult to control, and the throughput was small.[23]

In this study, a new strategy for cationic nitrogen-containing functional groups functionalized few-layer graphene (f-FLG) with synthesis from graphite was proposed. First, an IL, 1-ethyl-3-methylimidazolium dicyanamide (EMIM-DCA), and graphite flakes were mixed with water and processed by SP where an exchange of electrons between SP and graphite flakes takes place. The fabrication process can realize a high-throughput of f-FLG. The results indicated that SP serves as an effective field for the exchange of electrons between plasma and graphite

flakes via the IL, affording a considerable amount of f-FLG. The peeling mechanism was explained using a potential and kinetic energy diagram comprising electron excitation temperature (T_e), density of states (DOS) for bulk graphite and its subsurface, and ionization potential (I_P) and electron affinity (E_A) of EMIM-DCA in water, which were estimated by ab initio molecular orbital (MO) calculations, cyclic voltammetry (CV), optical emission spectroscopy (OES), and past study results based on band calculations.[22]

2.2. Experimental procedures

2.2.1 *Solution preparation and peeling process.*

Figure 2.1 shows the experimental procedure. First, as-received graphite flakes were added to an aqueous solution containing IL. Second, the graphite flakes were treated by SP or US, followed by filtration of the solutions and drying the products. Finally, the obtained samples were dispersed in *N*,*N*-dimethylformamide (DMF), and f-FLG was separated from the supernatant solution by centrifugation. f-FLG was characterized by X-ray diffraction (XRD), transmission electron microscopy (TEM) combined with selected-area electron diffraction (SAED), field emission scanning electron microscopy (FE-SEM), Raman spectroscopy, and Fourier transform infrared (FTIR) spectroscopy. Detailed conditions for material preparation and evaluation are described in the following sections.

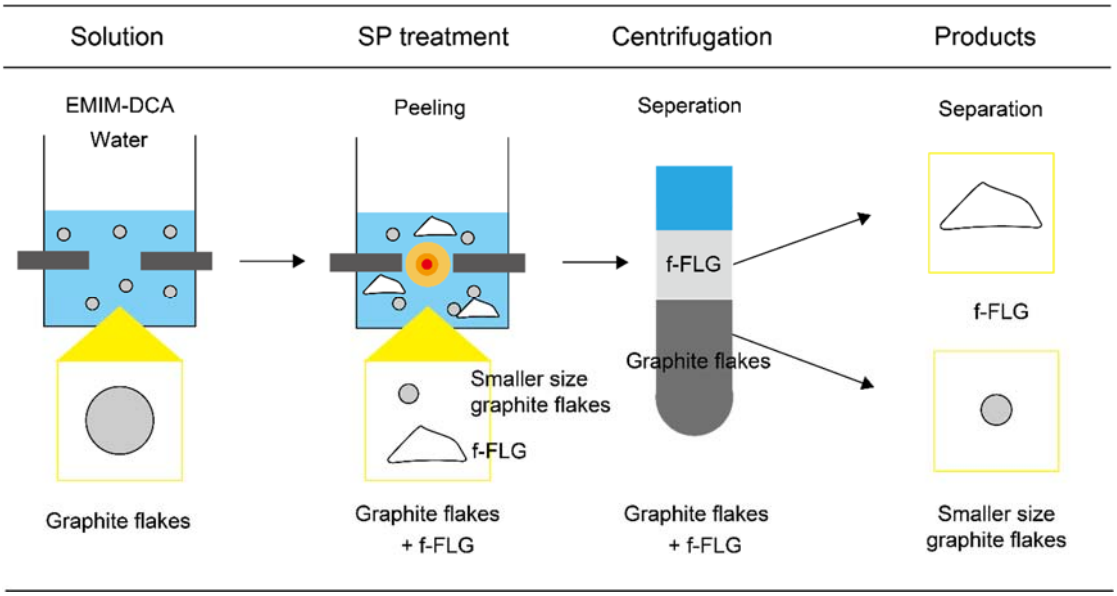

Figure 2.1. Experimental procedures of fabricating f-FLG from graphite flakes in an aqueous solution containing IL by SP.

EMIM-DCA (98.0% purity, Sigma-Aldrich) was used as the IL. Distilled water with an electrical conductivity of 0.055 μS cm^{-1} was obtained from a distillation apparatus (Aquarius RFD250NB, Advantec). The concentration of EMIM-DCA in water was adjusted to 10 wt%. A 50 mL aqueous solution of EMIM-DCA containing 200 mg of graphite (synthetic graphite flakes with a smaller diameter than 20 μm purchased from Sigma-Aldrich) was prepared. The final conductivity of the solution was 3.25 mS cm^{-1}.

Figure 2.2a shows the schematic of an SP reactor system. Tungsten electrodes (99.9% purity, Nilaco) with a diameter of 1 mm were shielded using an insulating ceramic tube and placed in the solution within a glass vessel. The electrode gap distance was adjusted at 1.0 ± 0.1 mm. A bipolar pulsed power supply (MPP-HV04, KURITA Seisakusho) was used to generate the SP. The voltage applied between the electrodes was about 1 kV at a repetition frequency of 100 kHz and a pulse width of 1.0 μs. **Figure 2.2b** shows the voltage and current waveforms generated between the electrodes during the SP in the solution used for f-FLG synthesis. The current and voltage waveforms were recorded using a high-voltage probe (P6015A, Tektronix) and a current probe (model 6595, Pearson Electronics), respectively, on an oscilloscope (DS1202CA, RIGOL).

A US bath (US-102, SND Co., Ltd.) operated at an oscillation frequency of 38 kHz and a power of 0.1 kW was also utilized as a source of energy to peel graphite flakes in a 10 wt% EMIM-DCA aqueous solution containing 200 mg graphite flakes. The products obtained by SP- and US-graphite flakes treated in EMIM-DCA aqueous solutions were analyzed and compared.

The processing time for all experiments was maintained at 30 min. The excess of EMIM-DCA was separated from the SP- and US-treated solutions by filtration using a polytetrafluoroethylene membrane with an average pore size of 0.1 μm (JVWP04700, Merck Millipore). Furthermore, the filter-trapped graphite flakes and f-FLG product were rinsed with distilled water and dried in an oven at 85 °C for 12 h. The dried product (50 mg) was dispersed in 50 mL DMF after a sonication treatment during one hour. The concentration of

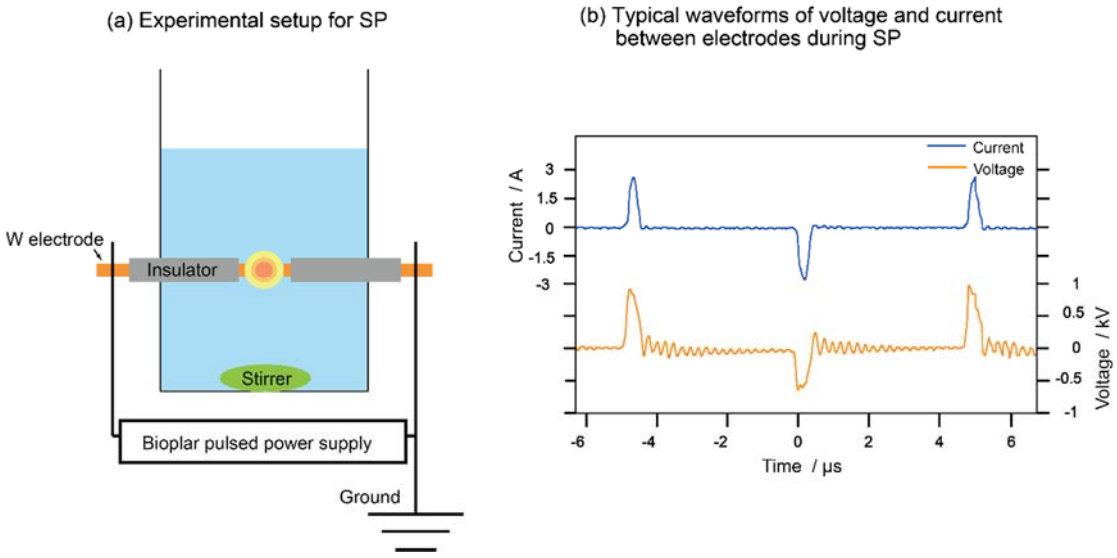

Figure 2.2. Solution plasma setup for the synthesis of f-FLG: (a) SP reactor system and (b) waveforms of voltage and current between electrodes. The maximum peak voltage applied between the electrodes was about 1 kV at a repetition frequency of 100 kHz and a pulse width of 1.0 μs. The corresponding maximum current was about 2.8 A.

Table 2.1. Total energies, I_P, and E_A of molecules in water at pH 7.

Adiabatic Transition

	Net Charges	Multiplicity	T_e (eV)	I_P (eV)	E_A (eV)
	+2	Doublet	−7942.882711		
EMIM	+1	Singlet	−7949.380194	6.50	0.61
	0	Doublet	−7949.990780		
	−2	Doublet	−5550.648986		
DCA	−1	Singlet	−5549.795614	5.28	0.85
	0	Doublet	−5544.514817		
	+3	Doublet	−15900.34054		
EMIM dimer	+2	Triplet	−15896.43032	4.88 (4.47)*	3.91 (3.49)*
	+1	Doublet	−15891.54700		

T_e: total energy; I_P: first ionization energy; E_A: electron affinity.

*; The values were estimated at pH 7.

the dispersed material in water was same as that in DMF, i.e., 1 mg/mL. Only the f-FLG was extracted in 50% proportion from the supernatant solution by centrifugation at 4000 rpm for 30 min.

2.2.2 *Characterization*

XRD (SmartLab, Rigaku) measurements were carried out using Cu Kα X-ray source (with a wavelength of 0.154 nm filtered by a Ni foil) to examine the stacked structure of graphite flakes, treated graphite flakes, and f-FLG. The XRD system was operated at 45 kV and 200 mA. For data acquisition, the 2θ angle was changed from 10° to 90° with a scan speed of 3° min^{-1} and a step size of 0.02°. High-purity semiconductor-grade silicon (eleven 9s, TOKUYAMA) was used as an internal standard for the correlation of the 2θ angle in XRD. The standard deviation was calculated using five different measurements.

X-ray photoelectron spectroscopy (XPS) (PHI 5000 VersaProbe II, ULVAC-PHI) measurements were carried out using a Mg Kα X-ray source with an energy of 1253.6 eV. Survey-scan XPS spectra were recorded from 0 to 1100 eV at a pass energy of 47 eV and an acquisition step of 0.5 eV. Narrow-scan spectra for the analysis of C 1s, N 1s, and O 1s were recorded at a pass energy of 12 eV and an acquisition step of 0.1 eV. The compensation of the charge-up was performed using a neutralization gun.

FTIR (Nicolet 8700, Thermo Fisher Scientific) spectra were recorded by the KBr method. KBr pellets were prepared by mixing the sample with KBr (sample : KBr weight ratio ≅ 1 : 200). The spectrum was collected by averaging 64 scans, with a resolution of 4 cm^{-1}, in the wavenumber range from 1000 to 4000 cm^{-1}.

TEM (JEM-2500SE, JEOL, with an accelerating voltage of 200 kV) and SAED (same acceleration voltage and a camera length of 300 cm) analyses were performed to observe the as-received graphite flakes and the f-FLG obtained from the supernatant after centrifugation. FE-SEM images were recorded on an S-4800 instrument (HITACHI High-Technologies) at an accelerating voltage of 10 kV, a probe current of 5 μA, and a working distance of 9.6 mm.

Raman spectroscopy (NRS-100, JASCO, with a laser excitation wavelength of 532.5 nm) was utilized to estimate the number of layers. The sample was prepared by casting a few drops of the supernatant on Si (100) wafer and drying it. The Raman microscope used a high magnification objective lens of 100X. The spectra were recorded in the wavenumber range of 1000–3000 cm^{-1} by averaging five acquisitions at an exposure time of 10 s at ambient temperature. Plasma OES has been collected with a spectrometer (USB4000, Ocean Optics) in the wavelength range of 280–900 nm.

To examine the EMIM-DCA electrochemical window at pH 7, the I_P and E_A of EMIM-DCA in water were estimated on the basis of the adiabatic transition by ab initio MO calculations with UB3LYP / 6-311++g (2d, p), including the solvent effect, in a self-consistent reaction field polarizable continuum model (SCRF / PCM). All calculations were carried out using the Gaussian 09 program code.[24] I_P and E_A were calculated by equations 1 and 2, respectively:[25,26]

$$I_P = E(A^+) - E(A) \quad (1)$$

$$E_A = E(A^-) - E(A) \quad (2)$$

where $E(A^+)$, $E(A^-)$, and $E(A)$ represent the energies of the cation, anion, and neutral state of molecule A, respectively. **Table 2.1** summarizes the total energies, I_P, and E_A of molecules in water at pH 7. Moreover, the electrochemical window from ab initio MO calculations was validated by CV measurements performed in two different solutions: an aqueous solution containing 0.5 M Na_2SO_4 and 10 wt% EMIM-DCA. The electrochemical cell with three electrodes (a Pt working electrode, a Pt wire as a counter electrode, and an Ag / AgCl electrode used as the reference) was connected to a potentiostat with a function generator (HZ5000, Hokuto Denko) to carry out the CV measurements.

2.3. Results and discussion

Figure 2.3a shows the XRD patterns of the SP- and US-treated EMIM-DCA aqueous solution, SP- and US-treated distilled water, and as-received graphite flakes. The peaks observed at $2\theta = 26.46°$ corresponding to the 002 diffraction was related to the layer-by-layer graphite structures. No peak shifts were detected in all cases, indicating that the distance between the layers does not change and that intercalation and expansion do not occur. The ratios ($I_{26.46}$ / $I_{28.42}$) between the peak intensities at 26.46° (graphite 002) and 28.42° (silicon 111) corresponded to the crystallite size along the c-axis (L_c) (as explained in **Figure 2.4**) and was related to the number of layers. The $I_{26.46}$ / $I_{28.42}$ ratio was normalized to the ratio of the as-received graphite flakes to silicon. **Figure 2.3b** shows the $I_{26.46}$ / $I_{28.42}$ ratios of the SP- and US-treated EMIM-DCA aqueous solution, SP- and US-treated distilled water, and as-received graphite flakes. After the treatment of graphite flakes in distilled water using SP and US, the $I_{26.46}$ / $I_{28.42}$ ratios slightly decreased to 0.85−0.9. For the US-treated EMIM-DCA aqueous solution, the $I_{26.46}$ / $I_{28.42}$ ratio decreased to about 0.80. Furthermore, the ratio for the SP-treated EMIM-DCA aqueous solution notably decreased to 0.34 compared with that observed for the as-received graphite flakes. The decreased $I_{26.46}$ / $I_{28.42}$ ratio implied a reduction in the crystallite size L_c of the layered graphite structure and can be related to the peeling of graphite.[21,27] Hence, the SP-treated EMIM-DCA aqueous solution can enhance the peeling of graphite flakes. L_c was evaluated from Scherrer's equation which provides the average crystallite size perpendicular to the layered graphite structure. **Figure 2.3b** shows L_c for all samples. The L_c of SP-treated EMIM-DCA was 26 ± 1 nm which is a smaller value than that of the as-received graphite flakes, i.e., 39 ± 1 nm. The decrease in the average crystallite size was related to the peeling of graphite and the f-FLG formation.

To confirm the f-FLG synthesis, the XRD pattern of a low-molecular-weight product extracted from SP-treated EMIM-DCA is shown in **Figure 2.5**. The 002 diffraction peak indicated an interlayer spacing of 0.340 nm ($2\theta = 26.20 \pm 0.2°$) and L_c of 5 ± 0.25 nm from peak broadening demonstrating that the obtained f-FLG comprises less than approximative15

layers. This value was overestimated because the XRD powder sample led to an increase in the apparent number of layers.

Figure 2.6a shows the Raman spectra of the graphite flakes, the US-treated EMIM-DCA aqueous solution, and the SP-treated EMIM-DCA aqueous solution. Three main bands were observed at 1300–1350 cm^{-1} (D band), 1580–1620 cm^{-1} (G band), and 2680–2700 cm^{-1} (2D band).[28] The D band (1340 cm^{-1}) corresponds to the edges and defects of the graphite structure.[29] The estimated in-plane crystallite size (L_a) values for the graphite flakes and products were low. In fact, the sizes of the graphite flakes and the obtained products derived from the Raman spectra[30] of the samples ranged from 60 to 100 nm. The 2D band depends on electron-phonon coupling, indicating that the position and the full width of half maximum (FWHM) are related to the number of layers. The 2D band of the f-FLG product extracted from the SP-treated EMIM-DCA aqueous solution was stronger than that of the US-treated EMIM-DCA aqueous solution and graphite flakes. The result indicated that the number of layers of the product obtained from the SP-treated EMIM-DCA aqueous solution is less than those in the graphite flakes and US-treated EMIM-DCA aqueous solution. The I_{2D} / I_G intensity ratios of the graphite flakes, US-treated EMIM-DCA aqueous solution, and SP-treated EMIM-DCA aqueous solution were 0.41, 0.52, and 0.84, respectively, as shown in **Figure 2.6a**. From these I_{2D} / I_G ratios, the approximate number of graphene layers in the sample can be estimated.[31,32] Thus, for the SP-treated EMIM-DCA aqueous solution, the I_{2D} / I_G ratio is 0.84, with a calculated FWHM of 62 cm^{-1}, indicating that f-FLG comprises three layers (**Figure 2.6b**).[31,32] The 2D band of the SP-treated EMIM-DCA aqueous solution was higher than 2D bands of US-treated EMIM-DCA aqueous solution and graphite flakes and shifted to lower Raman frequency, which means negative charge impurities on the synthesized f-FLG which might be due to the CN groups attached to the edges of graphene.[33]

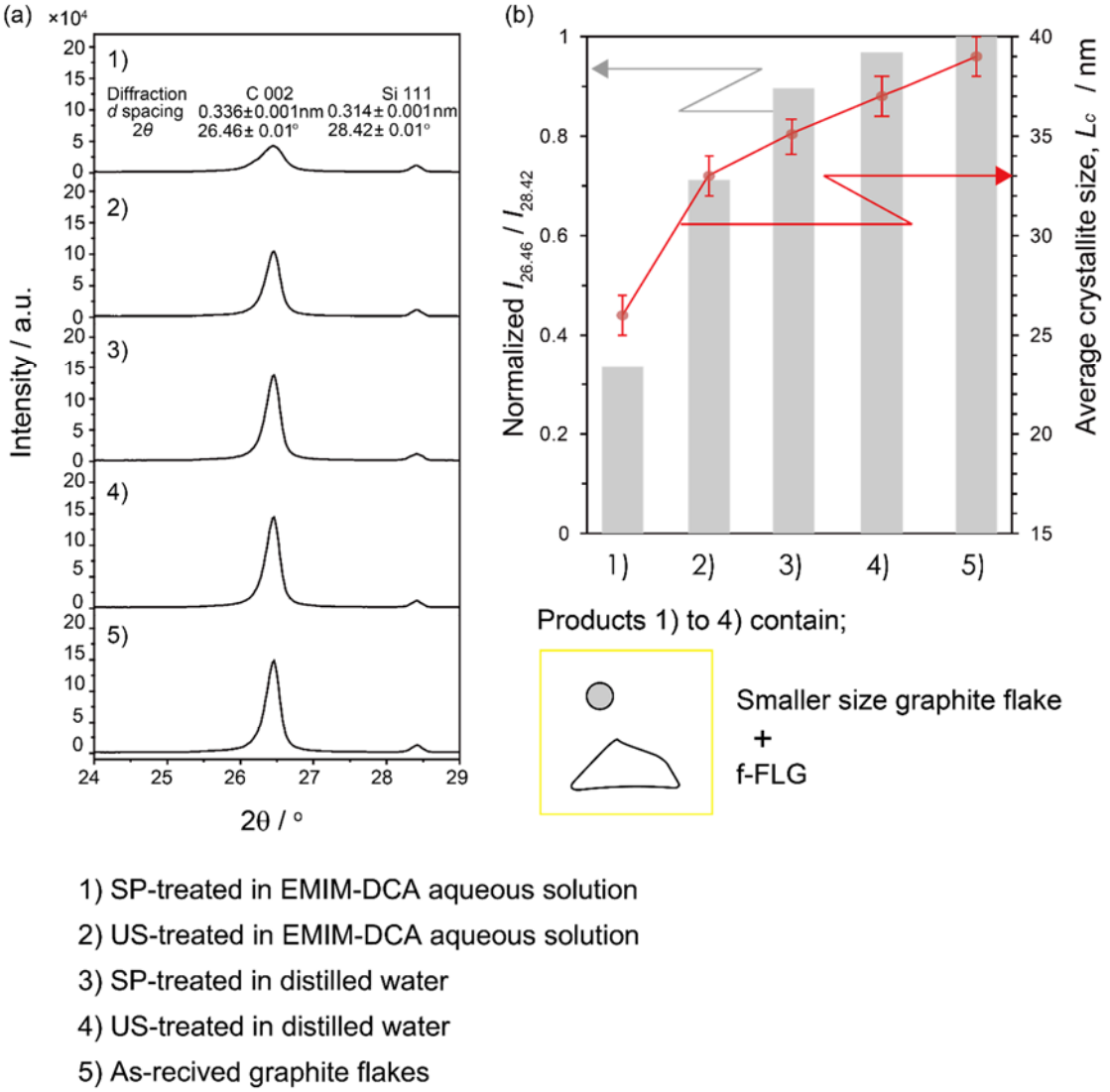

Figure 2.3. (a) XRD patterns of as-received graphite flakes 5) and treated products 1) to 4) without centrifugation and (b) ratio between $I_{26.46}$ (graphite 002) and $I_{28.42}$ (silicon 111) normalized to the silicon peak area (left side of Y axis) and the average crystallite size along the c-axis (right side of Y axis). All samples were mixed with silicon powder as a reference element.

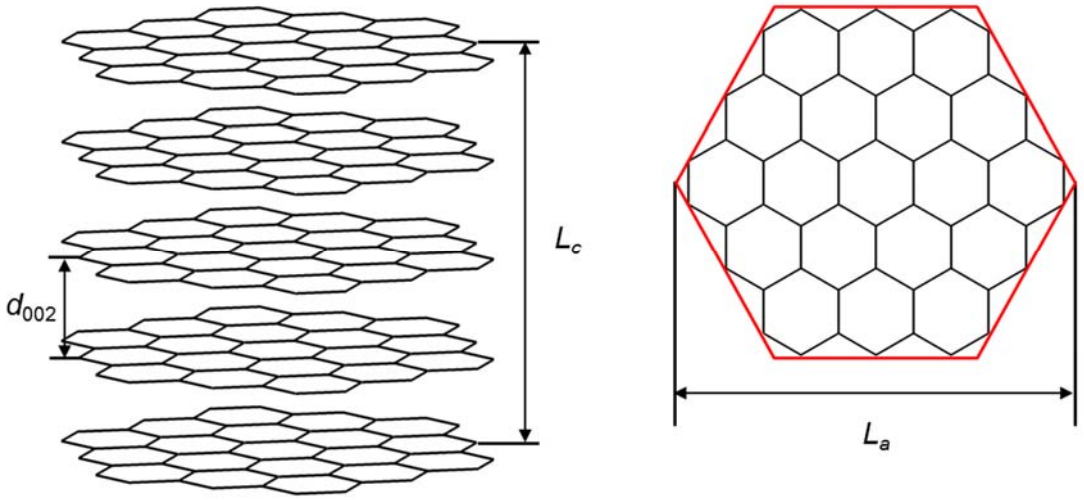

Figure 2.4. The average crystallite size along c-axis (L_c) and the crystallite size along the basal plane (L_a)

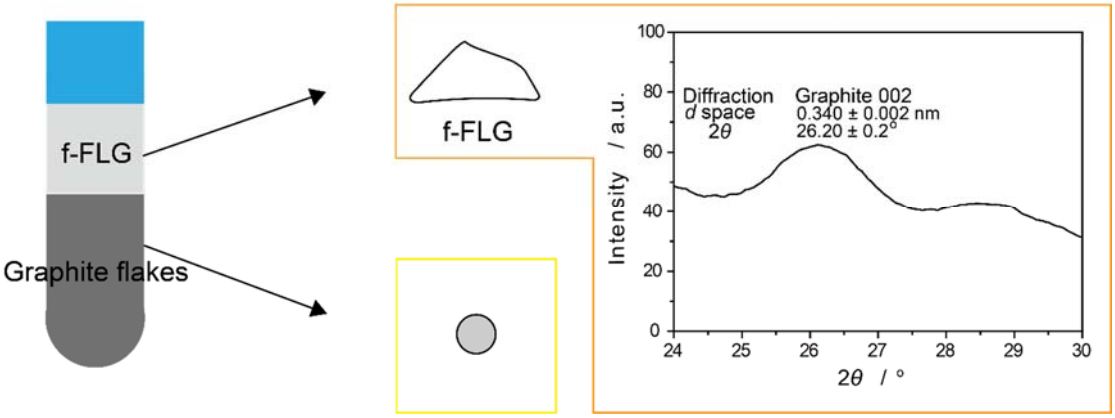

Figure 2.5. XRD pattern and *d* spacing calculated from the 002 diffraction peak for the product extracted by centrifugation from the SP-treated EMIM-DCA aqueous solution on Si (100) wafer.

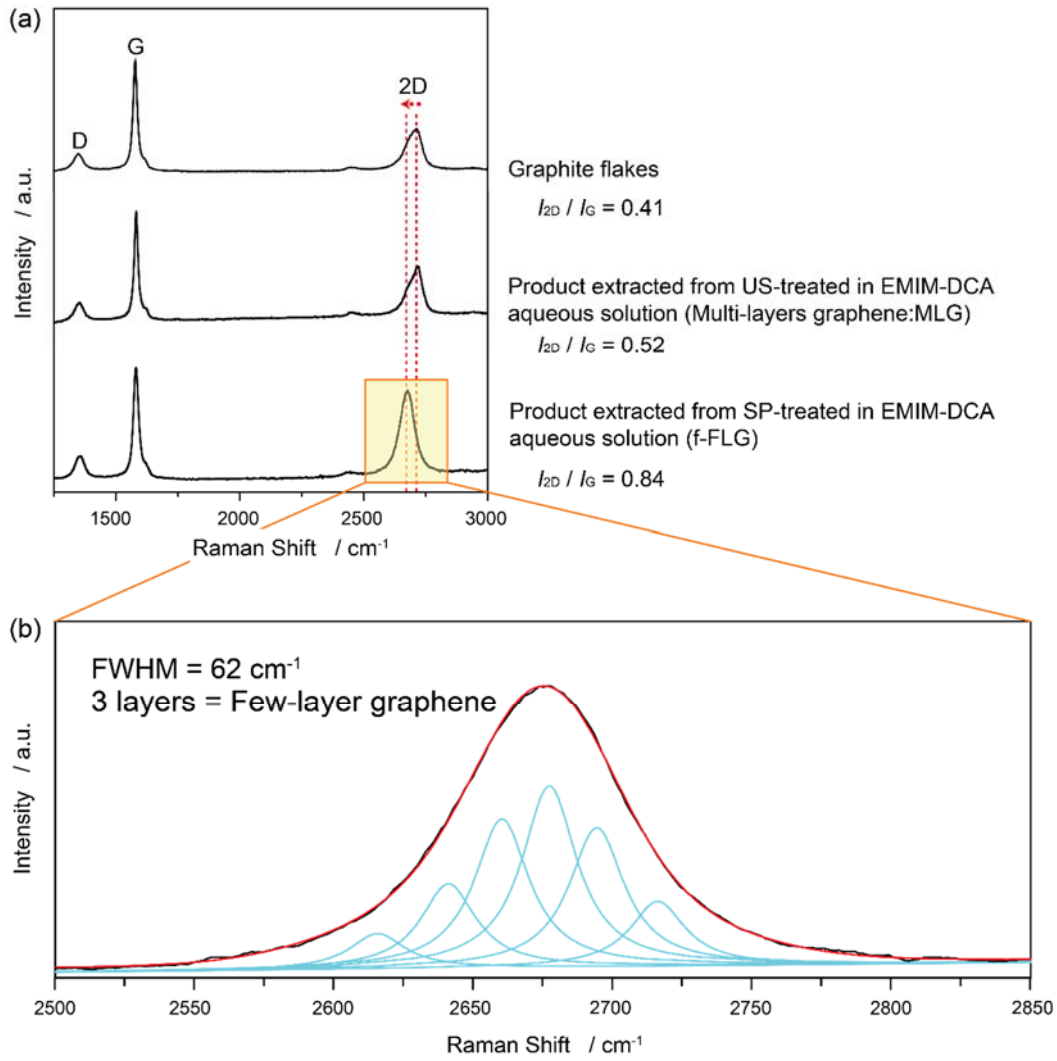

Figure 2.6. Raman spectra of (a) as-received graphite flakes, products extracted from SP-, US-treated EMIM-DCA aqueous solution (f-FLG and MLG), and the corresponding I_{2D} / I_G ratios; and (b) FWHM of f-FLG sample fitted with six Lorentzians corresponding to three graphene layers.

Figure 2.7a–2.7d shows the TEM and SAED images of (a) graphite flakes, (b) the f-FLG products extracted from the US-treated EMIM-DCA aqueous solution, and (c), (d) the f-FLG products extracted from the SP-treated EMIM-DCA aqueous solution. The TEM image shown in **Figure 2.7a** was dark compared with those of the other samples because of the largest sample thickness. The corresponding SAED pattern showed spots of polycrystalline and turbostratic graphite crystallized in $P6_3$ / *mmc* space group. The TEM image in **Figure 2.7b** was bright compared with that of the graphite flakes, indicating that the US-treated EMIM-DCA aqueous solution facilitates the peeling of graphite flakes and the formation of the MLG. Also, the corresponding SAED pattern showed spots of polycrystalline and turbostratic graphite. A similar SAED pattern was observed for the as-received graphite flakes. On the contrary, the TEM images of f-FLG from **Figure 2.7c** and **2.7d** showed a significantly increased brightness compared with those of the as-received graphite flakes and the US-treated EMIM-DCA. Moreover, the honeycomb structures of graphene were easily identified in the high-resolution TEM images. The SAED patterns along the [001] zone axis also showed spots of single-crystalline f-FLG on three circles: six spots with a sixfold axis on an inner circle, corresponding to the {100} plane of graphene, six spots on an intermediate circle, corresponding to the {110} plane, and six spots on an outer circle, corresponding to the {200} plane. The diffraction intensity of 100, I_{100}, was approximately the same as I_{110}, indicating the monolayer graphene (**Figure 2.7c**). In **Figure 2.7d**, the SAED image showed six spots and six rotated spots on an inner circle, and six spots and six rotated spots on an intermediate circle. This rotation indicated that the geometry of layers was disordered. The intensity of the spots on the outer circle, I_{110}, was around two times stronger than that of the spots on the inner circle, I_{100}, indicating that the number of layers is more than two.[34] Moreover, the third circle was not observed under the same SAED operation conditions, implying that the number of layers was greater than that shown in **Figure 2.7c**. These results indicated that the obtained product mainly comprises f-FLG, although graphene structure was also observed.

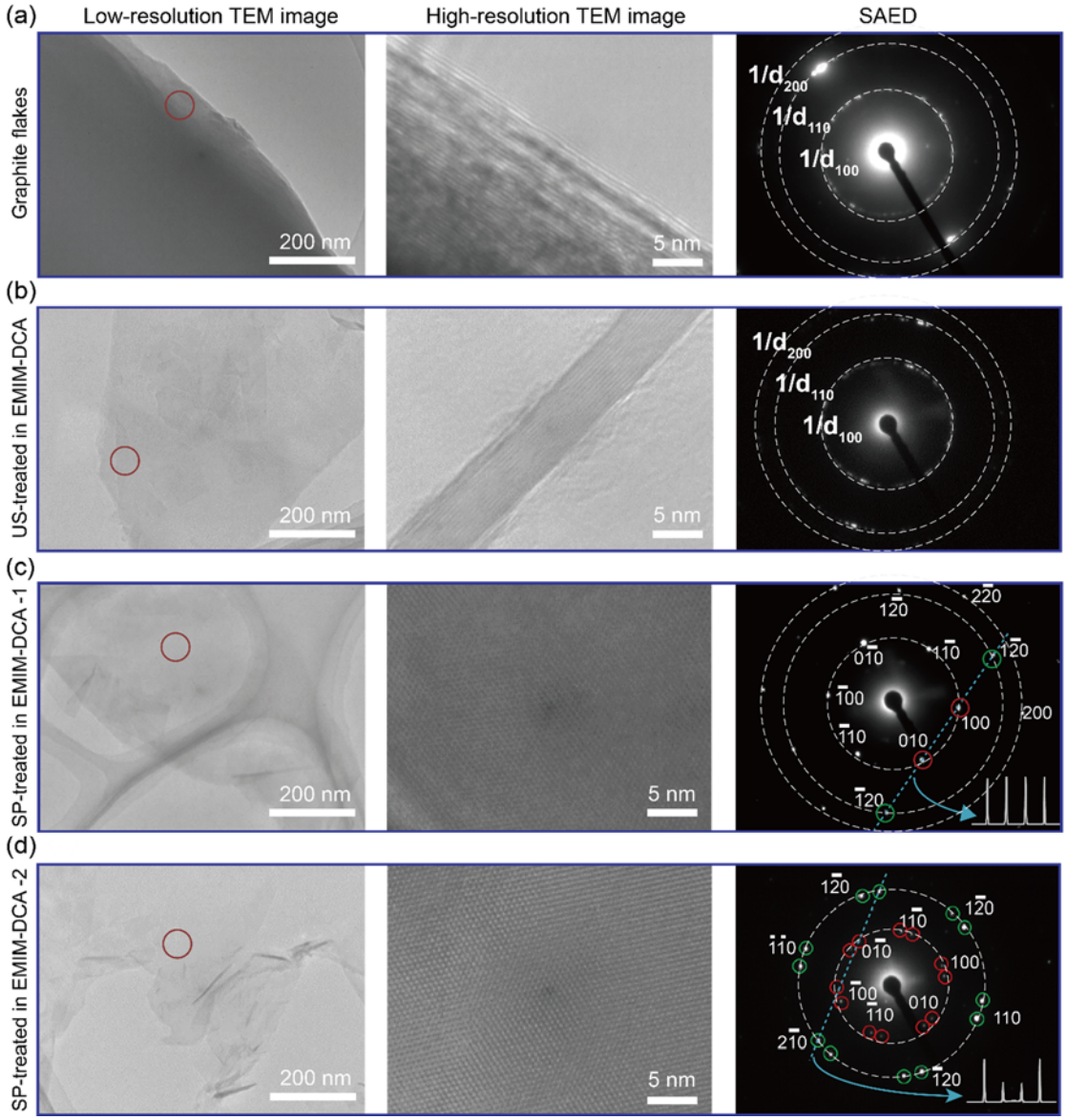

Figure 2.7. TEM images and SAED patterns of (a) as-received graphite flakes, (b) US-treated EMIM-DCA aqueous solution, (c) sample 1 of the SP-treated EMIM-DCA aqueous solution, and (d) sample 2 of the SP-treated EMIM-DCA aqueous solution. The SAED pattern corresponds to the marked circle area of the low-resolution images of (a), (b), (c), and (d). In the SAED pattern, the inset shows the intensity profile plots along the dotted line.

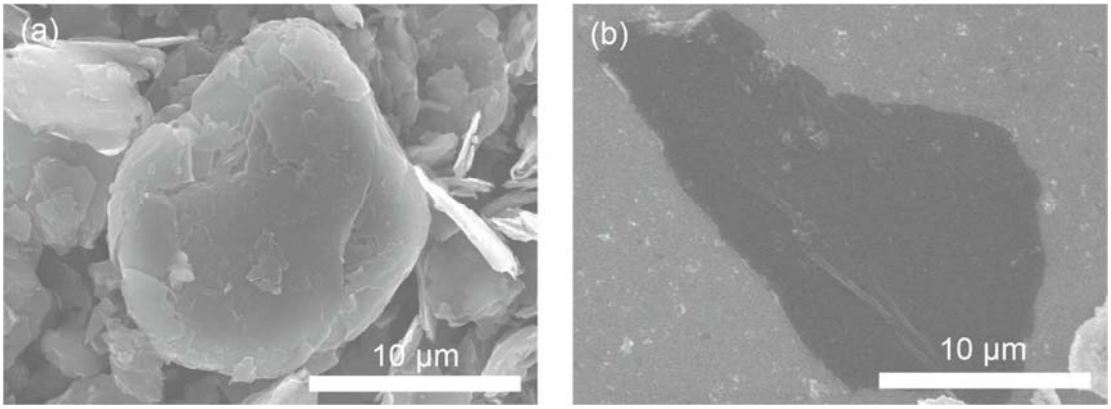

Figure 2.8. SEM images of (a) as-received graphite flakes and (b) f-FLG; the average size of f-FLG was approximately 20 μm.

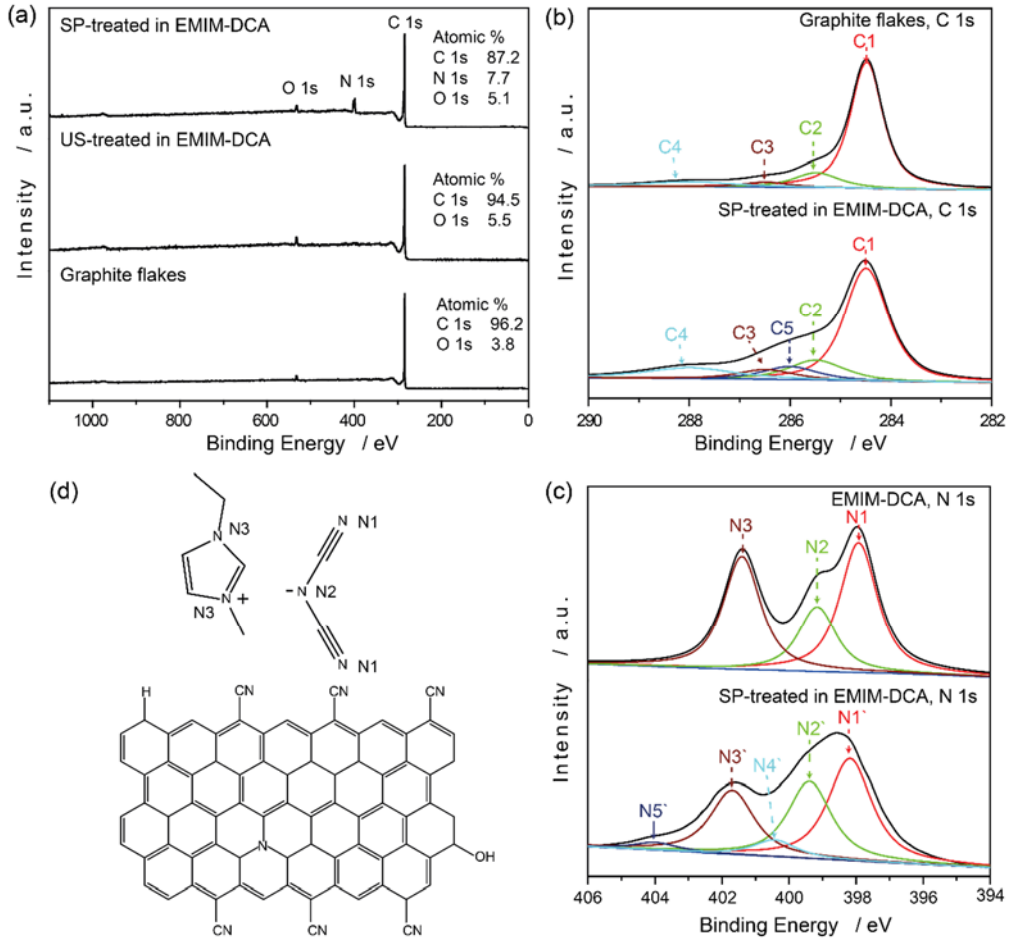

Figure 2.9. XPS spectra of SP-treated in EMIM-DCA, US-treated in EMIM-DCA and as-received graphite flakes; (a) wide survey spectra and the corresponding elemental composition; (b) narrow spectra of C 1s with deconvolution and peaks assignments; the XPS spectrum of the SP-treated in EMIM-DCA and graphite flakes contains the peaks sp^2-C at 284.5eV (C1), sp^3-C at 285.5 eV (C2), C-O at 286.5 eV (C3), C=O at 288.0 eV (C4), and C-N at 296.0 eV (C5). (c) narrow spectra of N 1s with deconvolution and peaks assignments; the XPS spectrum of the EMIM DCA sample contains the peaks N1 (398.0 eV), N2 (399.2 eV) and N3 (401.6 eV); the XPS spectrum of SP-treated in EMIM-DCA sample contains the peaks N1` (398.2 eV), N2` (399.4 eV), N3` (401.8 eV), N4` (400.4 eV), and N5` (403.8 eV). The black solid line represents the raw data, and the colored lines are the deconvoluted peaks; (d) chemical structures corresponding to EMIM DCA and SP-treated in EMIM-DCA material together with each component of the C 1s and N 1s spectra.

To confirm the morphology and size of the f-FLG, SEM images were recorded. **Figure 2.8** shows the SEM images of (a) graphite flakes and (b) f-FLG extracted from the SP-treated EMIM-DCA aqueous solution. The average diameters of graphite flakes and f-FLG were approximately 20 ± 7.5 μm, confirming that f-FLG can be formed from graphite flakes by the peeling process.

A C 1s peak (283–290 eV), O 1s peak (529–535 eV), and N 1s peak (394–406 eV) (**Figure 2.9**) were observed in the XPS wide-scan spectra of the products extracted from SP-treated EMIM-DCA aqueous solution, the US-treated EMIM-DCA aqueous solution, and graphite flakes. The N 1s peak was observed only in the product extracted from the SP-treated EMIM-DCA aqueous solution. From the XPS survey spectra, the total nitrogen and oxygen contents were estimated at 7.7 and 5.1 at%, respectively. The appearance of the N 1s peak indicated that f-FLG was functionalized with cationic nitrogen-containing functional groups.

The FTIR spectra of graphite flakes, a mixture of graphite flakes and EMIM-DCA, and the product extracted from the SP-treated EMIM-DCA aqueous solution were recorded to identify the functional groups added to f-FLG. Bands were observed at 1631 and 1585 cm^{-1}, corresponding to the skeletal vibrations of aromatic C=C bonds in graphite (**Figure 2.10a**).[35] **Figure 2.10b** shows the FTIR spectrum of the graphite flake / EMIM-DCA mixture. Bands were observed at 2237, 2198, and 2139 cm^{-1}, corresponding to the stretching vibrations of the C≡N bonds in the DCA anion.[36,40] Also, bands were observed at 2237, 2198, and 2139 cm^{-1}, corresponding to the antisymmetric (C–N) and symmetric (C–N) stretching vibrations, symmetric C≡N stretching, and antisymmetric C≡N stretching, respectively.[37] The C=N and C=C stretching vibrations of the imidazole groups were observed at 1630 and 1572 cm^{-1}, respectively, which overlapped with the aromatic C=C stretching vibration from graphite.[38] Also the bands at 1313 and 1171 cm^{-1} corresponded to the C–N and C–N–C bending vibrations of the imidazole groups, respectively, and the bands observed at 3104 and 3151 cm^{-1} corresponded to the C–H vibrations of the imidazole groups.[36] Broad bands at 2256 and 2206 cm^{-1} and a sharp peak at 2150 cm^{-1}, corresponding to the C≡N stretching vibrations of the

nitrile group, were observed in the spectrum of the product obtained from SP (**Figure 2.10c**).[41] Compared with those observed for graphite, the intensities of the bands observed at 2256 and 2206 cm^{-1} in the spectrum of the EMIM-DCA mixture relatively decreased; on the other hand, the peak at 2150 cm^{-1}, corresponding to the asymmetric C≡N vibration, became sharp, indicating that SP decomposed dicyanamide, and the C≡N functional group was added to f-FLG, i.e., f-FLG with CN. Compared with the FTIR spectra of graphite or the EMIM-DCA mixture and f-FLG with CN, the intensity of the C=N/C=C bond, corresponding to the stretching vibrations at 1628 cm^{-1}, increased, and the intensity of the C=C bond, corresponding to the stretching vibrations at 1576 cm^{-1}, decreased. The bands observed at 1331 and 1169 cm^{-1} also confirmed the presence of the C–N stretching vibrations of aromatic amine groups and the stretching vibrations of amine groups, respectively.[39] The extremely high reactivity at the edges of the f-FLG determines that the functional groups were attached to these parts of graphene.

Broad absorption bands were observed at 3435 cm^{-1}, corresponding to the OH stretching vibrations, in the FTIR spectra of graphite flakes, the graphite / EMIM-DCA mixture, and f-FLG with CN. This result indicated the presence of a partially terminated OH group in the as-received graphite flakes.

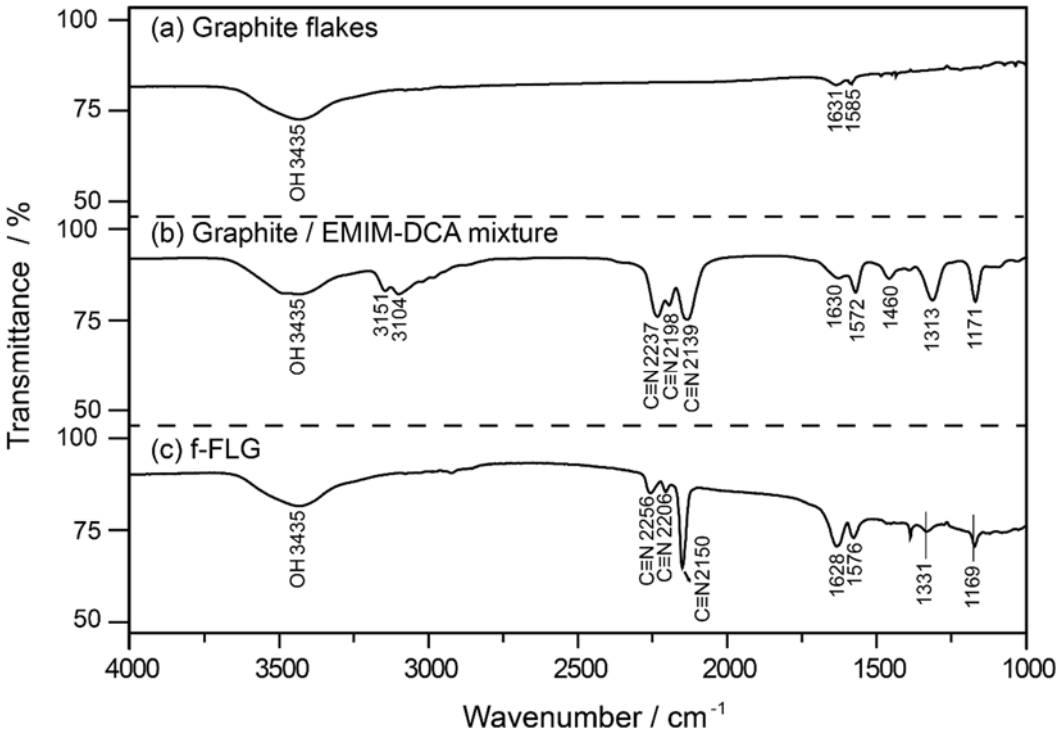

Figure 2.10. FTIR spectra of (a) as-received graphite flakes, (b) graphite / EMIM-DCA, and (c) f-FLG. To confirm the functional groups introduced by SP, sample (b) was prepared by mixing only graphite flakes and EMIM-DCA without SP.

To elucidate the mechanism for the formation of the f-FLG by peeling graphite flakes, OES spectra of the plasma generated during the synthesis of SP in the EMIM-DCA aqueous solution and SP in distilled water were recorded (**Figure 2.11a** and **2.11b**). In all the OES spectra, H·, O·, and OH· excited radicals were observed, related to water dissociation. The SP generated in EMIM-DCA and graphite flakes exhibited a higher electron density and electron excitation temperature than the plasma generated in distilled water and graphite flakes, explained by the high solution conductivity (**Figure 2.11**, **Figure 2.12a** and **2.12b**). **Figure 2.12** and **Tables 2.2**, and **2.3** provide details of the calculations of the electron density and excitation temperature. Highly reactive CN radicals easily interact with carbon materials.[42,43] Both ions of the IL dissociated in the plasma gas phase by electron collisions, affording radicals, but the high density of CN radicals might be predominantly generated from DCA anions (Figure 2.9a). The nitrile radicals attached to the edges of the f-FLG in the form of C≡N or an ionized and resonance structure of =C=N- was confirmed by the FTIR results. The attachment of the =C=N- anion can produce a repulsive force at the edges, leading to the weakening of the van der Waals force between the layers and aiding the peeling. The C≡N functional group attached to graphene sheets improved the solubility of the f-FLG in distilled water, which was easily observed (**Figure 2.13**).

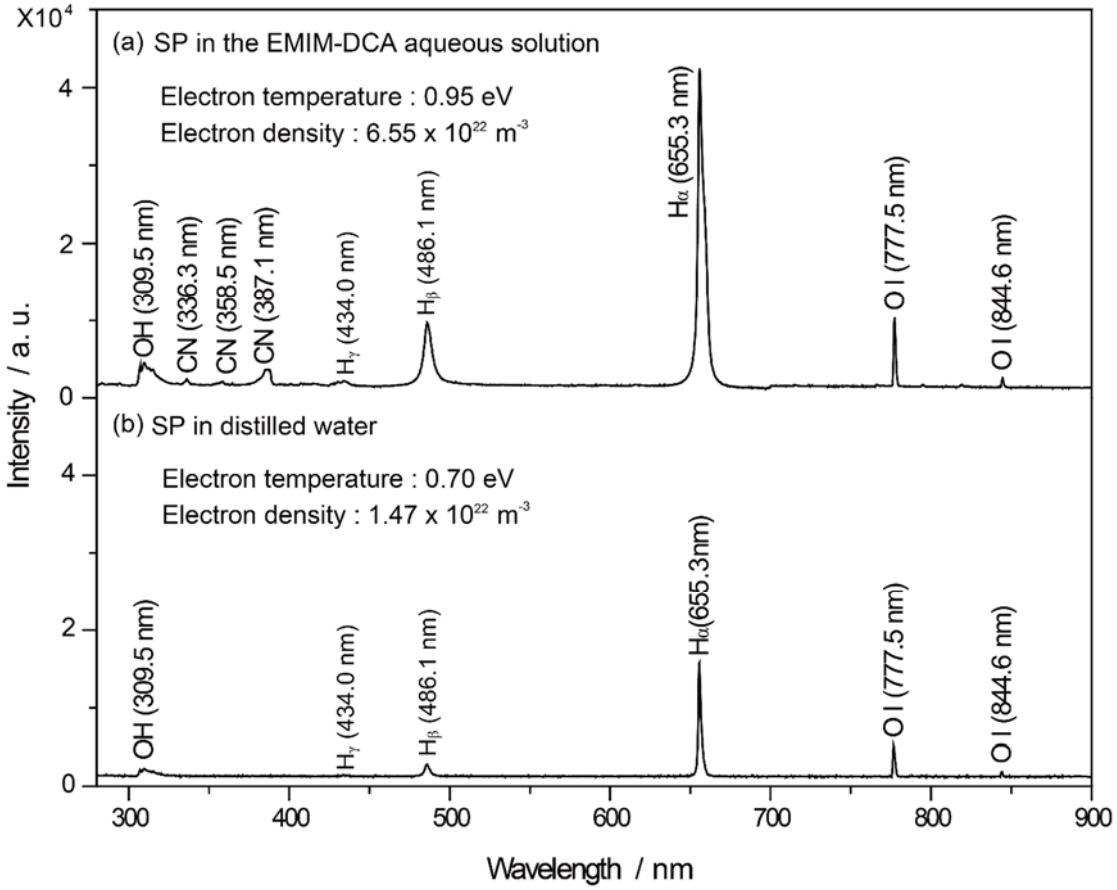

Figure 2.11. Optical emission spectra, electron excitation temperature, and density in the plasma for (a) SP in the EMIM-DCA aqueous solution and (b) SP in distilled water with graphite flakes. **Table 2.2** summarizes the assignment of the emissions from atoms, molecules, and radicals.

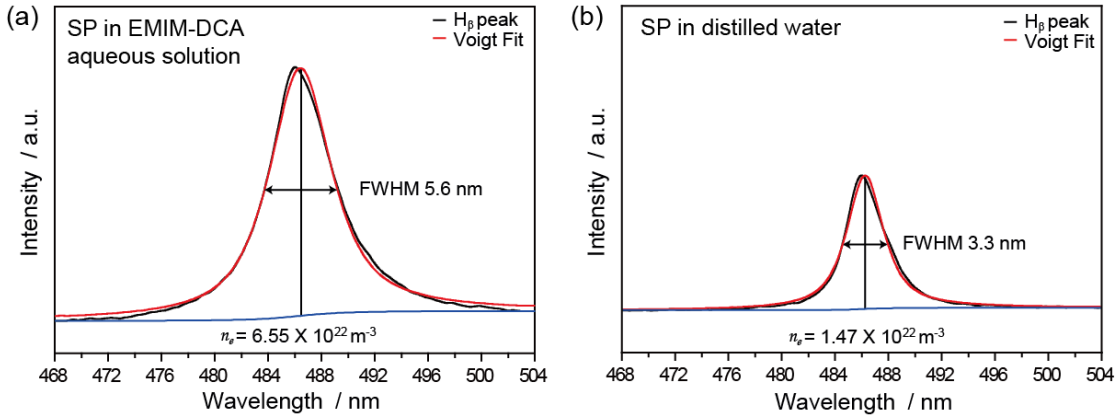

Figure 2.12 Profile of the H_β line (black line) fitted with a Voigt line profile (red line) corresponding to (a) SP in the EMIM-DCA aqueous solution containing graphite and (b) SP in distilled water containing graphite flakes. From the full-width at half-maximum (*FWHM*) the electron density was calculated. Electron density was calculated by $FWHM = 4.800 \times (n_e \times 10^{-23})^{0.681}$ [44] The measured FWHM of H_β line was corrected with the instrumental broadening of the spectrograph, which was 2 nm.

Table 2.2. Identification of the excited species from OES.[45-48]

Species	λ (nm)	Transition
H_α	655.3	$3d \rightarrow 2p$
H_β	486.1	$4d \rightarrow 2p$
H_γ	434.0	$5d \rightarrow 2p$
O	844.6 777.5	$^3P \rightarrow {}^3S^\circ$ $^5P \rightarrow {}^5S^\circ$
CN	387.1 358.5 336.3	$B^2\Sigma^+ \rightarrow X^2\Sigma^+$ $B^2\Sigma^+ \rightarrow X^2\Sigma^+$ $B^2\Sigma^+ \rightarrow X^2\Sigma^+$
OH	309.5	$A^2\Sigma^+ \rightarrow X^2\Pi$

Table 2.3. Atomic spectral data for hydrogen lines used to calculate the electron excitation temperature in SP.[49] Electron excitation temperature calculated by $kT_e(\alpha\beta) = -[(E_\alpha - E_\beta) / \ln(I_\alpha A_\beta g_\beta \lambda_\alpha / I_\beta A_\alpha g_\alpha \lambda_\beta)]$; 1) SP in EMIM-DCA aqueous solution: $kT_e(\alpha\beta) = 0.95$ eV, 2) SP in distilled water: $kT_e(\alpha\beta) = 0.70$ eV

H line	OES intensity / arb. units		gA / s^{-1}	E / cm^{-1}	λ / nm
	1)	2)			
α	42481.72	15800.08	7.94×10^8	97492.30	656.30
β	9700.92	2815.96	2.69×10^8	102823.90	486.10

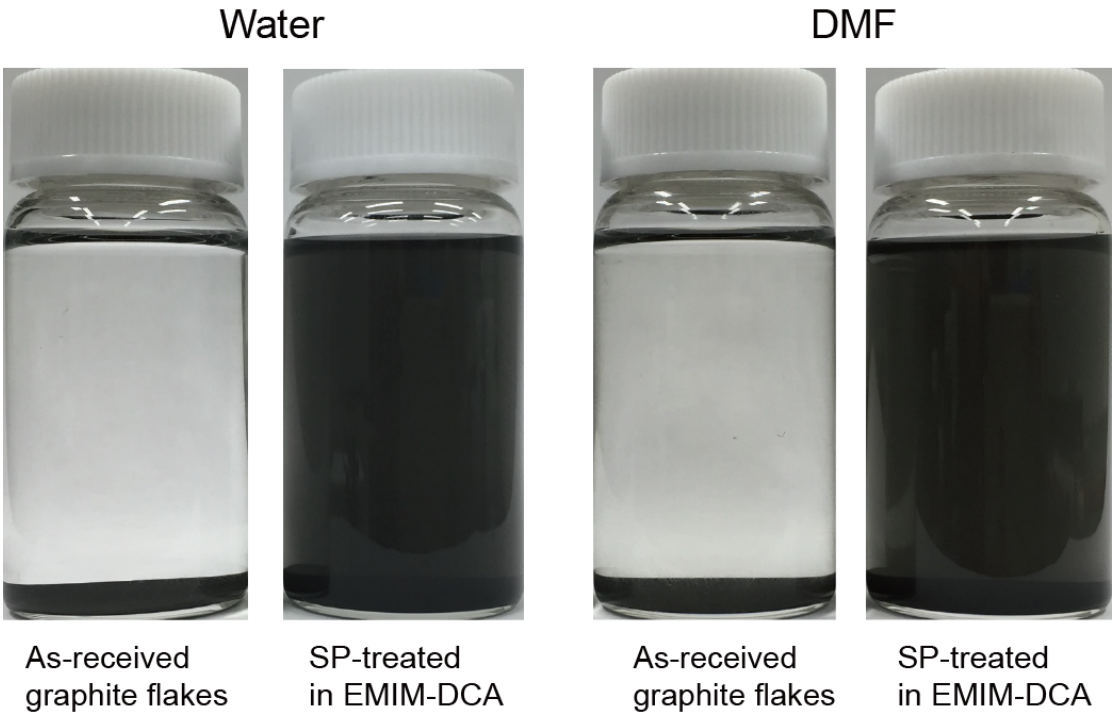

Figure 2.13. Digital photographs of the as-received graphite flakes and SP-treated in EMIM-DCA aqueous solution dispersed in water and DMF.

The adsorption of EMIM cations on the graphite surface that determined the reduction in the van der Waals force between the graphite layers, which was referred to the interaction between π-electrons and cations, was utilized to explain the exfoliation of graphite to produce graphene induced by ionic liquids and its dispersion in polar solvents.[50] In our experiment, the formation of the f-FLG cannot be completely clarified by the cation adsorption and electrostatic force. Peeling occurred efficiently with the application of a shear force from the lateral side of graphite.[51] From another viewpoint, if SP causes a localized lack of electrons on a subsurface (defined as a few layers above) of graphite flakes via electron exchange, the attractive force in a direction perpendicular to the basal plane will weaken. To validate the mechanism based on such a localized lack of electrons, the energy diagram for SP in the EMIM-DCA aqueous solution with graphite flakes is shown in **Figure 2.14**. In this diagram, the DOS of graphite and its subsurface,[52] EMIM-DCA in water, water, and SP are displayed together to explain the peeling process. In the diagram, the energy scale (right side) is negative and relative to the vacuum level (VL). The energy scale on the left side is versus the normal hydrogen electrode (NHE). The energies were calculated corresponding to pH 7, similar to the condition utilized during the SP process. If the work function (−4.19 eV) and DOS bands of graphite are known,[52] then it was imperative to calculate these values for EMIM-DCA in water by ab initio MO calculations using UB3LYP / 6-311++g (2d,p) with SCRF/PCM (**Figure 2.15**, **Tables 2.1** and **2.4**). The calculated I_P and E_A values for the EMIM dimer in water at pH 7 were −4.47 and −3.49 eV, respectively. The corresponding values of I_P and E_A for DCA were −5.28 and −0.85 eV, respectively.[53] The calculated values approximately agreed with those obtained from the CV measurements in 10 wt% EMIM-DCA aqueous solution. Thereby, the I_P and E_A values for EMIM were found at −5.86, and −3.94 V, respectively, and the corresponding values for DCA were determined to be −6.20 and −3.25 V, respectively (**Figure 2.15** and **Table 2.4**). The bonded states in SP corresponded to the energy levels of the species present in plasma, such as atoms, molecules, and radicals, from where electrons can escape by ionization via interparticle collisions, mainly electron collisions. The plasma served as a large reservoir of free electrons

with an energy of about 0.95 eV, from where electrons were supplied in the system.[54] First, electrons from the graphite subsurface were transferred to the I_P level of EMIM-DCA in water situated at −4.47 eV, which is close to the Fermi level of graphite at −4.19 eV. The induced lack of electrons in the graphite subsurface promoted the peeling of graphite because of a shear lateral force, affording f-FLG. The lack of electrons in f-FLG was compensated during the next steps, when electrons were transferred from SP, via the E_A level of the EMIM dimer in water situated at −3.49 eV, to f-FLG. Finally, electrons were transferred from the EMIM dimer to f-FLG, and f-FLG reached the electronic ground state.

SP in the EMIM-DCA aqueous solution with graphite flakes exhibited high solution conductivity, leading to a higher electron density as compared with that for plasma generated in water and graphite flakes (**Table 2.3**). At a concentration of 10 wt% EMIM-DCA in distilled water, US promoted the peeling of graphite in EMIM-DCA in an aqueous solution, albeit only marginally. Moreover, the product was MLG because the peeling was possibly related to the mechanical force. Furthermore, with the application of a high voltage without SP breakdown, the peeling of graphite barely occurred. Thus, only SP in the EMIM-DCA aqueous solution can enhance the formation of the f-FLG.

These results indicated that SP and the free electrons are crucial in the peeling process of graphite flakes. Hence, the above experiments confirmed that SP is responsible for the weakening of the attractive force perpendicular to the basal plane caused by a localized lack of electrons on the subsurface of graphite flakes, and EMIM-DCA plays a major role in inducing the peeling of graphite flakes and the formation of the f-FLG by electron exchange.

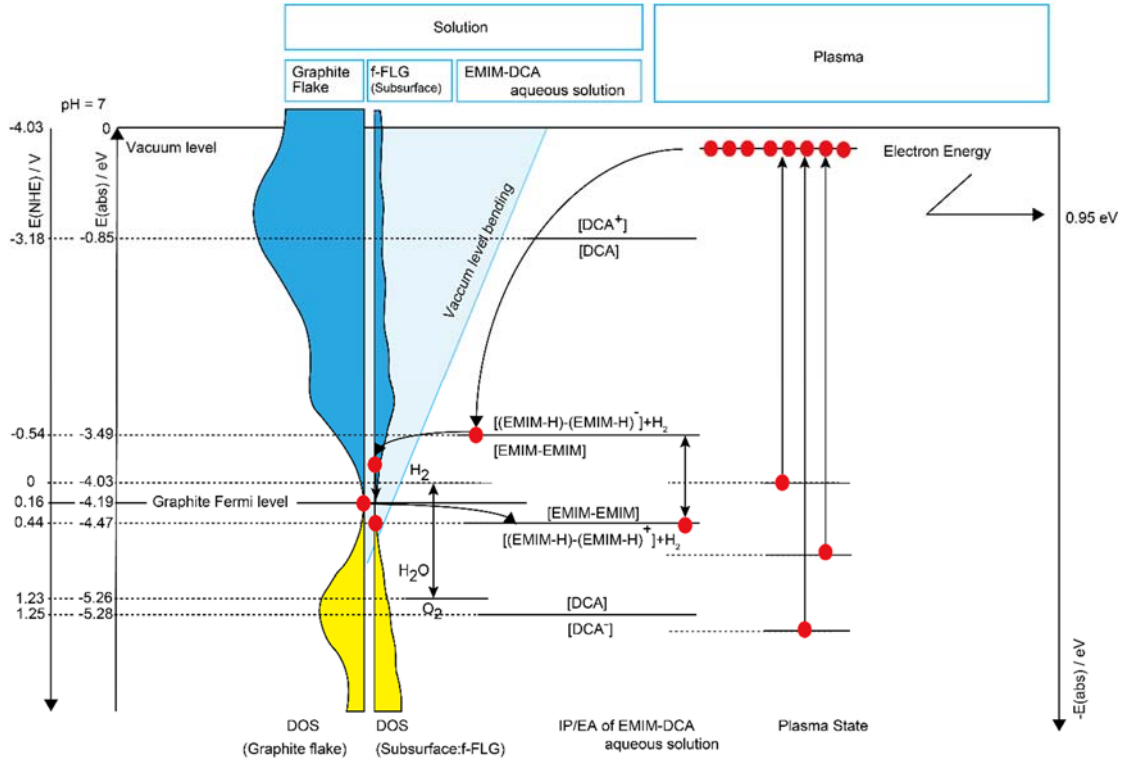

Figure 2.14. Schematic of the synthesis of f-FLG from graphite flakes by electron exchange induced by SP. The transfer of electrons from graphite flakes to EMIM-DCA led to the lack of electrons on the subsurface of graphite flakes, which in turn promoted peeling. The Fermi level of graphite flakes was at −4.19 eV, relative to VL. From SP with the maximum of the electron energy at about 0.95 eV (in the case of SP in water, EMIM-DCA, and graphite flakes), the electrons were transferred to the graphite subsurface via EMIM-DCA. The calculated I_P and E_A values for EMIM-DCA in water at pH 7 were −4.47 and −3.49 eV, respectively. Finally, electrons were transferred from EMIM dimer to f-FLG. In SP the collisional processes of excitation followed by ionization generated electrons.

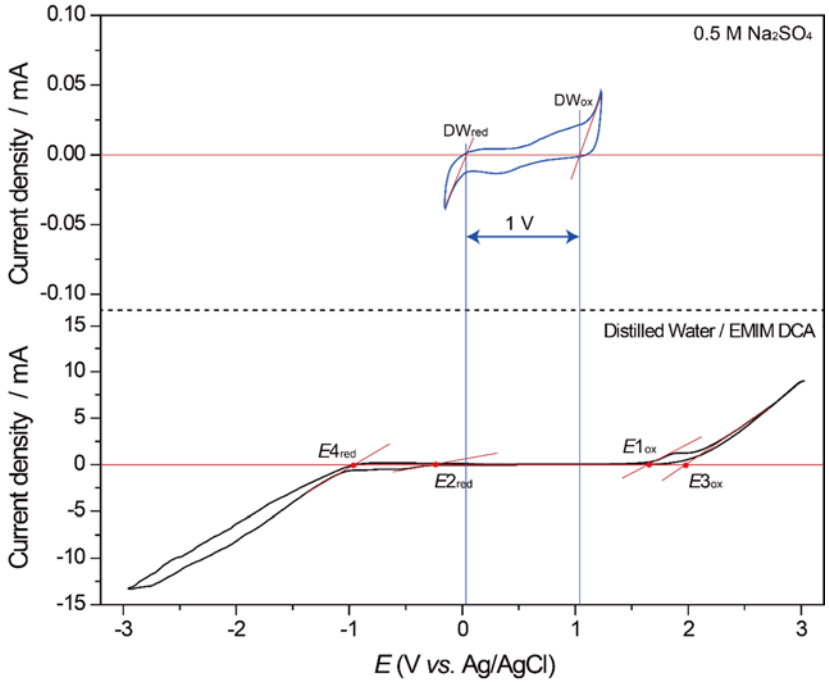

Figure 2.15. Cyclic voltammetry (CV) of the Pt working electrode in 0.5 M Na_2SO_4 solution and distilled water (90 wt%) / EMIM-DCA (10 wt%) electrolyte at a scan rate of 100 mV/s (oxidation: ox; reduction: red).

Table 2.4. Electrochemical data obtained from CV measurements of the solution.[55]

Molecule	Potential vs. Ag/AgCl in V	Potential vs. NHE in V	*IP* and *EA* in eV vs. vacuum level
$E1_{EMIM^+, ox}$	1.63	1.83	−5.86 I_P
$E2_{EMIM^{++}, red}$	−0.29	−0.09	−3.94 E_A
$E3_{DCA, ox}$	1.97	2.17	−6.20 I_P
$E4_{DCA^-, red}$	−0.98	−0.78	−3.25 E_A

2.4. Summary

In this study, a one-pot process for f-FLG synthesis in an EMIM-DCA aqueous solution by the SP method was successfully developed. OES analysis provided evidence for the presence of C≡N radicals in SP. XRD, TEM, XPS, and FTIR results confirmed the peeling of graphite and the simultaneous formation of f-FLG with CN. A high nitrogen content of 7.7 at% was observed. The broadening of the 2D band in the Raman spectra confirmed that f-FLG comprises three layers. The mechanism for the formation of the f-FLG can be explained by the SP-induced exchange of electrons via EMIM-DCA in water. The transfer of electrons from the graphite subsurface to the cationic IL led to a lack of electrons on the graphite flake subsurface, which in turn resulted in the weakening of the attractive force perpendicular to the basal plane and promoted peeling. After peeling, the lack of electrons was compensated by the electrons transferred from SP via IL. In conclusion, f-FLG was rapidly synthesized without the use of any substrate, permitting immediate use of the material. In this mechanism, the electron exchange of SP via ILs can be applied for the synthesis of various materials.

References

(1) A. K. Geim and K. S. Novoselov, *Nat. Mater.*, 2007, **6**, 183-191.

(2) X. Wang, L. Zhi and K. Müllen, *Nano Lett.*, 2008, **8**, 323-327.

(3) A. L. M. Reddy, A. Srivastava, S. R. Gowda, H. Gullapalli, M. Dubey and P. M. Ajayan, *ACS Nano*, 2010, **4**, 6337-6342.

(4) L. Qu, Y. Liu, J.-B. Baek and L. Dai, *ACS Nano*, 2010, **4**, 1321-1326.

(5) M. D. Stoller, S. Park, Y. Zhu, J. An and R. S. Ruoff, *Nano Lett.*, 2008, **8**, 3498-3502.

(6) D. Wei, Y. Liu, Y. Wang, H. Zhang, L. Huang and G. Yu, *Nano Lett.*, 2009, **9**, 1752-1758.

(7) Y. Wang, Y. Shao, D. W. Matson, J. Li and Y. Lin, *ACS Nano*, 2010, **4**, 1790-1798.

(8) K. S. Novoselov, A. K. Geim, S. V. Morozov, D. Jiang, Y. Zhang, S. V. Dubonos, I. V. Grigorieva and A. A. Firsov, *Science*, 2004, **306**, 666-669.

(9) S. Latil and L. Henrard, *Phys. Rev. Lett.*, 2006, **97**, 036803.

(10) S. Ghosh, W. Bao, D. L. Nika, S. Subrina, E. P. Pokatilov, C. N. Lau and A. A. Balandin, *Nat. Mater.*, 2010, **9**, 555-558.

(11) M. Aliofkhazraei, N. Ali, W. I. Milne, C. S. Ozkan, S. Mitura and J. L. Gervasoni, *Graphene Science Handbook: Nanostructure and Atomic Arrangement*, CRC Press, 2016.

(12) V. Schwartz, W. Fu, Y. T. Tsai, H. M. Meyer, A. J. Rondinone, J. Chen, Z. Wu, S. H. Overbury and C. Liang, *ChemSusChem*, 2013, **6**, 840-846.

(13) T. Ramanathan, A. Abdala, S. Stankovich, D. Dikin, M. Herrera-Alonso, R. Piner, D. Adamson, H. Schniepp, X. Chen and R. Ruoff, *Nat. Nanotechnol.*, 2008, **3**, 327-331.

(14) M. Cai, D. Thorpe, D. H. Adamson and H. C. Schniepp, *J. Mater. Chem.*, 2012, **22**, 24992-25002.

(15) A. E. Del Rio-Castillo, C. Merino, E. Díez-Barra and E. Vázquez, *Nano Res.*, 2014, **7**, 963-972.

(16) I.-Y. Jeon, Y.-R. Shin, G.-J. Sohn, H.-J. Choi, S.-Y. Bae, J. Mahmood, S.-M. Jung, J.-M. Seo, M.-J. Kim and D. W. Chang, *Proc. Natl. Acad. Sci. U. S. A.*, 2012, **109**, 5588-5593.

(17) S. Stankovich, D. A. Dikin, R. D. Piner, K. A. Kohlhaas, A. Kleinhammes, Y. Jia, Y. Wu, S. T. Nguyen and R. S. Ruoff, *Carbon*, 2007, **45**, 1558-1565.

(18) M. J. McAllister, J.-L. Li, D. H. Adamson, H. C. Schniepp, A. A. Abdala, J. Liu, M. Herrera-Alonso, D. L. Milius, R. Car and R. K. Prud'homme, *Chem. Mater.*, 2007, **19**, 4396-4404.

(19) Y. Hernandez, V. Nicolosi, M. Lotya, F. M. Blighe, Z. Sun, S. De, I. McGovern, B. Holland, M. Byrne and Y. K. Gun'Ko, *Nat. Nanotechnol.*, 2008, **3**, 563-568.

(20) J. Chen, W. Shi, Y. Chen, Q. Yang, M. Wang, B. Liu, Z. Tang, M. Jiang, D. Fang and C. Xiong, *Appl. Phys. Lett.*, 2016, **108**, 073105.

(21) M. Matsumoto, Y. Saito, C. Park, T. Fukushima and T. Aida, *Nat. Chem.*, 2015, **7**, 730-736.

(22) T. Morishita, T. Ueno, G. Panomsuwan, J. Hieda, A. Yoshida, M. A. Bratescu and N.

Saito, *Sci. Rep.*, 2016, **6**.

(23) H. Lee, M. A. Bratescu, T. Ueno and N. Saito, *RSC Adv.*, 2014, **4**, 51758-51765.

(24) M. J. Frisch, G. W. Trucks, H. B. Schlegel, G. E. Scuseria, M. A. Robb, J. R. Cheeseman, G. Scalmani, V. Barone, B. Mennucci, G. A. Petersson, H. Nakatsuji, M. Caricato, X. Li, H. P. Hratchian, A. F. Izmaylov, J. Bloino, G. Zheng, J. L. Sonnenberg, M. Hada, M. Ehara, K. Toyota, R. Fukuda, J. Hasegawa, M. Ishida, T. Nakajima, Y. Honda, O. Kitao, H. Nakai, T. Vreven, J. A. Montgomery Jr, J. E. Peralta, F. Ogliaro, M. Bearpark, J. J. Heyd, E. Brothers, K. N. Kudin, V. N. Staroverov, R. Kobayashi, J. Normand, K. Raghavachari, A. Rendell, J. C. Burant, S. S. Iyengar, J. Tomasi, M. Cossi, N. Rega, J. M. Millam, M. Klene, J. E. Knox, J. B. Cross, V. Bakken, C. Adamo, J. Jaramillo, R. Gomperts, R. E. Stratmann, O. Yazyev, A. J. Austin, R. Cammi, C. Pomelli, J. W. Ochterski, R. L. Martin, K. Morokuma, V. G. Zakrzewski, G. A. Voth, P. Salvador, J. J. Dannenberg, S. Dapprich, A. D. Daniels, O. Farkas, J. B. Foresman, J. V. Ortiz, J. Cioslowski, and D. J. Fox, Gaussian 09, Revision D.01, Gaussian, Inc., Wallingford CT, 2009.

(25) R. M. Richard, M. S. Marshall, O. Dolgounitcheva, J. Ortiz, J.-L. Brédas, N. Marom and C. D. Sherrill, *J. Chem. Theory Comput.*, 2016, **12**, 595-604.

(26) J. W. Knight, X. Wang, L. Gallandi, O. Dolgounitcheva, X. Ren, J. V. Ortiz, P. Rinke, T. Körzdörfer and N. Marom, *J. Chem. Theory Comput.*, 2016, **12**, 615-626.

(27) L. Liu, Z. Xiong, D. Hu, G. Wu and P. Chen, *Chem. Commun.*, 2013, **49**, 7890-7892.

(28) A. Ferrari, J. Meyer, V. Scardaci, C. Casiraghi, M. Lazzeri, F. Mauri, S. Piscanec, D. Jiang, K. Novoselov and S. Roth, *Phys. Rev. Lett.*, 2006, **97**, 187401.

(29) A. C. Ferrari and J. Robertson, *Phys. Rev. B*, 2000, **61**, 14095.

(30) L. Cançado, K. Takai, T. Enoki, M. Endo, Y. Kim, H. Mizusaki, A. Jorio, L. Coelho, R. Magalhaes-Paniago and M. Pimenta, *Appl. Phys. Lett.*, 2006, **88**, 163106.

(31) S. Lee, K. Lee and Z. Zhong, *Nano Lett.*, 2010, **10**, 4702-4707.

(32) A. Reina, X. Jia, J. Ho, D. Nezich, H. Son, V. Bulovic, M. S. Dresselhaus and J. Kong, *Nano Lett.*, 2008, **9**, 30-35.

(33) C. Casiraghi, S. Pisana, K. Novoselov, A. Geim and A. Ferrari, *Appl. Phys. Lett.*, 2007, **91**, 233108.

(34) N. Parveen, M. O. Ansari and M. H. Cho, *RSC Adv.*, 2015, **5**, 44920-44927.

(35) P. Khanra, C.-N. Lee, T. Kuila, N. H. Kim, M. J. Park and J. H. Lee, *Nanoscale*, 2014, **6**, 4864-4873.

(36) P. Li, D. Paul and T.-S. Chung, *Green Chem.*, 2012, **14**, 1052-1063.

(37) X. Xuan, M. Guo, Y. Pei and Y. Zheng, *Spectrochim. Acta, Part A*, 2011, **78**, 1492-1499.

(38) S. Indrawirawan, H. Sun, X. Duan and S. Wang, *J. Mater. Chem. A*, 2015, **3**, 3432-3440.

(39) Y. Murti, R. Agnihotri and D. Pathak, *Am. J. Chem.*, 2011, **1**, 42-46.

(40) J. W. Sprague, J. G. Grasselli and W. M. Ritchey, *J. Phys. Chem.*, 1964, **68**, 431-433.

(41) B. V. Lotsch, J. Senker, W. Kockelmann and W. Schnick, *J. Solid State Chem.*, 2003, **176**, 180-191.

(42) E. Wang, Z. Guo, J. Ma, M. Zhou, Y. Pu, S. Liu, G. Zhang and D. Zhong, *Carbon*, 2003, **41**, 1827-1831.

(43) T. J. Wasowicz, A. Kivimäki, M. Coreno and M. Zubek, *J. Phys. B: At., Mol. Opt. Phys.*, 2014, **47**, 055103.

(44) P. Bruggeman, D. Schram, M. Á. González, R. Rego, M. G. Kong and C. Leys, *Plasma Sources Sci. Technol.*, 2009, **18**, 025017.

(45) S. F. Durrant, E. C. Rangel and M. A. Bica de Moraes, *J. Vac. Sci. Technol., A*, 1995, **13**, 1901-1906.

(46) A. E. Lefohn, N. M. Mackie and E. R. Fisher, *Plasmas Polym.*, 1998, **3**, 197-209.

(47) Y. Himeno, Y. Ogura and T. Shirafuji, *J. Phys. Conf. Ser.* 2014, 518, 012021.

(48) A. Kramida, Y. Ralchenko and J. Reader, NIST ASD Team (2016), *NIST Atomic Spectra Database* (version 5.4).

(49) N. Liu, F. Luo, H. Wu, Y. Liu, C. Zhang and J. Chen, *Adv. Funct. Mater.*, 2008, **18**, 1518-1525.

(50) T. Gould, Z. Liu, J. Z. Liu, J. F. Dobson, Q. Zheng and S. Lebègue, *J. Chem. Phys.*, 2013, **139**, 224704.

(51) M. D. Williams, D. K. Samarakoon, D. W. Hess and X.-Q. Wang, *Nanoscale*, 2012, **4**, 2962-2967.

(52) T. Takahashi, H. Tokailin and T. Sagawa, *Phys. Rev. B*, 1985, **32**, 8317.

(53) L. Šištík, M. Ončák and P. Slavíček, *Phys. Chem. Chem. Phys.*, 2011, **13**, 11998-12007.

(54) P. Bruggeman, D. Schram, M. Á. González, R. Rego, M. G. Kong and C. Leys, *Plasma Sources Sci. Technol.*, 2009, **18**, 025017.

(55) T. Johansson, W. Mammo, M. Svensson, M. R. Andersson and O. Inganäs, *J. Mater. Chem.*, 2003, **13**, 1316-1323.

Chapter 3

P-type Doping of Graphene with Cationic Nitrogen via Solution Plasma

Chapter 3 - P-type Doping of Graphene with Cationic Nitrogen via Solution Plasma

3.1. Introduction

Graphene is currently considered as the most attractive 2D material for a broad range of potential applications in electronic, sensor, and electrochemical energy devices[1-3] due to its fascinating properties, such as planar structure, large surface area, high thermal/electrical conductivity, and tunable electrical properties. Chemical doping of graphene by heteroatoms can effectively tailor its electronic, chemical, and optical properties to realize graphene with desired functional properties. Among several types of heteroatoms studied, nitrogen can easily be incorporated into the hexagonal lattice of graphene, thus creating redistribution of charge and spin density state in the graphene.[4] In general, when a nitrogen atom is doped into graphene, three typical bonding configurations are detectable: (1) quaternary N (or graphitic N) at the basal plane of graphene,[5] (2) pyridinic N and (3) pyrrolic N at the edge site.[6] Bonding configuration of N atom doping plays an essential role in influencing electron and hole transport behaviors of graphene. Over the past decade, a significant progress has been paid on the control of N bonding configuration in nitrogen-doped graphene (NG) at specific position by altering processing temperature, synthetic method, and starting precursor[7]. Graphitic N could result in n-type semiconducting graphene with high mobility of charge carriers since the excess valence electrons are delocalized.[8] In contrast, pyridinic N and pyrrolic N atoms resulted in either weak n-type or p-type semiconducting behavior.[9] Another possible N bonding configuration in graphene is in a cationic form.[10] Graphene doped with cationic N is expected to preserve its planar structure as compared to other N bonding configurations at high N doping levels.[11] However, cationic N has been rarely investigated and not well understood at the present stage. Its electrical and charge transport properties are also still unresolved. Therefore, controlling the

N bonding configuration with a cationic form in NGs is very challenging for further development towards this exiting area.

In recent experimental studies on NGs, they have extensively been synthesized via either direct synthesis (e.g., chemical vapor deposition, solvothermal, and arc discharge[12]) or post-synthesis treatment (e.g., thermal treatment in NH_3 and plasma treatment[13]). However, most of these methods are complex and requires high processing temperature under a vacuum system. Precursors used are also expensive and highly toxic. With the aim to scale up production of NGs, development of the simpler synthesis method with balance between cost, time, and controllability is urgently needed. Very recently, our group has demonstrated a powerful strategy to synthesize nitrogen-doped carbons (NCs) by a simple method called "*solution plasma (SP)*". SP is non-thermal plasma in liquid phase, which can keep reaction temperature close to room temperature during synthesis at atmospheric pressure. A number of both aliphatic and aromatic organic precursors has been used in the synthesis of NCs by SP (e.g. pyridine, aniline, acrylonitrile, etc.).[14-16] The N bonding configuration and N doping content in NCs varied broadly from 0.5 to 7.8 at%, depending on the synthesis conditions and type of precursors.[17-19] Unintentionally, Hyun *et al* have successfully synthesized N-doped carbon nanosheets (NCNSs) through SP by using *N*-methyl-2-pyrrolidone (NMP) at specific SP conditions without post-heat treatment.[20] This interesting finding has shed light on the potential of SP as an alternative bottom-up method to synthesize sheet-like carbon structure.

Here, we report for the first time the successful synthesis of cationic N-doped graphene (CN–G) by SP. A mixture of 10% 1-Ethyl-3-methylimidazolium dicyanamide (EMIM DCA, $C_8H_{11}N_5$) and 90% dimethylformamide (DMF, C_3H_7NO) was used as a precursor. The EMIM DCA ionic liquid (IL) was selected since its high nitrogen content, environmentally friendly solvent (green solvent), stable liquid solution at high temperatures, and very low vapor pressure.[21] A bipolar high voltage pulse with high frequency of 200 kHz was applied to a pair of tungsten electrodes that were submerged in the mixed precursor. After discharge for 15 min, the black solid product was obtained and then collected by a vacuum filtration. The resultant

product is hereafter denoted as CN–G. More detailed information on synthesis procedure can be found in **Figure 3.1**.

3.2. Experimental procedures

3.2.1 *Solution preparation and synthesis of CN–G by SP.*

A mixture of 10% 1-Ethyl-3-methylimidazolium dicyanamide (EMIM DCA, $C_8H_{11}N_5$, 98.0% purity, Sigma-Aldrich) and 90% organic solution was prepared, as shown in **Figure 3.1**. The organic solution used, dimethylformamide (DMF, C_3H_7NO, >99.5% purity,) was purchased from Kanto Chemical.

Figure 3.1 illustrates the ionic liquid solution plasma for the produced CN–G. The discharge was generated at the distance between a pair of tungsten electrode (1.0 mm in diameter, 99.9% purity, Nilaco) that were placed at the center of a glass reactor. A gap distance between two tungsten electrodes shielded with an insulating ceramic tube was fixed at 1.0 mm. Mixture of ILs / OSs (EMIM DCA, 10% / DMF, 90%) was inserted in glass reaction. A bipolar high voltage pulse was applied to the tungsten electrodes using a bipolar-DC pulsed power supply (KURITA Seisakusho) set to use a pulse voltage of 1 kV, a pulse frequency of 200 kHz and a pulse width of 1.0 μs. **Figure 3.1** shows a schematic illustration of experimental setup for the solution plasma process in this study. After discharging for 5 min, the synthesized powder was separated by vacuum filtration through a polytetrafluoroethylene (PTFE, Merck Millipore, JVWP04700) membrane filter with a pore size of 0.1 μm. The obtained specimens of this ionic liquids solution plasma process were then washed with distilled water and ethanol and then dried in oven at 85 °C for 12 h.

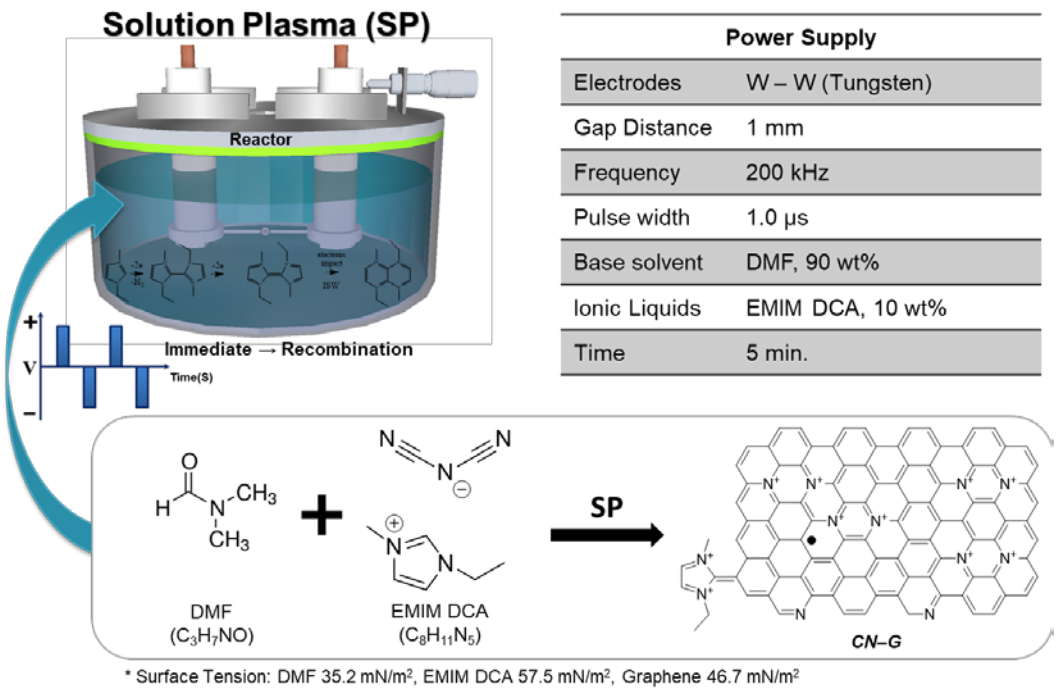

Power Supply	
Electrodes	W – W (Tungsten)
Gap Distance	1 mm
Frequency	200 kHz
Pulse width	1.0 μs
Base solvent	DMF, 90 wt%
Ionic Liquids	EMIM DCA, 10 wt%
Time	5 min.

Figure 3.1. Schematic image of experimental setup for the solution plasma process

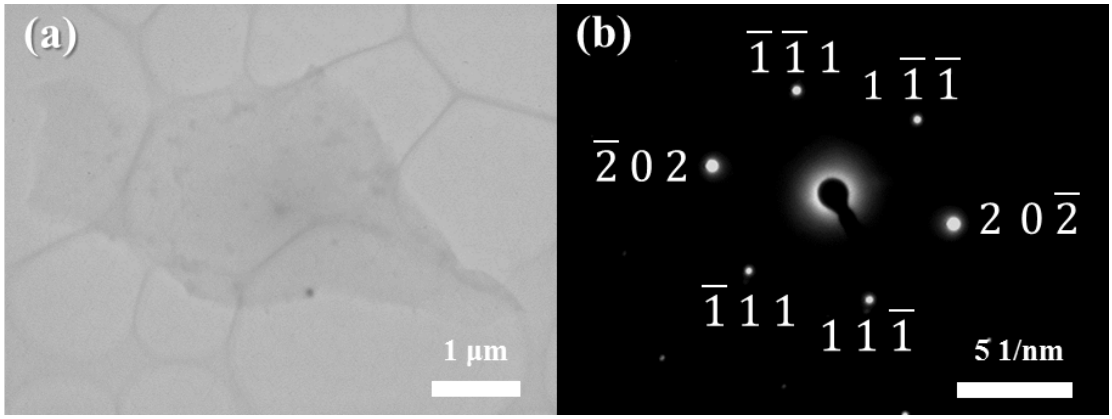

Figure 3.2. (a) TEM images and corresponding (b) SAED pattern of CN–G.

Table 3.1. Crystallographic calculation of pristine graphene and CN–G.

	Pristine Graphene	**Cationic N-doped Graphene**
Space Group	P 63mc	C mmm
Point Group	D_{6v}^{4}	D_{2h}^{19}
3D Lattice	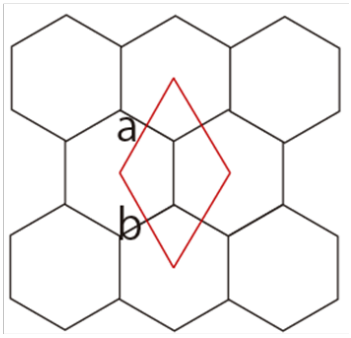	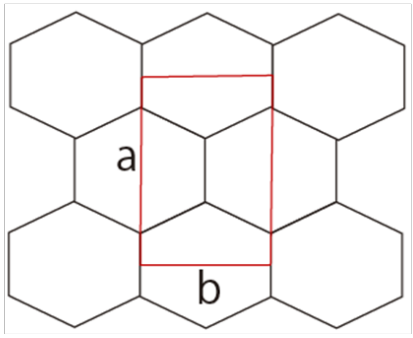
Lattice Condition	a = b c = 2.4700 Å b =2.4700 Å c = 6.7900 Å α = β = 90.00° γ =120.00°	a ≠ b a = 4.01602 Å b = 2.34994 Å c = 6.89 Å α = β = γ = 90°

2.2.2 *Characterization*

The X-ray diffraction (XRD, Smartlab, Rigaku) patterns of the synthesized sample were recorded on XRD instrument with Cu Kα radiation of 0.154 nm, an accelerating voltage of 45 kV and a current of 200 mA. The morphology of sample was observed by transmission electron microscopy (TEM, JEM-2500SE, JEOL) at an accelerating voltage of 200 kV, using selected-area electron diffraction (SAED) patterns. The Raman spectra of the synthesized sample were recorded on a Raman spectrometer (NRS-100, JASCO) equipped with a laser-excitation wavelength of 532.5 nm at room temperature. The spectra were recorded in the wavenumber range from 1000 to 3000 cm^{-1}. X-ray photoelectron spectroscopy (XPS, PHI 5000 VersaProbe II, ULVAC-PHI) analysis was carried out using a Mg Kα X-ray source, a pass energy of 46.9 eV, and an acquisition step of 0.5 eV. The resistivity measurement was accomplished with a four probes device (Loresta-GP MCP-T610, Mitsubishi Chemical).

3.3. Results and discussion

We first verified the formation of graphene-like structure of CN–G by transmission electron microscopy (TEM). Clearly, TEM image in **Figure 3.2a** revealed that CN–G had sheet-like morphology with lateral size of about 20–30 μm. The corresponding selected area electron diffraction (SAED) pattern of CN–G was composed of six spots in asymmetrical hexagonal arrangement (*P*63*mc*), which refer to $11\bar{1}$, $\bar{1}11$, $\bar{1}\bar{1}1$, $1\bar{1}\bar{1}$, $20\bar{2}$, and $\bar{2}02$ lattice points (**Figure 3.2b**). This diffraction feature was different from the pristine graphene, which typically has six spots with symmetrical hexagonal arrangement ($a = b$).[22] Based on crystallographic calculation, lattice constants, *a* and *b*, of CN–G were not identical since its atomic arrangement was distorted to be an orthorhombic structure (*Cmmm*) rather than hexagonal structure (see **Table 3.1**).

The structural properties of CN–G were examined by X-ray diffraction (XRD), as shown in **Figure 3.3a**. The XRD pattern showed two pronounced peaks at 25.9° and 43.1°, corresponding to the (002) and (111) planes of graphite, respectively. An intense and sharp 002 diffraction

peak indicates high degree of graphitization for CN–G. The 002 interlayer spacing was calculated to be 0.340 nm, which was slightly larger than that of pristine graphite (0.335 nm). Such a larger 002 interlayer spacing might be induced by the presence of defect and N doping in the carbon framework structure. Furthermore, to gain more structural information, Raman spectroscopic measurement was carried out and is shown in **Figure 3.3b**. Raman spectrum of CN–G showed the D band at ~1340 cm^{-1}, G band at ~1580 cm^{-1}, 2D band at ~2700 cm^{-1}, and G + D band at ~2940 cm^{-1} (a combination scattering peak). These four peaks are typically found for graphene and graphite.[23] The D band at about 1340 cm^{-1} is typically observed only when the graphene has defects in the crystal structure on the edge of the graphene or has disordered structure.[24] Therefore, the emergence of D band of CN–G is caused by its internal defects in the graphene structure and the functionalization of the graphene sheet edge. Moreover, the D' band is observed only at N doping, which is not observed in pure graphene.[25] The intensity ratio of 2D band to G band (I_{2D}/I_G) was 0.82 and the full width at half maximum of the 2D band was about 68 cm^{-1}, which corresponded to three-layer graphene.[26] Another important aspect should be noted here is a shift of 2D peak toward lower wavenumber, which is normally found in the NGs as reported elsewhere.[27]

The X-ray photoelectron spectroscopy (XPS) survey spectrum of CN–G was composed of C 1s peak (284.5 eV), O 1s peak (532.5 eV) and N 1s peak (399.5 eV), as shown in **Figure 3.3c**. From the quantitative analysis of elemental composition, the content of C, O, and N were 81.4, 5.2, and 13.4 at%, respectively. The N doping content in CN–G had a higher level than those reported in previous works (ca. 1–7 at%) (**Table 3.2**). Such a high N doping level in CN–G is likely due to less decomposition of N atoms under low reaction temperature of SP. The XPS N 1s spectrum can be deconvoluted into four peaks associated with various types of N bonding configurations, including pyridinic N (N_P: 398.5 ± 0.1 eV), pyrrolic N (N_{PR}: 400.0 ± 0.1 eV), cationic N (N_C: 401.3 ± 0.2 eV), and oxidized-N (N_{OX}: 403.5 ± 0.2 eV).[18,28,29] The N 1s peak was mainly contributed by N_P (48.5%), N_C (28.4%), while N_{PR} (20.9%) and N_{OX} (2.2%) were minor contribution. This result indicates that most of N atoms were bonded to the surrounding

carbon atoms in the forms of N_C and N_P. Typically, when a nitrogen atom is doped into graphene lattice, there are three common bonding configurations, including quaternary N (or graphitic N), pyridinic N, and pyrrolic N. However, in this work, the N atoms favored to exist in form of N_C rather than N_G. This is likely due to two possible reasons as follows: (i) use of ILs containing cationic N as precursor and (ii) low-temperature reaction occurred in SP preventing its transformation to N_G (typically formed at high temperature). The N_P and N_{PR} measured here support Raman spectra results since they induced internal defects of the graphene structure and functionalization of the graphene sheet edge.[25]

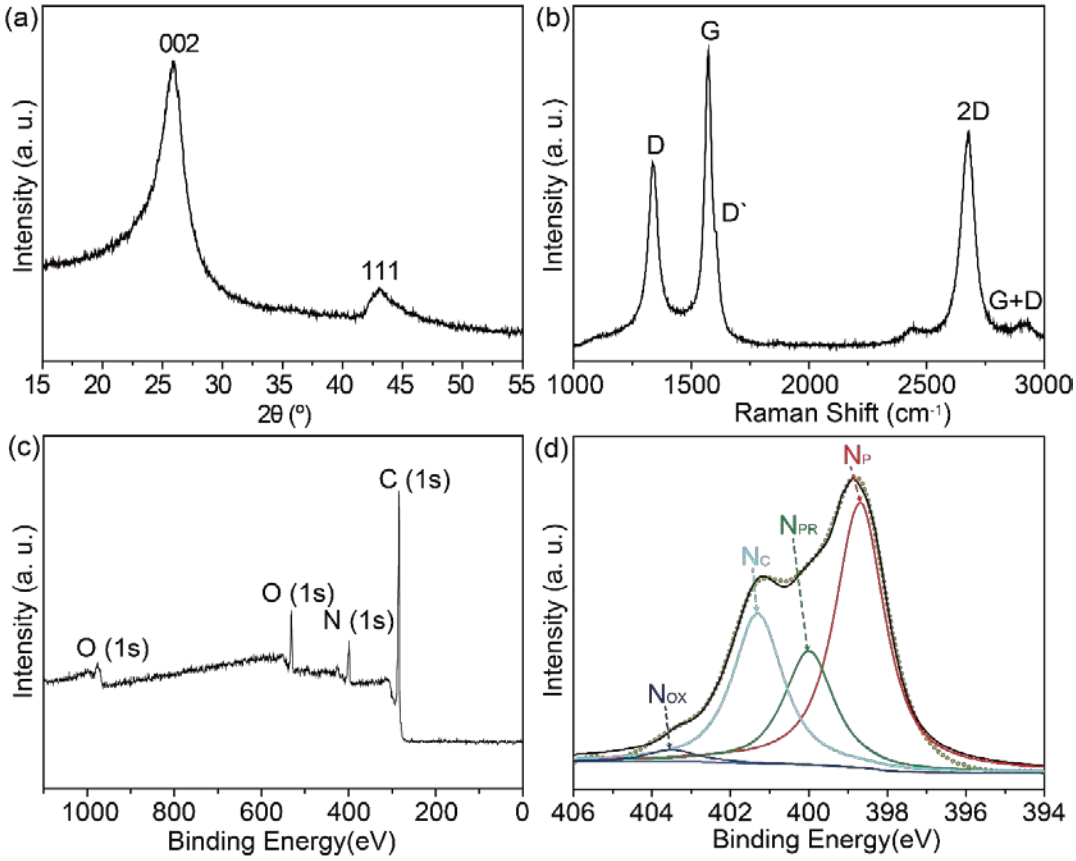

Figure 3.3. (a) XRD pattern, (b) Raman spectrum, (c) XPS survey spectrum, and high-resolution XPS N 1s spectrum of CN–G.

Table 3.2. N-doped methods and nitrogen concentration on carbon

Materials	Elemental composition (at%)			Method	Ref.
	C	O	N		
CNG	81.4	5.2	13.4	SP	Present work
N-doped carbon sheet	-	-	3.1	SP	20
N-doped graphene oxide	-	-	6.7	Hydrothermal	30
N-doped graphene sheet	-	-	3.0-5.0	Thermal treatment	31
N-doped CNFs	-	-	5.4	Electrospinning	32
N-doped graphene	-	-	4.0	CVD	33
N-doped graphene	-	-	1.0	N_2H_4 treatment	34

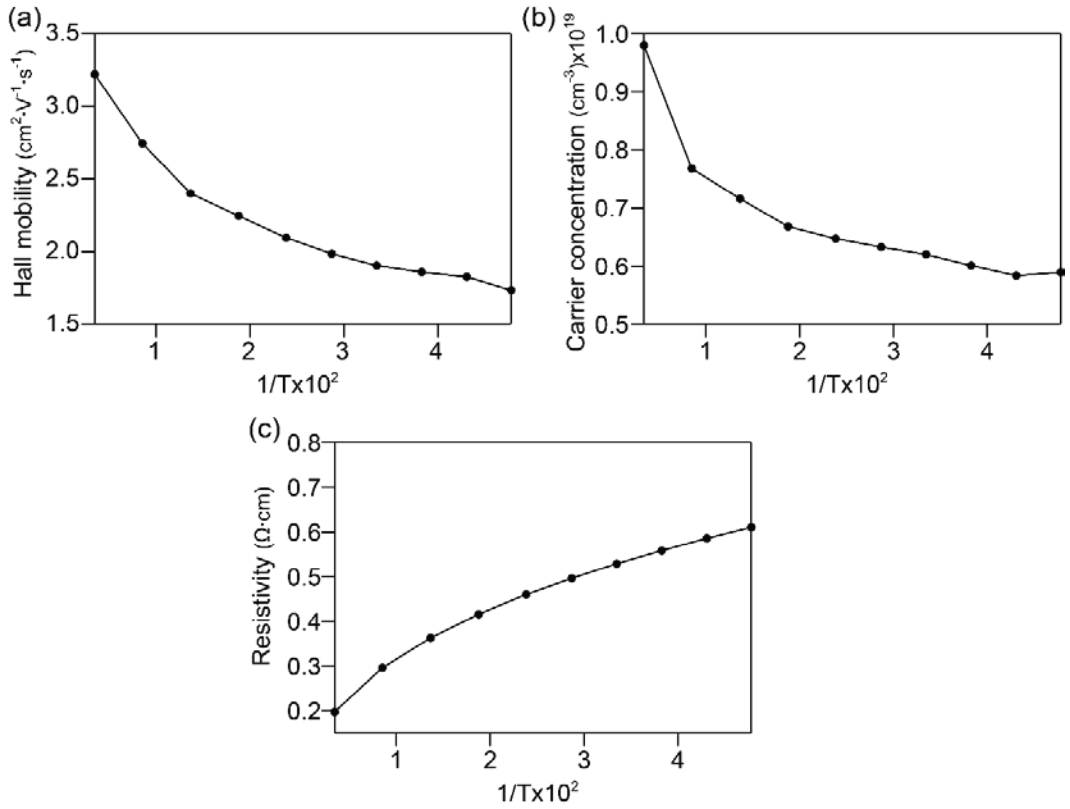

Figure 3.4. Hall-effect measurements of CN–G: (a) hall mobility, (b) carrier concentration, (c) resistivity, (d) electrical properties versus 1/*T* (*T* = 20–290 K).

Table 3.3. Electrical conductivity of CN–G by SP compared to other carbon materials in literature.

Materials	Type	Doping	Surface resistance [Ω sq^{-1}]	Hall mobility [cm² V·s^{-1}]	Carrier concentration [cm^{-3}]	Ref.
CNG	P	N	16.0	3.4	1.00E+19	Present work
PECVD	P	Au	-	25	7.00E+17	35
P-doped graphene by MBE	P	P	-	25	1.40E+17	36
Graphene-GaN	P	-	-	2.4	8.00E+17	37
Graphene-Zinc Phosphide	P	-	-	-	6.00E+16	38
Graphite	Pristine	-	-	-	5.00E+18	39

For the electrical measurements, Hall-effect measurement was performed at 20–290 K on area 4 × 4 mm^2 that was patterned on the sample using copper pressure clips in a van der Pauw configuration, at a magnetic field of 0.5 T and current of 70 mA. To test reproducibility, samples were re-measured several times and the measured data were found to be deviated less than 1%. As the temperature was lowered, the mobility and carrier concentration decreased, whereas the resistance increased (**Figure 3.4a-3.4c**). This characteristic trend indicates that CN–G behave like a semiconductor. Hall mobility and carrier concentration at 290 K were measured to be 3.4 $cm^2 \cdot V^{-1} \cdot s^{-1}$ and 10^{19} cm^{-3}, respectively. The carrier concentration is considerably high at the same level of organic semiconductors (see **Table 3.3**). The sheet resistance was measured to be 16.0 $\Omega \cdot sq^{-1}$, which is very low for carbon-based materials ever reported. The result of 4-probe measurement also showed sheet resistance of 15.0 $\Omega \cdot sq^{-1}$ and resistivity of 0.25 Ω·cm.

Normally, high N doping level in NGs can inevitably lead to the strong repulsive interactions between N dopants, which destabilize the C–C bond in graphene. Strain induced by N atoms is released by out-of-plane relaxation of carbon atoms in graphene, thus deteriorating the planar structure. This in turn leads to degradation of electrical conductivity of NG.[40] In contrast to three common N bonding configurations, the presence of cationic N can stabilize and retain the planar structure of graphene. The presence of cationic N in graphene lattice can also facilitate the electron transfer by moving through the cationic sites on the surface of the CN–G. Therefore, the superior carrier concentration and electrical conductivity of CN–G is possibly attributed to the synergistic contributions of cationic N and its planar structure.

Presumable formation mechanism of CN–G is schematically illustrated in **Figure 3.5**. Under the SP reaction field, each EMIM cation of ILs is first bound to another one through the CH activation. The combined two EMIM cations are subsequently oxidized, which make all of the N contained in the EMIM cations transform into cationic N. Due to instability of π-conjugated bonds in the 5 ring, they transform from the 5 + 5 ring to the 6 + 6 ring through the inverse stone wales (ISW) reaction.[40] Further growth and formation proceed repeatably via the above reactions,[42] eventually forming a large graphene sheet containng cation N.

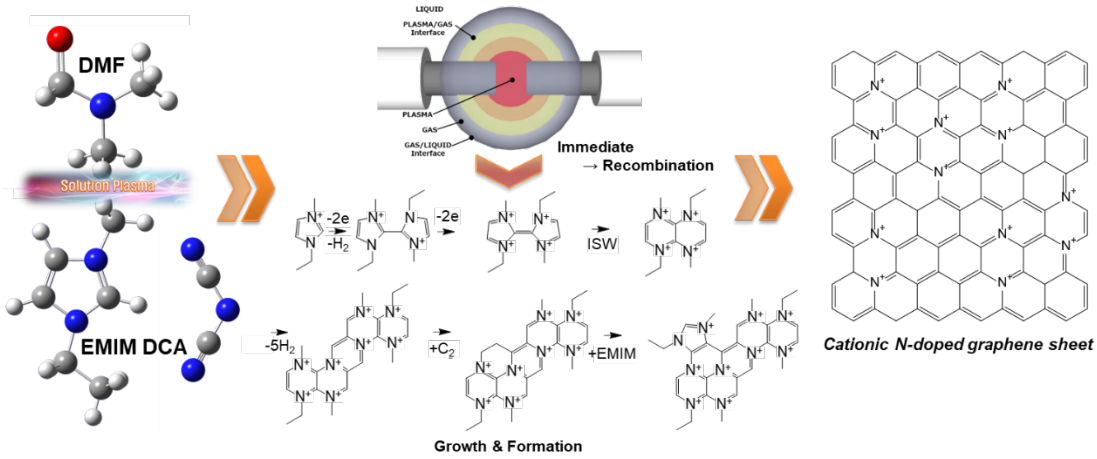

Figure 3.5. Schematic illustration showing the synthesis of CN–G from the mixture of EMIM DCA and DMF by SP.

3.4. Summary

We have successfully synthesized a novel type of graphene with cationic N doping by plasma assisted method with use of ILs and DMF as precursor. It is believed that EMIM cation and free radicals of ILs serve as the intermediate molecules for the formation of the CN–G via the ISW reaction. The characterization results revealed that CN–G exhibited a few layer graphene with high N doping content of 13.4 at%. CN–G behave like p-type semiconductors with high carrier concentration and electrical conductivity, which is likely due to the presence of cationic N and its preserved planar structure. The combination of SP and ILs shows a promising strategy in design and synthesis of NGs with cationic N doping, which cannot be achieved in other existing methods. The CN–G will be enable to potentially use in many applications in various fields, such as sensor, electronic, and energy devices.

References

(1) P. Avouris, *Nano Lett.*, 2010, **10**, 4285-4294.

(2) D. Chen, L. Tang and J. Li, *Chem. Soc. Rev.*, 2010, **39**, 3157-3180.

(3) C. Xu, B. Xu, Y. Gu, Z. Xiong, J. Sun and X. Zhao, *Energy Environmental Science*, 2013, **6**, 1388-1414.

(4) D. Wei, Y. Liu, Y. Wang, H. Zhang, L. Huang and G. Yu, *Nano Lett.*, 2009, **9**, 1752-1758.

(5) H. M. Jeong, J. W. Lee, W. H. Shin, Y. J. Choi, H. J. Shin, J. K. Kang and J. W. Choi, *Nano Lett.*, 2011, **11**, 2472-2477.

(6) L. Lai, J. R. Potts, D. Zhan, L. Wang, C. K. Poh, C. Tang, H. Gong, Z. Shen, J. Lin, R. S. J. E. Ruoff and E. Science, 2012, **5**, 7936-7942.

(7) R. Yadav and C. Dixit, *J. Sci. Adv. Mater. Devices*, 2017, **2**, 141-149.

(8) T. Schiros, D. Nordlund, L. Pálová, D. Prezzi, L. Zhao, K. S. Kim, U. Wurstbauer, C. Gutiérrez, D. Delongchamp and C. Jaye, *Nano Lett.*, 2012, **12**, 4025-4031.

(9) H.-L. Guo, P. Su, X. Kang and S.-K. Ning, *J. Mater. Chem. A*, 2013, **1**, 2248-2255.

(10) K. Xu, Y. Fu, Y. Zhou, F. Hennersdorf, P. Machata, I. Vincon, J. J. Weigand, A. A. Popov, R. Berger and X. Feng, *Angew. Chem. Int. Ed.*, 2017, **56**, 15876-15881.

(11) G.-L. Chai, Z. Hou, D.-J. Shu, T. Ikeda and K. Terakura, *J. Am. Chem. Soc.*, 2014, **136**, 13629-13640.

(12) Y. Shao, S. Zhang, M. H. Engelhard, G. Li, G. Shao, Y. Wang, J. Liu, I. A. Aksay and Y. J. J. o. M. C. Lin, 2010, **20**, 7491-7496.

(13) H. Wang, T. Maiyalagan and X. Wang, *ACS Catal.*, 2012, **2**, 781-794.

(14) S. Lee, Y. Heo, M. A. Bratescu, T. Ueno and N. Saito, *Phys. Chem. Chem. Phys.*, 2017, **19**, 15264-15272.

(15) K. Hyun, T. Ueno and N. Saito, *Jpn. J. Appl. Phys.*, 2015, **55**, 01AE18.

(16) G. Panomsuwan, N. Saito and T. Ishizaki, *Phys. Chem. Chem. Phys.*, 2015, **17**, 6227-6232.

(17) G. Panomsuwan, S. Chiba, Y. Kaneko, N. Saito and T. Ishizaki, *J. Mater. Chem. A*, 2014, **2**, 18677-18686.

(18) G. Panomsuwan, N. Saito and T. Ishizaki, *ACS Appl. Mater. Interfaces*, 2016, **8**, 6962-6971.

(19) K. Hyun and N. Saito, *Sci. Rep.*, 2017, **7**, 3825.

(20) K. Hyun, T. Ueno, O. L. Li and N. Saito, *RSC Adv.*, 2016, **6**, 6990-6996.

(21) J. S. Lee, X. Wang, H. Luo and S. J. A. M. Dai, 2010, **22**, 1004-1007.

(22) S. Xu, Q. Xu, N. Wang, Z. Chen, Q. Tian, H. Yang and K. Wang, *Chem. Mater.*, 2015, **27**, 3262-3272.

(23) L. G. Cançado, A. Jorio, E. M. Ferreira, F. Stavale, C. Achete, R. Capaz, M. Moutinho, A. Lombardo, T. Kulmala and A. Ferrari, *Nano Lett.*, 2011, **11**, 3190-3196.

(24) M. M. Lucchese, F. Stavale, E. M. Ferreira, C. Vilani, M. Moutinho, R. B. Capaz, C. Achete and A. Jorio, *Carbon*, 2010, **48**, 1592-1597.

(25) D. Deng, X. Pan, L. Yu, Y. Cui, Y. Jiang, J. Qi, W.-X. Li, Q. Fu, X. Ma and Q. Xue,

Chem. Mater., 2011, **23**, 1188-1193.

(26) P. R. Kidambi, C. Ducati, B. Dlubak, D. Gardiner, R. S. Weatherup, M.-B. Martin, P. Seneor, H. Coles and S. Hofmann, *J. Phys. Chem. C*, 2012, **116**, 22492-22501.

(27) C. Casiraghi, S. Pisana, K. Novoselov, A. Geim and A. Ferrari, *Appl. Phys. Lett.*, 2007, **91**, 233108.

(28) J. Wei, Y. Hu, Y. Liang, B. Kong, J. Zhang, J. Song, Q. Bao, G. P. Simon, S. P. Jiang and H. Wang, *Adv. Funct. Mater.*, 2015, **25**, 5768-5777.

(29) F. Ye, B. Zhao, R. Ran and Z. Shao, *J. Power Sources*, 2015, **290**, 61-70.

(30) J. Yang, M. R. Jo, M. Kang, Y. S. Huh, H. Jung and Y.-M. Kang, Carbon, 2014, 73, 106-113.

(31) Y. Qiu, X. Zhang and S. Yang, Phys. Chem. Chem. Phys., 2011, 13, 12554-12558.

(32) K. Huang, M. Li, Z. Chen, Y. Yao and X. Yang, Electrochim. Acta, 2015, 158, 306-313.

(33) L. Qu, Y. Liu, J.-B. Baek and L. Dai, ACS Nano, 2010, 4, 1321-1326.

(34) D.-W. Wang, I. R. Gentle and G. Q. M. Lu, Electrochem. Commun., 2010, 12, 1423-1427.

(35) W. Wang, K. Leung, W. Fong, S. Wang, Y. Hui, S. Lau, Z. Chen, L. Shi, C. Cao and C. Surya, J. Appl. Phys., 2012, 111, 093520.

(36) J.-H. Min, W.-L. Jeong, H.-M. Kwak and D.-S. Lee, Sci. Rep., 2017, 7, 10225.

(37) H. Tian, Q. Liu, A. Hu, X. He, Z. Hu and X. Guo, Opt. Express, 2018, 26, 5408-5415.

(38) O. Vazquez-Mena, J. P. Bosco, O. Ergen, H. I. Rasool, A. Fathalizadeh, M. Tosun, M. Crommie, A. Javey, H. A. Atwater and A. Zettl, Nano Lett., 2014, 14, 4280-4285.

(39) K. Novoselov, A. Geim, S. Morozov, S. Dubonos, Y. Zhang and D. Jiang, arXiv preprint cond-mat/0410631, 2004.

(40) W. J. Lee, U. N. Maiti, J. M. Lee, J. Lim, T. H. Han and S. O. Kim, *Chem. Commun.*, 2014, **50**, 6818-6830.

(41) M. T. Lusk and L. D. Carr, *Phys. Rev. Lett.*, 2008, **100**, 175503.

(42) T. Morishita, T. Ueno, G. Panomsuwan, J. Hieda, A. Yoshida, M. A. Bratescu and N. Saito, *Sci. Rep.*, 2016, **6**, 36880.

Chapter 4

Cationic Nitrogen-Doped Carbon-Wrapped Single-Walled Carbon Nanotubes with High Electrical Conductivity

Chapter 4 - Cationic Nitrogen-Doped Carbon-Wrapped Single-Walled Carbon Nanotubes with High Electrical Conductivity

4.1. Introduction

Tuning the electronic properties of carbon nanotubes (CNTs) by chemical doping with heteroatoms has been considered as one of the most promising approaches to extend the applications of CNTs in diverse areas of electronic, optical, sensor, and energy applications.[1,2] Thus far, doping with a single atom or multiple atoms of nitrogen, phosphorus, and boron in heteroatom-doped CNTs has been carried out often.[3] Nitrogen and phosphorus are electron-donating atoms, yielding n-type semiconducting behavior.[4] On the contrary, boron is an electron-withdrawing atom, yielding p-type semiconducting behavior.[5] Among the above-mentioned heteroatoms, considerable attention has been focused on the incorporation of nitrogen into the sp^2 structure of CNTs as it can significantly tailor their electronic structure.[6] According to the recent experimental data and theoretical calculations by density function theory, the electronic and transport properties of nitrogen-doped CNTs can be systematically tuned depending on the manner in which nitrogen atoms are incorporated into the carbon structure.[7] There are three main possible types of configurations of bonded nitrogen incorporated in the carbon structure, i.e., (i) graphitic or quaternary N, (ii) pyridinic N, and (iii) pyrrolic N, respectively.[8] A majority of studies have reported a similar tendency, i.e., the direct substitution of graphitic N or quaternary N plays a vital role in maximizing the electrical and transport properties of n-type CNT semiconductors to meet practical needs of advanced electronic devices.[9] However, the *in situ* and *ex situ* doping of nitrogen at high levels may inevitably cause unwanted side effects, i.e., distortion and breaking of the crystallity of the

tubular structure, leading to the deterioration of electrical and transport properties of nitrogen-doped CNTs.[10] Therefore, it is imperative to preserve their tubular strucure as much as possible to realize the desired electrical conductivity and charge transport.

From a molecular viewpoint, another possible configuration of nitrogen exists, i.e., the cationic form (N^+), which has not been focused much in the literatures of nitrogen-doped carbon materials. Cationic nitrogen can be incorporated into the carbon structure via direct substitution similar to that of graphitic or quaternary configuration via bonding with three neighboring carbon atoms, with no remaining electrons because nitrogen exhibits valence electrons equivalent to carbon.[6,11] Such cationic nitrogen can lead to a dramatic change in the local density of state around the Fermi level, thereby tailoring the electronic structure of the sp^2 carbon framework.[12] On the basis of theoretical simulations, unlike other nitrogen-bonding configurations, cationic nitrogen can preserve the planar or tubular structure without breaking crystallinity.[13] Thus far, the study of cationic nitrogen-doped carbons is still a dubious topic that needs to be unraveled. Despite significant progress in the synthesis method of nitrogen-doped carbon (i.e., by using chemical vapor deposition, thermal treatment, and pyrolysis),[9] the development of a simple, effective method to dope nitrogen of a selective cationic form with control is still a longstanding challenge.

In this study, cationic nitrogen-doped carbons wrapped around single-walled carbon nanotubes (CN–C@SWCNT) were synthesized by solution plasma (SP) for the first time to the best of our knowledge. Cationic nitrogen was not directly doped into SWCNTs, but in the carbon materials wrapped around SWCNTs. SP is a powerful tool developed by our group for synthesizing nitrogen-doped nanocarbons using a wide selection of nitrogen-containing organic precursors, including aniline,[14] pyridine,[15] acrylonitrile,[16] cyanopyrazine,[17] and *N*-methyl-2-pyrrolidone.[18] In this study, CN–C@SWCNTs were synthesized via the generation of SP at the wire-to-wire electrode gap immersed in a mixture of aniline, water, and HCl with dispersed SWCNTs (**Figure 4.1**). Aniline is an essential molecule due to the presence of lone-pair electrons on the nitrogen atom. The aniline in 1M HCl aqueous solution provide

phenylammonium ions ($C_6H_5NH_3^+$), which are electrically attracted to the negatively charged surface of SWCNTs.[19] Phenylammonium ions can serve as a precursor for the formation of doped cationic nitrogen in CN–C.[20] After the generation of plasma, phenylammonium ions attracted on the SWCNT surface are converted into carbon materials in the presence of doped cationic nitrogen. Raman spectroscopy and X-ray photoelectron spectroscopy (XPS) verified the presence of doped cationic nitrogen. Electrical conductivity was evaluated by a four-point probe measurement. In addition, the carrier concentration and carrier mobility were evaluated by hall measurements with a van der Pauw configuration.

4.2. Experimental procedures

4.2.1 *Solution preparation and synthesis of CN–C@SWCNT by SP.*

Aniline ($C_6H_5NH_2$, purity 99.0%), hydrochloric acid (HCl, purity 35.0–37.0%), hydrogen peroxide (H_2O_2, purity 34.5%), *N*-methyl-2-pyrrolidinone (NMP, $CH_3NC_4H_6O$, purity 99.0%), and sulfuric acid (H_2SO_4, 0.5 M) were purchased from Kanto Chemicals. All chemicals were used without any further purification. Ultrapure water with a resistivity of 18.2 MΩ cm at 25 °C was obtained from an Aquarius water purification system (RFD250NB, Advantec, Japan).

1 M HCl (100 mL), aniline (1.25 mL), SWCNT (200 mg, Meijo Carbon), and ultrapure water (30 mL) were mixed and stirred for 15 min in a 200 mL glass beaker, which was specially designed for an SP reactor. **Figure 4.1a** shows the schematic of the experimental setup for SP. Nickel (Ni, purity 99.99%, Nilaco) wire electrodes with a diameter of 1 mm were shielded using an insulating ceramic tube and placed into the SP reactor. The electrode gap distance was adjusted at 0.5 mm. A bipolar pulsed power supply (MPP-HV04, Kurita Seisakusho) was employed to generate and sustain the SP in the mixture. The applied voltage between the electrodes was maintained to produce plasma for 15 min at a repetition frequency of 35 kHz and a pulse width of 1.0 μs. The plasma was generated under vigorous stirring at ambient temperature and atmospheric pressure. Then, 18 mL of a 6 wt% H_2O_2 solution was slowly dropped to neutralize the solution. After 12 h, the synthesized sample was obtained by vacuum

filtration using a polytetrafluoroethylene (PTFE, JVWP04700, Merck Millipore) membrane filter (pore size of 0.1 μm), washed several times with distilled water and 0.5 M H_2SO_4, and dried in a vacuum oven at 80 °C for 3 h. The synthesis rates of CN–C and CN–C@SWCNT were ~93 and 130 mg min^{-1}, respectively.

4.2.2 *Characterization*

The dried sample was dispersed in ethanol under ultrasonication for 10 min. Then, the suspension was dropped onto a TEM grid, which was analyzed by TEM (JEM-2500SE, JEOL) and STEM-EDS at an acceleration voltage of 200 kV. FE-SEM (S-4800, Hitachi High-Technologies) images were recorded at an acceleration voltage of 10 kV, with a probe current of 5 μA, and a working distance of 40 mm. XPS (PHI 5000 VersaProbe II, ULVAC-PHI) spectra recorded using a Mg Kα line as the X-ray source were accumulated with a pass energy of 46.9 eV and an acquisition step of 0.5 eV. XRD patterns were recorded on an X-ray diffractometer (SmartLab, Rigaku) using Cu Kα as the X-ray source with an accelerating voltage of 45 kV and a current of 200 mA. The diffraction angle (2θ) was scanned from 10° to 80° at a scan speed of 2.4° min^{-1}, step size of 0.02°, a distributing slit of 0.5°, a scattering slit of 0.5°, and a receiving slit of 0.15 mm. Raman spectra were recorded on a Raman spectroscope (NRS-100, JASCO) with a laser excitation wavelength of 532.5 nm. A high-magnification objective lens of 50× was used in the Raman microscope. Raman spectra were recorded at wavenumbers ranging from 100 to 3000 cm^{-1} by averaging five acquisitions at an exposure time of 10 s at ambient temperature. Resistivity was estimated using a four-point probe device (Loresta-GP MCP-T610, Mitsubishi Chemicals) at room temperature. For the measurements, the samples were pressed into a pellet using a metal mold at 5 MPa in air. In addition, the sample used for Hall-effect measurements was prepared by using the same method.

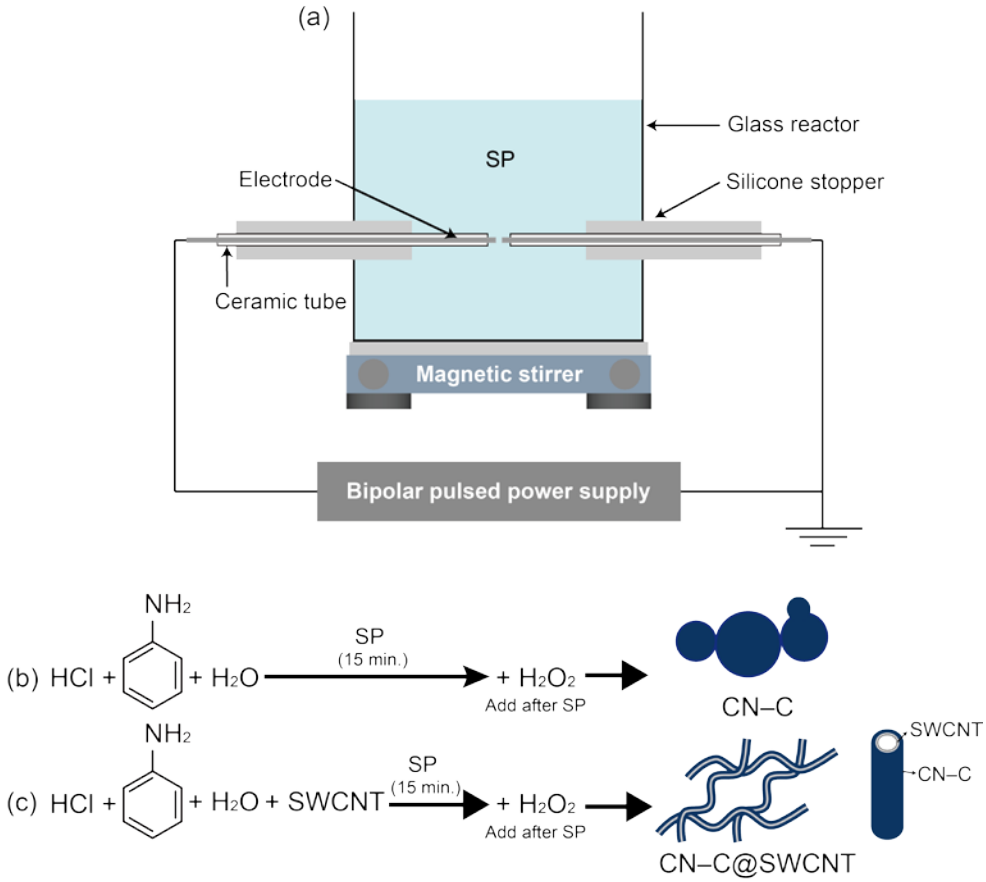

Figure 4.1. (a) Schematic of the SP experimental setup with a wire-to-wire electrode configuration. The synthesis of (b) CN–C in an aniline aqueous solution and (c) CN–C@SWCNT in an aniline aqueous solution with the SWCNT dispersion.

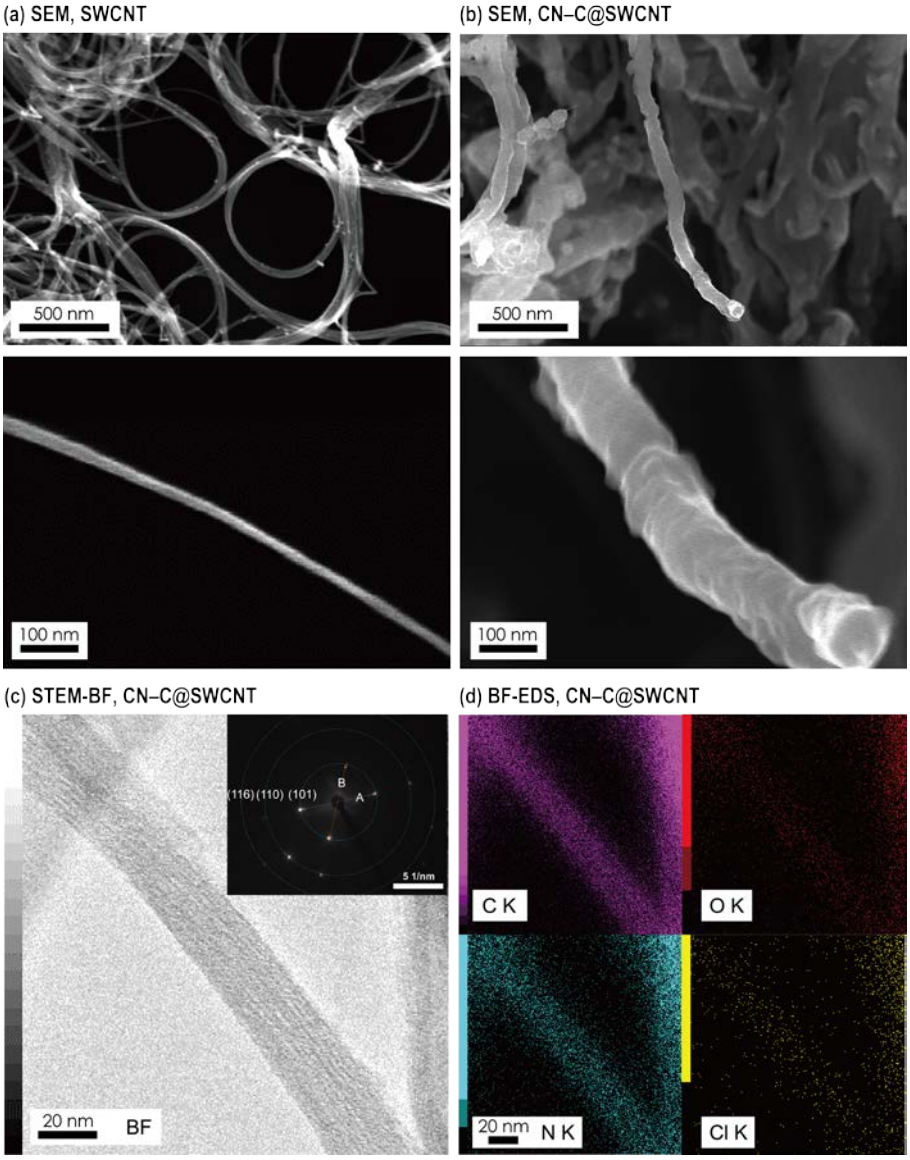

Figure 4.2. FE-SEM images of (a) bundle SWCNT and (b) CN–C@SWCNT. (c) STEM-BF image of the bundle SWCNT wrapped by CN–C (inset shows the electron diffraction (ED) pattern), (d) EDS mapping images of CN–C@SWCNT in (c) confirming the presence of C, O, N, and Cl.

Table 4.1. Crystal structural parameters and experimental ED pattern in the reflection configuration of CN–C@SWCNT.

CN–C@SWCNT	**Graphite, JCPDS card 41-1487**		
d spacing (nm, ± 0.02)	*d* spacing	hkl	Intensity
	0.338	002	100
0.206	0.204	101	50
	0.168	004	80
0.124	0.123	110	30
	0.116	112	50
	0.099	114	40
0.084	0.083	116	40

4.3. Results and discussion

First, field-emission scanning electron microscopy (FE-SEM) and transmission electron microscopy (TEM) images of CN–C@SWCNT were recorded to observe their morphology. **Figure 4.2a** and **4.2b** show the FE-SEM images of pristine SWCNT and CN–C@SWCNT, respectively. Each SWCNT bundle was uniformly wrapped by CN–C. **Figure 4.2d** shows the elemental mapping image: C, N, O, and Cl were evenly distributed over CN–C@SWCNT. In the ED pattern of CN–C@SWCNT (inset of **Figure 4.2c**), discrete diffraction spots in each circle corresponding to Bragg reflections were observed, which were assigned to the (101), (110), and (116) planes of graphite (JCPDS card no. 41-1487, **Table 4.1**).[21] Four diffraction spots were clearly observed along the (101) ring, possibly revealing the presence of CN–C wrapped around the SWCNTs. Typically, the angle between line A and line B should be 60° in case of a hexagonal structure for graphene. However, the angle between line A and line B for CN–C@SWCNT was 65.09°, and such an angle distortion is thought to be related to a structural change induced by the presence of cationic nitrogen in the carbon structure.

Figure 4.3 shows the Raman spectra of CN–C, SWCNT, and CN–C@SWCNT. Two pronounced peaks were observed for CN–C at 1590 and 1350 cm^{-1}, respectively. The former and latter bands corresponded to the G band, related to the sp^2 carbon systems, and to the D band, related to structural defects. For pristine SWCNT, the G and 2D bands were observed, whereas the D band was not detected. After wrapping with CN–C, the G and 2D bands of CN–C@SWCNT became broader compared with pristine SWCNT. Notably, several small bands were observed at 1000–1500 cm^{-1}. The weak band at 1473 cm^{-1} corresponded to the C=N stretching mode of imine. In addition, the bands corresponding to $C–N^+$ stretching in the polaron bond (cationic amine unit of the benzenoid ring) and $C–N^{\bullet+}$ stretching in the bipolaron form (cationic amine units of the quinoid ring) were observed at 1338 and 1312 cm^{-1}, respectively.[22,23] This result is further evidence for the presence of cationic nitrogen in CN–C@SWCNT. Oppositely, these peaks were not observed for CN–C because of carbon structure become disorder..

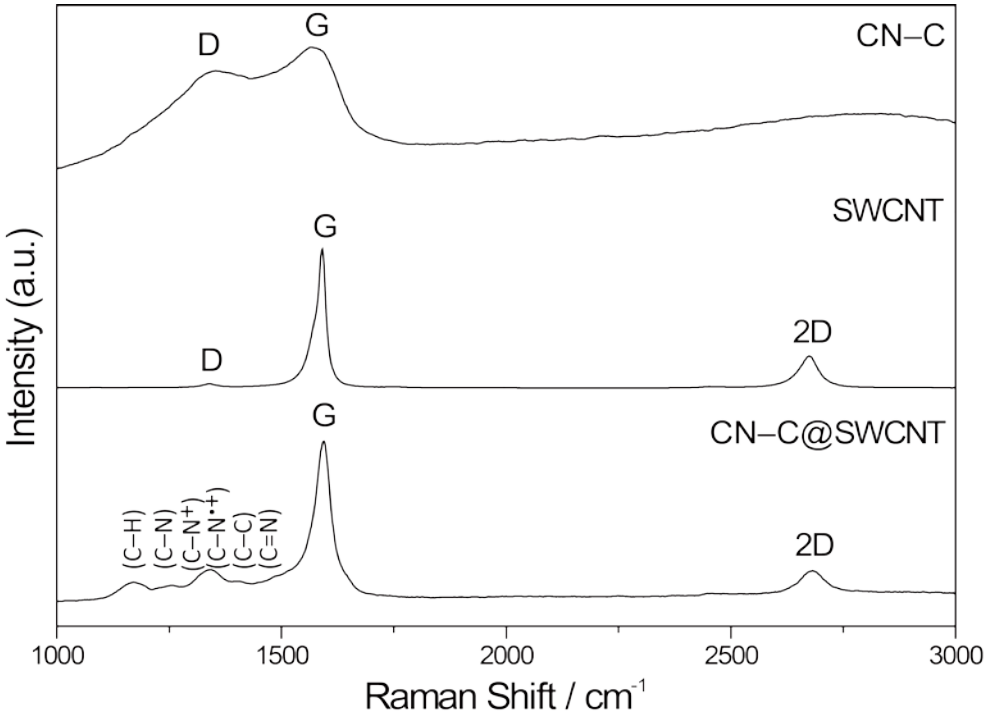

Figure 4.3. Raman spectra of (a) CN–C, SWCNT, and CN–C@SWCNT.

The XPS survey spectra of CN–C and CN–C@SWCNT revealed four peaks at 284.5, 399.5, 532.5, and 200.0 eV, corresponding to C 1s, N 1s, O 1s, and Cl 2p, respectively (**Figure 4.4**). This result is in good agreement with the aforementioned elemental mapping analysis, again confirming the presence of C, N, O, and Cl. From XPS quantitative analysis, the content of N in CN–C and CN–C@SWCNT was at the same level (7.8 at%). However, the [N]/[C] ratios for CN–C and CN–C@SWCNT were 0.09 and 0.08, respectively. The lower [N]/[C] ratio for CN–C@SWCNT was related to the high carbon content originating from SWCNT (86.3 at%). The high-resolution C 1s XPS spectra of CN–C and CN–C@SWCNT were deconvoluted into three peaks (**Figure 4.5a**). The most intense peak was observed at 284.4 ± 0.1 eV, revealing that carbon is present as a C=C (sp^2) bond in the graphite form. The other two peaks of the C 1s XPS peak corresponded to C–N (285.4 ± 0.1 eV) and C–O (286.4 ± 0.1 eV), respectively. The high-resolution Cl 2p XPS spectra (**Figure 4.5c**) corresponded to chloride anion Cl $2p_{3/2}$ (197.1 ± 0.1 eV), chloride anion Cl $2p_{1/2}$ (199.0 ± 0.1 eV), covalent chlorine Cl $2p_{3/2}$ (200.2 ± 0.1 eV), and covalent chlorine Cl $2p_{1/2}$ (202.2 ± 0.2 eV).[24] The [Cl]/[N] ratios for CN–C and CN–C@SWCNT were 0.09 and 0.13, respectively. A high [Cl]/[N] ratio for CN–C@SWCNT aided in the production of increased cationic nitrogen.[25]

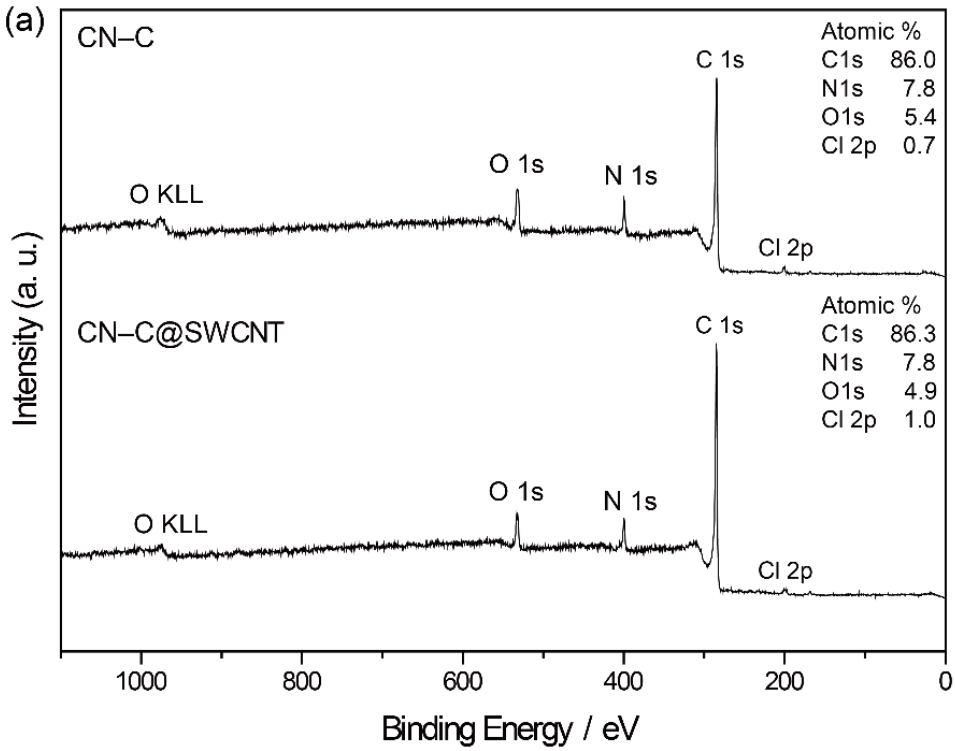

Figure 4.4. XPS survey spectra of CN–C and CN–C@SWCNT.

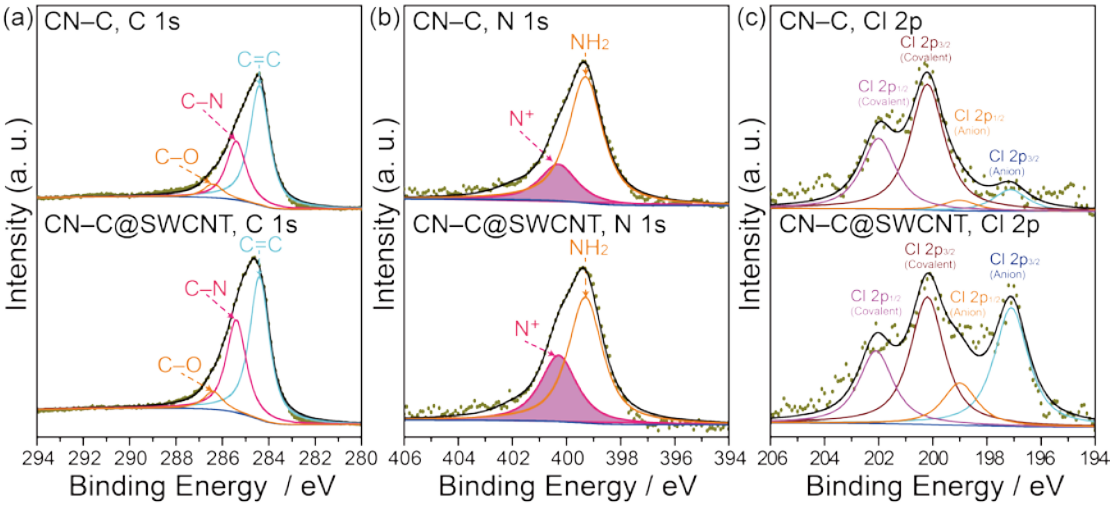

Figure 4.5. High-resolution XPS spectra with peak deconvolution of (a) C 1s, (b) N 1s, and (c) Cl 2p for CN–C and CN–C@SWCNT.

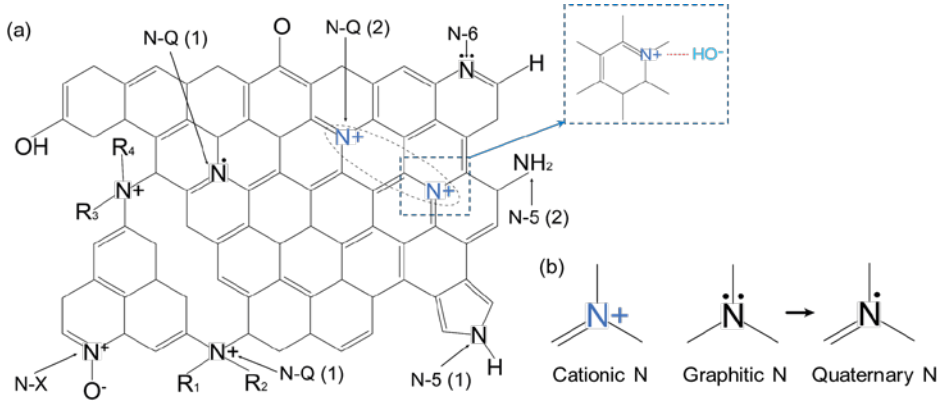

Figure 4.6. (a) Various nitrogen-bonding configurations in the carbon structure. (b) Chemical structures of cationic N, graphitic N, and quaternary N, with similar XPS binding energies.

Table 4.2. Classification of various nitrogen-bonding states according to XPS binding energies.

N-bonding denoted / Structure	N-bonding states name	BE (eV) literature	Ref.
N-6 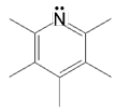	Pyridinic (398.2–398.8 eV)	398.2 398.3 398.4 398.5 398.6 398.7 398.8	26 27 28 29 30 31 32
N-5 (1) 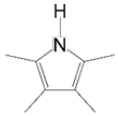	Pyrrolic (399.7–400.2 eV)	399.7 399.8 399.9 400.1 400.2	30 32 29 33 27
N-5 (2) 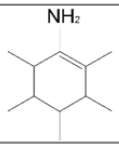	Amino (399.3–399.6 eV)	399.3 399.4 399.5 399.6	25 29 34 26
N-Q (1) 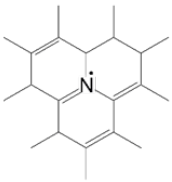	Quaternary or Graphitic (401.2–401.8 eV)	401.2 401.3 401.4 401.5 401.6 401.7 401.8	30 27 35 36 37 38 26
N-Q (2) 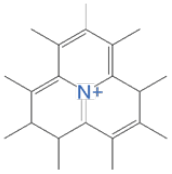	Cationic (400.3–401.4 eV)	400.3 400.3 400.4 400.4 >401.0 401.4	39 40 41 42 25 43
N-X 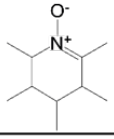	Oxidized (402.0–405.0 eV)	402.0–405.0 402.0–405.0 402.0–405.0 402.0–405.0	44 45 46 47

Table 4.3. Chemical structure descriptor in the literature.

Descriptor in other papers	Descriptor in our paper	N-bonding states name	Ref.
		N-Q (1) Quaternary	26, 33, 34
		N-Q (1) Graphitic	28, 37
		N-Q (2) Cationic	27, 47

Table 4.4 Chemical-state compositions of CN–C and CN–C@SWCNT.

Sample	Composition (at%)									
	C=C	C–N	C–O	NH_2	N^+	OH^-	CHO	C–OH	Cl^-	Cl
CN–C	53.6	26.3	6.3	5.9	1.9	2.0	1.9	1.5	0.1	0.6
CN–C@SWCNT	48.7	31.6	6.0	4.8	3.0	2.6	1.0	1.3	0.4	0.6

Figure 4.6 shows the various possible types of nitrogen-bonding states observed in the carbon materials. The most frequently observed types included pyridinic (N-6, 398.5 eV),[48,49] pyrrolic (N-5 (1), 400.1 eV),[50,51] and quaternary (N-Q (1), 401.1 eV).[33,34] Other possible types included amine (N-5 (2) 399.3 eV),[29,52] pyridinic N oxide (N-X, 402–405 eV), and cationic N (N-Q (2), 400.3 eV).[44,47] **Table 4.2** summarizes the classification of the different nitrogen-bonding states according to the XPS binding energies. Several studies have utilized different chemical structure descriptors; however, in this paper, the exact descriptor was defined and illustrated in **Table 4.3**. Owing to cationic N enhanced by chloride anions, the nitrogen atoms should be incorporated in the carbon structure in the form of cationic N rather than graphitic N or quaternary N, as indicated by Raman spectra and ED results. Thus, the high-resolution N 1s XPS spectra are deconvoluted into two main peaks, corresponding to amino N (399.3 ± 0.1 eV) and cationic N (400.3 ± 0.2 eV), respectively (**Figure 4.5b**).[25,47] The relative percentage of amino for CN–C was found to be dominant (65.7%), whereas that of cationic N was found to be minor (24.3%). For CN–C@SWCNT, the relative percentage of cationic N increased to 38.6%, possibly enhanced by the electrostatic effect between phenylammonium ions and SWCNT.[19] **Table 4.4** shows the composition of each chemical state (at%) for CN–C and CN–C@SWCNT as obtained from XPS measurements. Chloride anions are thought to play an essential role for promoting the generation of doped cationic nitrogen in CN–C and CN–C@SWCNT.

For the electrical measurements, electrical conductivity was estimated by a four-point probe method at room temperature. The electrical conductivities of SWCNT and CN–C were 0.74 and 4.31 S cm^{-1}, respectively. Interestingly, CN–C@SWCNT exhibited an excellent electrical conductivity of 120 S cm^{-1}; this value is approximately 160-fold greater than that of pristine SWCNTs. This value constitutes the highest electrical conductivity ever reported for nitrogen-doped carbon materials in literatures (**Table 4.5**). Furthermore, hall-effect measurements were further carried out at 298.6 K on an area that was patterned on the samples using copper pressure clips in the van der Pauw configuration under a magnetic field of 0.5 T and a current

of 70 mA. **Table 4.6** shows the Hall mobility and carrier concentration were estimated to be 2.1 $cm^2 V^{-1}$ and 4.6×10^{20} cm^{-3}, respectively. Interestingly, holes serve as majority carriers in CN–C and CN–C@SWCNTs rather than electrons (n-type), indicative of p-type semiconducting behavior. The carrier concentration of CN–C@SWCNT was considerably greater than those of p-type CNT and p-type graphene (~10^{16} to 10^{18} cm^{-3}),[53,54] as well as at the same level of a p-type organic semiconductor.[55] The sheet resistance was found to be 0.12 Ω/sq; this value is less than those observed for other carbon-based materials.[56] The samples were tested several times, and the data were found to vary within 1%. The remarkably enhanced electrical conductivity and charge carrier concentration for CN–C@SWCNT were related to the synergistic combination of the following reasons: (i) doping of cationic nitrogen in CN–C induces a change in the electronic structure of the sp^2 carbon framework,[57] (ii) SWCNT serves as a conductive bridge between the conductive domains of CN–C,[19] and (iii) among SWCNTs enables good contact by wrapped CN–C. **Figure 4.7** shows a schematic highlighting the excellent conductivity of CN–C@SWCNT.

Table 4.5. Electrical conductivities of CN–C, SWCNT, and CN–C@SWCNT compared with other carbon materials reported previously.

Material	Electrical conductivity / S cm^{-1}	Ref.
N-doped carbon nanosheet	18.87	18
N-doped CNF	15.38	58
N-doped CNT	25.00	59
N-doped graphene	6.67	60
Graphene	10.00	Aldrich 900561
XC–72	12.50	60
Super P–Li	9.30	61
PANI/MWCNT composite	33.37	62
CN–C	4.31	This work
SWCNT	0.74	This work
CN–C@SWCNT	120.00	This work

Table 4.6. Electrical characteristics of CN–C and CN–C@SWCNT.

Sample	Hall mobility ($cm^3\ V^{-1}\ s^{-1}$)	Carrier type	Carrier concentration (cm^{-3})	Sheet resistance ($\Omega\ sq^{-1}$)	Electrical conductivity ($S\ cm^{-1}$)
CN–C	0.4	p-type	7.3×10^{18}	10.60	4.31
CN–C@SWCNT	2.1	p-type	4.6×10^{20}	0.12	120.00

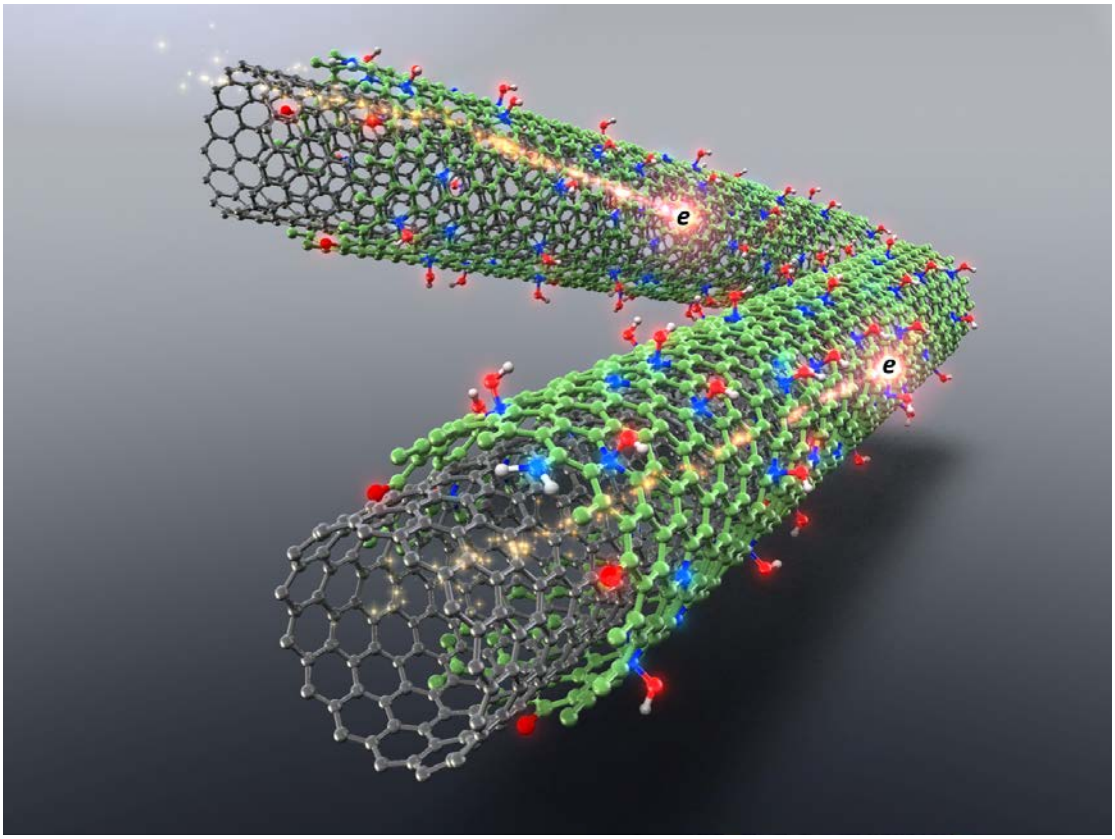

Figure 4.7. Schematic of the CN–C@SWCNT in the presence of cationic nitrogen (blue)..

4.4. Summary

In summary, CN–C@SWCNT was successfully synthesized via SP using an aniline aqueous solution as the precursor. Raman spectroscopy, ED patterns, and XPS verified the presence of cationic nitrogen in CN–C@SWCNT. CN–C@SWCNT exhibited p-type semiconducting behavior, with an excellent electrical conductivity of 120 S cm^{-1} and a high carrier concentration of 4.6×10^{20} cm^{-3}. Such an electrical property of CN–C@SWCNT was mainly related to the synergistic effects of cationic nitrogen, a conducting bridge between CN-C and SWCNT conducting domains, and good contact among SWCNTs. The successful approach by SP in this study has paved a new, efficient method for synthesizing cationic nitrogen-doped carbon materials. In addition, p-type CN–C@SWCNT with excellent electrical conductivity can be anticipated to demonstrate potential for advanced electronic devices.

References

(1) M. F. De Volder, S. H. Tawfick, R. H. Baughman and A. J. Hart, *Science*, 2013, **339**, 535-539.

(2) P. W. Barone, S. Baik, D. A. Heller and M. S. Strano, *Nat. Mater.*, 2005, **4**, 86.

(3) a) Y. Zhao, L. Yang, S. Chen, X. Wang, Y. Ma, Q. Wu, Y. Jiang, W. Qian and Z. Hu, *J. Am. Chem. Soc.*, 2013, **135**, 1201-1204. B) R. Czerw, M. Terrones, J.-C. Charlier, X. Blase, B. Foley, R. Kamalakaran, N. Grobert, H. Terrones, D. Tekleab and P. Ajayan, *Nano Lett.*, 2001, **1**, 457-460. c) B. Wei, R. Spolenak, P. Kohler-Redlich, M. Rühle and E. Arzt, *Appl. Phys. Lett.*, 1999, **74**, 3149-3151. d) I. Maciel, J. Campos-Delgado, E. Cruz-Silva, M. Pimenta, B. Sumpter, V. Meunier, F. López-Urías, E. Munoz-Sandoval, H. Terrones and M. Terrones, *Nano Lett.*, 2009, **9**, 2267-2272.

(4) E. Cruz-Silva, F. Lopez-Urias, E. Munoz-Sandoval, B. G. Sumpter, H. Terrones, J.-C. Charlier, V. Meunier and M. Terrones, *ACS Nano*, 2009, **3**, 1913-1921.

(5) L. Panchakarla, K. Subrahmanyam, S. Saha, A. Govindaraj, H. Krishnamurthy, U. Waghmare and C. Rao, *Adv. Mater.*, 2009, **21**, 4726-4730.

(6) W. J. Lee, U. N. Maiti, J. M. Lee, J. Lim, T. H. Han and S. O. Kim, *Chem. Commun.*, 2014, **50**, 6818-6830.

(7) F. Xu, Z. Yu, Z. Gong and H. Jin, *Front. Phys.*, 2017, **12**, 127306.

(8) Z.-H. Sheng, L. Shao, J.-J. Chen, W.-J. Bao, F.-B. Wang and X.-H. Xia, *ACS Nano*, 2011, **5**, 4350-4358.

(9) Q. Wei, X. Tong, G. Zhang, J. Qiao, Q. Gong and S. Sun, *Catalysts*, 2015, **5**, 1574-1602.

(10) a) E. Ibrahim, V. O. Khavrus, A. Leonhardt, S. Hampel, S. Oswald, M. H. Rümmeli and B. Büchner, *Diamond Relat. Mater.*, 2010, **19**, 1199-1206. b) O. Y. Podyacheva, S. V. Cherepanova, A. I. Romanenko, L. S. Kibis, D. A. Svintsitskiy, A. I. Boronin, O. A. Stonkus, A. N. Suboch, A. V. Puzynin and Z. R. Ismagilov, *Carbon*, 2017, **122**, 475-483.

(11) H. Kim, K. Lee, S. I. Woo and Y. Jung, *Phys. Chem. Chem. Phys.*, 2011, **13**, 17505-17510.

(12) K. Xu, Y. Fu, Y. Zhou, F. Hennersdorf, P. Machata, I. Vincon, J. J. Weigand, A. A. Popov, R. Berger and X. Feng, *Angew. Chem. Int. Ed.*, 2017, **56**, 15876-15881.

(13) G.-L. Chai, Z. Hou, D.-J. Shu, T. Ikeda and K. Terakura, *J. Am. Chem. Soc.*, 2014, **136**, 13629-13640.

(14) K. Hyun, T. Ueno and N. Saito, *Jpn. J. Appl. Phys.*, 2015, **55**, 01AE18.

(15) S. Lee, Y. Heo, M. A. Bratescu, T. Ueno and N. Saito, *Phys. Chem. Chem. Phys.*, 2017, **19**, 15264-15272.

(16) G. Panomsuwan, N. Saito and T. Ishizaki, *Phys. Chem. Chem. Phys.*, 2015, **17**, 6227-6232.

(17) G. Panomsuwan, N. Saito and T. Ishizaki, *Carbon*, 2016, **98**, 411-420.

(18) K. Hyun and N. Saito, *Sci. Rep.*, 2017, **7**, 3825.

(19) C. Oueiny, S. Berlioz and F.-X. Perrin, *Prog. Polym. Sci.*, 2014, **39**, 707-748.

(20) K. Tan, B. Tan, E. Kang and K. Neoh, *Phys. Rev. B*, 1989, **39**, 8070.

(21) R. Matassa, S. Orlanducci, E. Tamburri, V. Guglielmotti, D. Sordi, M. L. Terranova, D. Passeri and M. Rossi, *J. Appl. Crystallogr.*, 2014, **47**, 222-227.

(22) M. Kim, C. Lee and J. Jang, *Adv. Funct. Mater.*, 2014, **24**, 2489-2499.

(23) Z. Wei, M. Wan, T. Lin and L. Dai, *Adv. Mater.*, 2003, **15**, 136-139.

(24) S. Venkatesh and K. Vishista, *Electrochim. Acta*, 2018, **263**, 76-84.

(25) E. Kang, K. Neoh and K. Tan, *Polym. J.*, 1989, **21**, 873.

(26) X. Wang, C.-G. Liu, D. Neff, P. F. Fulvio, R. T. Mayes, A. Zhamu, Q. Fang, G. Chen, H. M. Meyer and B. Z. Jang, *J. Mater. Chem. A*, 2013, **1**, 7920-7926.

(27) B. Kumar, M. Asadi, D. Pisasale, S. Sinha-Ray, B. A. Rosen, R. Haasch, J. Abiade, A. L. Yarin and A. Salehi-Khojin, *Nat. Commun.*, 2013, **4**, 2819.

(28) J. Wei, Y. Hu, Y. Liang, B. Kong, J. Zhang, J. Song, Q. Bao, G. P. Simon, S. P. Jiang and H. Wang, *Adv. Funct. Mater.*, 2015, **25**, 5768-5777.

(29) 32 T. Kondo, S. Casolo, T. Suzuki, T. Shikano, M. Sakurai, Y. Harada, M. Saito, M. Oshima, M. I. Trioni and G. F. Tantardini, *Phys. Rev. B*, 2012, **86**, 035436.

(30) G. Zhou, E. Paek, G. S. Hwang and A. Manthiram, *Nat. Commun.*, 2015, **6**, 7760.

(31) A. J. Rennie and P. J. Hall, *Phys. Chem. Chem. Phys.*, 2013, **15**, 16774-16778.

(32) D. Liu, W. Lei, D. Portehault, S. Qin and Y. Chen, *J. Mater. Chem. A*, 2015, **3**, 1682-1687.

(33) 31 R. Arrigo, M. Hävecker, R. Schlögl and D. S. Su, *Chem. Commun.*, 2008, 4891-4893.

(34) 30 R. Arrigo, M. Hävecker, S. Wrabetz, R. Blume, M. Lerch, J. McGregor, E. P. Parrott, J. A. Zeitler, L. F. Gladden and A. Knop-Gericke, *J. Am. Chem. Soc.*, 2010, **132**, 9616-9630.

(35) M. Boutchich, H. Arezki, D. Alamarguy, K.-I. Ho, H. Sediri, F. Güneş, J. Alvarez, J. Kleider, C. Lai and A. Ouerghi, *Appl. Phys. Lett.*, 2014, **105**, 233111.

(36) S. Jia, Y. Wang, G. Xin, S. Zhou, P. Tian and J. Zang, *Electrochim. Acta*, 2016, **196**, 527-534.

(37) L. Tang, R. Ji, X. Li, K. S. Teng and S. P. Lau, *J. Mater. Chem. C*, 2013, **1**, 4908-4915.

(38) D. Zhou, Y. Cui, P.-W. Xiao, M.-Y. Jiang and B.-H. Han, *Nat. Commun.*, 2014, **5**, 4716.

(39) B.-X. Zou, Y. Liang, X.-X. Liu, D. Diamond and K.-T. Lau, *J. Power Sources*, 2011,

196, 4842-4848.

(40) Q. Hu, C. Guo, D. Sun, Y. Ma, B. Qiu and Z. Guo, *ACS Sustainable Chem. Eng.*, 2017, **5**, 11788-11796.

(41) L. Shi, R.-P. Liang and J.-D. Qiu, *J. Mater. Chem.*, 2012, **22**, 17196-17203.

(42) Y. Y. Smolin, M. Soroush and K. K. Lau, *Beilstein J. Nanotechnol.*, 2017, **8**, 1266.

(43) F. Ye, B. Zhao, R. Ran and Z. Shao, *J. Power Sources*, 2015, **290**, 61-70.

(44) 35 X. Y. Chen, C. Chen, Z. J. Zhang, D. H. Xie, X. Deng and J. W. Liu, *J. Power Sources*, 2013, **230**, 50-58.

(45) E. N. Nxumalo and N. J. Coville, *Materials*, 2010, **3**, 2141-2171.

(46) J. Zhang, Z. Xia and L. Dai, *Sci. Adv.*, 2015, **1**, e1500564.

(47) 34 W. Ding, Z. Wei, S. Chen, X. Qi, T. Yang, J. Hu, D. Wang, L. J. Wan, S. F. Alvi and L. Li, *Angew. Chem.*, 2013, **125**, 11971-11975.

(48) B. Kumar, M. Asadi, D. Pisasale, S. Sinha-Ray, B. A. Rosen, R. Haasch, J. Abiade, A. L. Yarin and A. Salehi-Khojin, *Nat. Commun.*, 2013, **4**, 2819.

() J. Wu, S. Ma, J. Sun, J. I. Gold, C. Tiwary, B. Kim, L. Zhu, N. Chopra, I. N. Odeh and R. Vajtai, *Nat. Commun.*, 2016, **7**, 13869.

(49) J. Zhang, L. Qu, G. Shi, J. Liu, J. Chen and L. Dai, *Angew. Chem. Int. Ed.*, 2016, **55**, 2230-2234.

(50) N. Mahmood, C. Zhang, H. Yin and Y. Hou, *J. Mater. Chem. A*, 2014, **2**, 15-32.

(51) R. Arrigo, M. Hävecker, S. Wrabetz, R. Blume, M. Lerch, J. McGregor, E. P. Parrott, J. A. Zeitler, L. F. Gladden and A. Knop-Gericke, *J. Am. Chem. Soc.*, 2010, **132**, 9616-9630.

(52) D. Zhou, Y. Cui, P.-W. Xiao, M.-Y. Jiang and B.-H. Han, *Nat. Commun.*, 2014, **5**, 4716.

(53) D. Wei, Y. Liu, Y. Wang, H. Zhang, L. Huang and G. Yu, *Nano Lett.*, 2009, **9**, 1752-1758.

(54) O. Vazquez-Mena, J. P. Bosco, O. Ergen, H. I. Rasool, A. Fathalizadeh, M. Tosun, M. Crommie, A. Javey, H. A. Atwater and A. Zettl, *Nano Lett.*, 2014, **14**, 4280-4285.

(55) W. Wang, K. Leung, W. Fong, S. Wang, Y. Hui, S. Lau, Z. Chen, L. Shi, C. Cao and C.

Surya, *J. Appl. Phys.*, 2012, **111**, 093520.

(56) M.-S. Lee, K. Lee, S.-Y. Kim, H. Lee, J. Park, K.-H. Choi, H.-K. Kim, D.-G. Kim, D.-Y. Lee and S. Nam, *Nano Lett.*, 2013, **13**, 2814-2821.

(57) G.-L. Chai, Z. Hou, D.-J. Shu, T. Ikeda and K. Terakura, *J. Am. Chem. Soc.*, 2014, **136**, 13629-13640.

(58) Z. R. Ismagilov, A. E. Shalagina, O. Y. Podyacheva, A. V. Ischenko, L. S. Kibis, A. I. Boronin, Y. A. Chesalov, D. I. Kochubey, A. I. Romanenko and O. B. Anikeeva, *Carbon*, 2009, **47**, 1922-1929.

(59) K. Fujisawa, T. Tojo, H. Muramatsu, A. L. Elías, S. M. Vega-Díaz, F. Tristán-López, J. H. Kim, T. Hayashi, Y. A. Kim and M. Endo, *Nanoscale*, 2011, **3**, 4359-4364.

(60) D. Deng, X. Pan, L. Yu, Y. Cui, Y. Jiang, J. Qi, W.-X. Li, Q. Fu, X. Ma and Q. Xue, *Chem. Mater.*, 2011, **23**, 1188-1193.

(61) N. Rey-Raap, E. Calvo, J. Bermúdez, I. Cameán, A. García, J. Menéndez and A. Arenillas, *Measurement*, 2014, **56**, 215-218.

(62) H. Zengin, W. Zhou, J. Jin, R. Czerw, D. Smith Jr, L. Echegoyen, D. L. Carroll, S. H. Foulger and J. Ballato, *Adv. Mater.*, 2002, **14**, 1480-1483.

Chapter 5

Summary

Chapter 5 – Summary

Rational design and development of a novel carbon material system have emerged as the promising strategy to create unique and unconventional functional properties. Herein, CN–C materials was synthesized by a one-step SP at room temperature and atmospheric pressure. The SP was generated between wire-to-wire electrodes which were submerged in the solution. Room-temperature Hall-effect measurement demonstrated that CN–C materials exhibited p-type semiconducting behavior with an excellent hole concentration. More interestingly, CN–C materials had an excellent electrical conductivity, which is the highest value ever reported for carbon-based materials. A remarkable enhancement of electrical conductivity and p-type characteristic of CN–C materials is attributed to contributions of high conductive pathway by cationic nitrogen and the existence of cationic nitrogen doping. In other words, the presence of the cationic nitrogen maintaining planarity of the carbon material and improves the crystallinity, thereby contributing to the improvement of the electrical properties.

Chapter 2 focuses on the f-FLG was easily synthesized via a new route in solution plasma in an ionic liquid from graphite flakes at ambient temperature and atmospheric pressure. A simple method to fabricate f-FLG from graphite flakes using solution plasma was reported. f-FLG with a narrow distribution regarding the number of layers was obtained, as verified by X-ray diffraction, Raman spectroscopy, electron microscopy, infrared spectroscopy, and X-ray photoelectron spectroscopy. The mechanism of f-FLG synthesis was explained by the induced electron exchange in graphene flakes and the ionic liquid via solution plasma. An energy diagram of the density of states of graphite, ionic liquid in water, and plasma were used to confirm the electron exchange during f-FLG synthesis, which in turn led to a lack of electrons

on the graphite flakes subsurface. The peeling of graphite flakes was proposed to occur because of this lack of electrons. Therefore, the electronic structure of the ionic liquid in water was calculated by ab initio molecular orbital calculations and confirmed by cyclic voltammetry.

Chapter 3 describes that CN–G have been successfully synthesized by one-pot synthesis of SP with high-repetition frequency discharges. TEM and XPS results showed that the graphene containing a high nitrogen content. Broadening of the 2D band in the Raman spectra, CN–G confirmed that the three layers graphene. In addition, nitrogen doping content was found as high as 13.4 at% and a high amount of cationic nitrogen appeared. CN–G behave like p-type semiconductor with a high sheet resistance of 16 Ω sq^{-1} and a high carrier concentration of 10^{19} cm^{-3}; indicating that process can significantly control the electrical properties of graphene.

Chapter 4 reveals that CN–C and CN–C@SWCNT were successfully synthesized via a solution plasma process using an aniline aqueous solution with the SWCNT dispersion. Cationic nitrogen produced from the plasma discharge in the liquid led to the formation of CN–C wrapped uniformly around the SWCNT. Characterization results revealed that CN–C@SWCNT exhibits p-type semiconducting behavior, with an excellent electrical conductivity of 120 S cm^{-1} and a high carrier concentration of 4.6×10^{20} cm^{-3}; these values are greater than those of the previously reported carbon-based materials. The outstanding electronic and transport properties of CN–C@SWCNT were mainly attributed to the doped cationic nitrogen from the CN–C wrapped around the SWCNT surface and SWCNT serving as a conductive bridge among the CN–C domains.

In this study, we succeeded to synthesize CN–C materials without thermal treatment, high-performance carbon with excellent electrical properties using solution plasma. Particularly, through 4 chapters, we have confirmed the infinite possibilities of development on CN–C

materials. We have confirmed the possibility of manufacturing a new form (N+) of carbon material with a high heteroatom content, which is expected to greatly improve the electrical conductivity, field emission, catalyst and storage properties. From all we mentioned, CN–C really showed a great potential to be a promising p-type semiconductor for advanced technological applications.

Achievement

List of publication

[1] Sangwoo. Chae, Maria Antoaneta Bratescu, and Nagahiro Saito, “Synthesis of Few-Layer Graphene by Peeling Graphite Flakes via Electron Exchange in Solution Plasma”, *Journal of Physical Chemistry C*, 2017, 121, 23793–23802.

[2] Sangwoo Chae, Kazuo Hashimi, Maria Antoaneta Bratescu, and Nagahiro Saito, “The nano-structure and their properties of exfoliation several layers-stacked graphene prepared from graphite dispersed in aqueous solutions by solution plasma”, *Nanoscience and Nanotechnology Letters*, 2018, 10, 784-789.

[3] Sangwoo Chae, Gasidit Panomsuwan, Maria Antoaneta Bratescu, Takahiro Ishizaki, Katsuya Teshima and Nagahiro Saito, “Highly Cationic Nitrogen-Doped Carbon Wrapping Single-Wall Carbon Nanotubes with High Electrical Conductivity”, *Chemical Communications*, 2018, under review.

[4] Sangwoo Chae, Gasidit Panomsuwan, Maria Antoaneta Bratescu, Katsuya Teshima and Nagahiro Saito, “P-type Graphene with Cationic N dopants”, *ACS Applied Nano Materials*, 2018, under review.

List of patent

[1] Patent number: PCT / JP2018 / 085585 Title: “窒素ドープカーボンCNT複合体”; Investigators: 齋藤永宏、プラテスク マリア アントワネッタ、蔡尚佑、橋見一生、虎澤研示、橋本剛、八名拓実; Investor: 名古屋大学, (株)名城ナノカーボン.

[2] Patent number: PCT / JP2018 / 00000; Title: “高結晶性窒素高含有グラファイトシート及び

グラファイト"; Investigators: 齋藤永宏、虎澤研示, プラテスク マリア アントワネッタ、橋見一生, 蔡尚佑、牟田幸浩; Investor: 名古屋大学.

List of awards

Best Poster Rewards: "The nano-structure and their properties of exfoliation several layers-stacked graphene prepared from graphite dispersed in aqueous solutions by solution plasma, The 4th International Symposium on Hybrid Materials and Processing (Hymap 2017), Busan, South Korea, November, 2017.

List of international presentation

[1] Sangwoo Chae, Maria Antoaneta Bratescu, and Nagahiro Saito, "Peeled and CN-Graphene from Graphite by Ionic Liquid via Solution Plasma", The 5th International Workshop & The 4th International Mini Workshop on Solution Plasma and Molecular Technology (SPM-5 & Mini SPM-4), Greifswald, Germany, June, 2017.

[2] Sangwoo Chae, Maria Antoaneta Bratescu, and Nagahiro Saito, "The nano-structure and their properties of exfoliation several layers-stacked graphene prepared by solution plasma in graphite dispersed in aqueous solutions.", The 4th International Symposium on Hybrid Materials and Processing, Busan, South Korea, November, 2017.

[3] Sangwoo Chae, Maria Antoaneta Bratescu, and Nagahiro Saito, "Few-Layers Graphene Sheets Synthesis from Graphite by Solution Plasma", 2017 workshop on Biomimetic Materials and Energy-Saving Materials, Shanghai, China, November, 2017.

[4] Sangwoo Chae, Maria Antoaneta Bratescu, and Nagahiro Saito, "Synthesis and Properties of Cationic Nitrogen-Doped Carbon Wrapped SWCNTs", The Final Seminar on JSPS Core-to-Core Program (B. Asia-Africa Science Platforms) Establishment of Research Hub for Compact

Mobility Model in the ASEAN Region, Thailand, Bangkok, December, 2018.

[5] Sangwoo Chae, Maria Antoaneta Bratescu, and Nagahiro Saito, “Synthesis of Cationic Nitrogen-Doped Carbon Wrapping Carbon Nanotubes with High Electrical Conductivity”, The International Conference on Advanced and Applied Petroleum, Petrochemicals, and Polymers (ICAPPP 2018), Thailand, Bangkok, December, 2018.

List of domestic presentation

[1] Sangwoo Chae, Maria Antoaneta Bratescu, and Nagahiro Saito, “ソリューションプラズマを用いたグラファイトの剥離・修飾による機能化グラフェンシートの作製”, 平成28年度表面技術若手研究者・技術者研究交流発表会, 名古屋市工業研究所, 2016年 12月.

[2] Sangwoo Chae, Maria Antoaneta Bratescu, and Nagahiro Saito, “N-doped carbon r apping CNTs to enhance electrical conductivity”, The Third Seminar on JSPS Core-to-Core Program (B. Asia-Africa Science Platforms) “Establishment of Research Hub for Compact Mobility Model in the ASEAN Region”, 名古屋大学, 2018年 2月.

[3] Sangwoo Chae, Maria Antoaneta Bratescu, and Nagahiro Saito, “Cationic N-doped carbon wrapping CNT to enhance electrical conductivity”, 2018年第79回応用物理学会秋季学術講演会, 名古屋国際会議場, 2018年 9月.